Landau and Van Kampen Spectra in Discrete Kinetic Plasma Systems

Vasil Bratanov

Master Thesis
Physics Department
LMU Munich

Scientific Advisor: Prof. Dr. Frank Jenko
Advisor at the LMU: Prof. Dr. Hartmut Zohm

25.09.2011

Declaration of Authorship

I declare that this thesis was composed by myself and that the work contained therein is my own, except where explicitly stated otherwise in the text.

Vasil Bratanov

July 13, 2012

Acknowledgements

First and foremost I would like to express my gratitude to my supervisor Prof. Dr. Frank Jenko for his support and guidance that helped me to understand the framework of Kinetic Theory and made my work possible. I am extremely thankful both to him and Prof. Dr. Hartmut Zohm for their patience and valuable remarks during the process of writing my thesis, and for giving me the opportunity to write my Master thesis at the Max-Plank-Institut für Plasmaphysik, Garching. Sincere thanks are given also to David Hatch, Ph.D. for the many useful discussions regarding the physics behind the mathematical models, for making a comparison with GENE possible, and helping me improve my English. I would also like to thank Dr. Stephan Brunner for the discussions, his introductory notes about the slab ITG model and examples for MATLAB routines. I am also grateful to Prof. Dr. Semjon Wugalter, whose lectures provided useful insights into the topic of operator theory. Further, I would like to express my gratitude to the German Academic Exchange Service (DAAD) for its financial support during my studies.

Contents

Chapter 1

Introduction

1.1 Plasma physics and its relation to nuclear fusion

More than 99% of the matter in the Universe that can be observed directly exists as plasma, to which one often refers as the fourth state of matter. Its large abundance and the great variety of phenomena that occur in plasmas make the study of this state of matter an important part of physics. Nowadays, the interest in plasma physics research is also driven by more pragmatic reasons, namely the need for a powerful, compact, and environmentally safe source of energy that has also practically inexhaustible fuel reserves. The only power source known to mankind that has the potential to fulfil these conditions is nuclear fusion. This is the same process to which stars owe their energy production. The fundamental physics behind fusion reactions became clear already in the first half of the 20th century, and since the 1950s, scientists have been making a great effort to produce energy from fusion in a controlled way on Earth. For fusion reactions to happen, the distance between the two nuclei should be small enough such that the short-ranged strong nuclear force dominates and the nuclei merge. However, all atomic nuclei are positively charged and repel each other via the Coulomb force. One way to overcome these repelling forces is to heat the plasma. This increases the average kinetic energy of the particles and allows them to come closer to each other and thus enhances the probability for a quantum mechanical tunnel effect that makes fusion possible. The approach that has made the greatest progress with respect to a net energy gain from fusion reactions is magnetic confinement. In such machines, hot and dilute plasma is confined via a strong magnetic field that forces the charged particles in the plasma to gyrate rapidly around the magnetic field lines. This gyromotion considerably reduces the particle transport perpendicular to the field lines and makes interactions between plasma particles and the containing vessel infrequent such that plasma temperatures of the order of $10^8 K$ are possible. Because of this effect the optimal containing vessel for a magnetically confined plasma is such that at every point of the boundary the magnetic field lines are roughly tangent to the wall of the vessel. For a non-vanishing continuous vector field (e.g., a magnetic field), this condition cannot be fulfilled on a sphere (Hairy Ball Theorem due to Poincaré) but it can be fulfilled for a toroidal

surface. Therefore, in the field of nuclear fusion based on magnetic confinement, one uses predominantly Tokamaks or Stellarators, both of which have topologically the same shape, namely that of a torus.
In the beginning of magnetic confinement fusion research it was thought that particles (as well as energy and momentum) are transported across the nested toroidal magnetic surfaces, formed by the field lines, due to collisions. When a collision between two gyrating particles occurs, the particles can 'jump' to different field lines inducing cross-field transport. However, after a thorough mathematical analysis of such processes, it became clear that the corresponding diffusivities are too small and cannot explain the shorter energy confinement time observed in experiments. With the advance of fusion research, another effect was discovered that affects this collision-induced transport. In the twisted magnetic field of a Tokamak, the plasma particles move along complicated trajectories called 'banana orbits' that can lead them rapidly from the inner to the outer part of the torus where only few collisions can distort their orbit such that they do not return back in the inner part of the plasma. In total, this effect, called 'neoclassical transport', results in an outward energy transport and thus cooling the plasma which is an undesirable effect for fusion machines. The neoclassical transport expresses itself in enhancing the total transport coefficient and, therefore, decreasing the energy confinement time. However, the corresponding correction can be computed, and it still cannot explain the experimental results. The residual effect was called 'anomalous transport', and represents one of the biggest hurdles on the way to harnessing nuclear fusion.
In order to understand the reason for the anomalous transport, one first looked at fluid-like models of the plasma. In typical fusion machines, there are enormous density and temperature differences over the plasma volume. For instance, the temperature in the plasma core is of the order of $10^8 K$, such that the conditions necessary for the nuclei to fuse are met. On the other hand, the materials which the containing vessel is made of impose an upper limit on the energy flux that is tolerable. This leads to the fact that the outer plasma layers have a temperature of the order of $10^4 K$. The consequences of such a limitation are that in fusion plasmas there exist immense temperature gradients, that are of the order of $10^8 K/m$. Analogous considerations for the density show that its gradient is also enormous. From fluid theory, it is known that in situations where large gradients of temperature and density are present, turbulent flows arise that form eddies in the plasma. These eddies mix the fluid and, therefore, work against the gradients. The total effect of the turbulence results in a rapid energy transport from hotter to colder areas of the plasma. After nearly two decades of research in that area, it is widely agreed upon in the fusion community that turbulence is the cause for the anomalous transport. This discovery showed that a good understanding of the fundamental features of turbulence is needed in order to improve the predictability of the behaviour of magnetized plasmas.
An essential question in this context is how exactly turbulent flows arise. Strictly speaking, there exist stationary solutions for the plasma with large gradients. However, in the real world, such a state of the plasma cannot be realized exactly. There will always be some deviations, to which we shall refer as perturbations, of the realized state from the one that is desired. If even an arbitrarily small perturbation of the initial condition grows steadily

in the linear approximation for some set of parameters, then this is called an instability. It is physically clear that such an instability cannot continue to grow indefinitely and has to be saturated via nonlinear effects. According to our current understanding, such instabilities give rise to the turbulent flows observed. Therefore, understanding the formation and saturation of unstable modes is of great importance for the study of turbulence and its influence on the particle and energy transport in hot plasmas.
Although turbulence is a notion of fluid theory, it can be influenced by kinetic effects because they can cause instabilities or additional damping of the modes that determine the turbulent behaviour. Therefore, a study of kinetic effects is often needed for a thorough understanding of the origin and development of turbulent flows. In this work, we are going to focus on one of the well known and widely studied kinetic effects, namely Landau damping. The simple linear models we shall use will allow us to avoid unnecessary mathematical complications and concentrate on gaining physical insights that can then be used to better understand the results of nonlinear numerical simulations.

1.2 Importance of Landau damping

Since the subject of this work is the Landau damping of plasma waves, it will be beneficial to focus our attention on its importance in plasma physics and fusion research. We shall show that in the case of electrostatic perturbations of a Maxwellian background, there are no unstable (i.e., steadily growing in time) solutions. However, as we will see in this work, this is not always the case. In some models and for some sets of parameters, this simple linear approach can lead to waves that grow with time. This is called an instability. Such instabilities are of great importance in fusion research since they are the main obstacle for plasma confinement. Properties of the unstable solution, like growth rate and wave number, are essential because they contain the information for the time scales on which the instability has to be taken into account and the spatial scales on which it occurs. As in conventional fluid mechanics, the instabilities are those effects that start and drive the turbulence. It appears also that turbulence is the major hurdle in magnetic confinement devices that prevents achievement of large energy confinement times. Strictly speaking, discovering an unstable solution of the equations means that linear theory is not valid any more, since in the framework of the linear approximation, every instability can grow indefinitely, and thus at some point the approximation made by neglecting terms quadratic in the perturbations no longer applies. The real physical picture in such cases is that the instabilities are saturated at some point, i.e., the energy that is injected into the perturbed system equals the energy that is dissipated. Nonlinear effects, however, can rarely be treated analytically. In such cases a numerical approach is often the only possible way to proceed. Computer simulations of plasma turbulence show that many modes which are damped in the framework of linear theory, are excited by nonlinear effects. These damped modes can then couple to the unstable modes via nonlinear effects and thus facilitate saturation. Although linear theory is too simplified to describe the behaviour of a real plasma, it is often used to easily gain physical insights into the model. For instance, from computer

simulations it is known that the nonlinear frequency spectrum peaks at the position of the linear instability.
From the point of view of conventional fluid theory, energy is usually injected on large scales (i.e., small wave numbers) and then dissipated on small scales (corresponding to large k) via viscosity (Kolmogorov cascade) [10]. Although it was thought for decades that this is also the case in plasmas, recent findings show that this is not the complete picture [25], [24], [28], [27]. In plasmas, a great amount of energy dissipation appears at the same spatial scales as the energy injection which means that the most important nonlinear coupling is that between damped and unstable modes that have similar k. This important feature of energy dissipation in plasmas resembles the physical picture of Landau damping, since for this phenomenon at the same wave number there exist many damped and unstable modes that have different frequencies. This is one of the indications that Landau damping plays an important role in the saturation of plasma turbulence. However, the connection between these two effects has yet to be solidified, and a necessary step in this direction is a thorough study of the linear Landau damping also in the Van Kampen picture, investigating important aspects of this phenomenon that can then be qualitatively recognized in nonlinear simulations.

1.3 Structure of the thesis

This thesis is organised as follows. In chapter 2, we describe the theoretical background of Langmuir waves, and then study a well known kinetic effect, called 'Landau damping', which damps the wave amplitude exponentially for large times. The first section presents the physical picture of this effect via a simplified calculation which, however, preserves the most prominent feature of the Langmuir waves, namely that they are damped away. In the next two parts of the second chapter we describe two different approaches for solving the problem that are more mathematical in nature. The first method is due to Landau (1946) who solved the initial value problem and discovered the damping effect. After that, Van Kampen (1955) found the eigenmodes of the equation which have real frequencies. Since damped waves have a complex frequencies, at this point confusion often arises and this issue is clarified at the end of the second subsection.
In chapter 3, we present our approach for finding the Van Kampen spectrum that is based on operator theory. This new method improves our understanding of the problem and shows that some standard references (e.g., [13]) regarding Landau damping actually do not give completely correct results about the general conditions on which the presence and the form of the Van Kampen spectrum depend.
Chapter 4 deals with the numerical description of Langmuir waves and is divided into two sections. In the first part, we neglect collisions and reproduce some of the known analytical results. Here, also a short subsection is dedicated to the 'bump-on-tail' instability. Incorporating collisions into the system via different collision operators is the topic of the second section, where we test if a discretization scheme in velocity space reproduces the analytical

results stated in [18], [26] and [16], namely that the collisionless Van Kampen spectrum is altered profoundly when collisions are introduced. Further, we investigate which part of the collision operator causes this abrupt change.
In chapter 5, we consider electrostatic perturbations in the slab ITG model. From the equations it is evident that all we learned in chapter 3 can be applied to the ITG system. By introducing collisions into this model, we discover the same effect as in the case of Langmuir waves.
The last chapter gives a short summery of the thesis and outlines the open issues that are going to be the subject of subsequent work.

Chapter 2

Theoretical model of Langmuir waves in a collisionless plasma

In this chapter, we will discuss a simple one-dimensional model of Langmuir waves in a collisionless plasma, and consider electron oscillations with a small amplitude with respect to a homogeneous background of immobile ions such that quasi-neutrality holds. The small amplitude of the electron oscillations allows linearisation of the equations and thus an exact analytic solution of the problem. In this simplified model, one should also think about the physical correctness of neglecting collisions. From a naive physical point of view, one could argue using a time scale argument. In a real plasma, particle collisions are always going to be present. However, if one is interested in processes that develop on time scales that are much smaller than the average collision time, it appears to be physically reasonable to neglect the collision operator for time intervals that are sufficiently small. Although such an argument is at first sight adequate from a physical point of view, later on in this work we will see that collisions are of great importance for the physical system. In mathematical terms, the collision operator, for which we shall use an approximative one-dimensional model, will turn out to be a singular perturbation to the system. Therefore, if the collision frequency is not exactly zero, this will alter the results profoundly, no matter how small its value is.

Let $f(z, v, t)$ be the one-dimensional electron distribution function where v is the velocity in the $z-$direction. From kinetic theory, it is known that $f(z, v, t)$ should satisfy the one-dimensional Boltzmann equation. In the case when there are no external fields, and considering only the electric field $E(z, t)$ produced by f, we can write the Boltzmann equation in the form

$$\frac{\partial f}{\partial t} + v\frac{\partial f}{\partial z} - \frac{e}{m_e}E(z,t)\frac{\partial f}{\partial v} = \left(\frac{\partial f}{\partial t}\right)_{col}, \tag{2.1}$$

where e is the absolute value of the electron charge, m_e is the electron mass, and the right-hand side represents the general collision operator influencing the dynamics of the system. In a collisionless model, the right-hand side of (2.1) is set to zero. The equation above is not sufficient in order to find a solution $f(z, v, t)$. The behaviour of a system consisting of

charged particles is determined by Maxwell's equations that are necessary to solve (2.1). Since we have neglected the influence of magnetic fields, we are left only with the Poisson equation, and in one dimension it reads

$$\frac{\partial E(z,t)}{\partial z} = \frac{\rho(z,t)}{\varepsilon_0}. \tag{2.2}$$

Now, the only remaining step is to express the charge density ρ via the particle distribution function $f(z,v,t)$. For this reason, we first represent f as

$$f(z,v,t) = f_0(v) + f_1(z,v,t), \tag{2.3}$$

where $f_0(v)$ is the equilibrium distribution function of the electrons and f_1 is the deviation from this equilibrium. This splitting is always possible and there is yet no approximation made with regard to the distribution function. f_0 depends only on v because the ion background is homogeneous (no z dependence), and the definition of equilibrium implies no time independence. The whole dynamics of the system (in space as well as in time) comes from the perturbation f_1. The electron density is by definition the integral of $f(z,v,t)$ over velocity space. Since we have split the distribution function, we can, without any loss of generality, also split the density as $n(z,t) = n_0 + n_1(z,t)$, where these two terms are defined as

$$n_0 := \int_{-\infty}^{+\infty} f_0(v)dv \quad ; \quad n_1(z,t) := \int_{-\infty}^{+\infty} f_1(z,v,t)dv. \tag{2.4}$$

These definitions are useful because there is a direct connection between the charge density and n_1. In order to see this, one should recall that in this model the ions (that have the charge $+e$) are immobile, so they are always in equilibrium, and because of quasineutrality, the particle density of ions and electrons must be the same: $n_{ions} = n_0$. This means that

$$\rho(z,t) = e(n_{ions} - n_{el}(z,t)) = e(n_0 - (n_0 + n_1(z,t))) = -e\int_{-\infty}^{+\infty} f_1(z,v,t)dv. \tag{2.5}$$

Thus, recalling (2.2), one notes that the electric field is produced by f_1 and depends on it linearly. Now we go back to (2.1) and rewrite it in a slightly different way using (2.3):

$$\frac{\partial f_1}{\partial t} + v\frac{\partial f_1}{\partial z} - \frac{e}{m_e}E(z,t)\frac{\partial f_0}{\partial v} - \frac{e}{m_e}E(z,t)\frac{\partial f_1}{\partial v} = \left(\frac{\partial f}{\partial t}\right)_{col}. \tag{2.6}$$

The last term on the left-hand side includes a product between E and f_1. Assuming that the perturbation f_1 is very small with respect to the equilibrium distribution f_0, we can neglect this term because it is of the order of f_1^2. Performing this linearisation procedure and neglecting the collision operator yields the so-called linearised Vlasov equation. Together with the Poisson equation, this gives us a self-consistent system of one differential and one integral equation

$$\frac{\partial f_1}{\partial t} + v\frac{\partial f_1}{\partial z} - \frac{e}{m_e}E(z,t)\frac{\partial f_0}{\partial v} = 0 \tag{2.7}$$

$$\frac{\partial E(z,t)}{\partial z} = -\frac{e}{\varepsilon_0}\int_{-\infty}^{+\infty} f_1(z,v,t)dv. \tag{2.8}$$

Since we have a numerical approach in mind, it is convenient to normalize the terms in this system of equations in such a way that the new quantities have no physical dimension. In order to do this, we consider length and time scales which are typical for the system. In our simple model of an unmagnetized homogeneous plasma, the typical length is the Debye length λ_D, and the typical time during which considerable changes of the system occur is the inverse of the electron plasma frequency ω_{pe}. In SI units they are given by

$$\lambda_D = \sqrt{\frac{\varepsilon_0 k_B T_0}{n_0 e^2}} \; ; \; \omega_{pe} = \sqrt{\frac{n_0 e^2}{m_e \varepsilon_0}} \tag{2.9}$$

where k_B is the Boltzmann constant, ε_0 the dielectric constant of the vacuum, T_0 and n_0 are the equilibrium temperature and density, respectively, which are defined via $f_0(v)$. The velocity will be normalized over the thermal velocity which we define via

$$v_{th} := \sqrt{\frac{k_B T_0}{m_e}} = \lambda_D \omega_{pe}. \tag{2.10}$$

Taking into account the above consideration, we introduce normalized expressions for the quantities which appear in our equations and denote them by a tilde over the usual symbol:

$$\widetilde{f}_{1,0} := \frac{v_{th}}{n_0} f_{1,0} \; ; \; \widetilde{E} := \frac{\lambda_D e}{k_B T_0} E \; ; \; \widetilde{z} := \frac{z}{\lambda_D} \; ; \; \widetilde{t} := t\omega_p \; ; \; \widetilde{v} := \frac{v}{v_{th}}. \tag{2.11}$$

This gives us a system of normalized equations:

$$\frac{\partial \widetilde{f}_1}{\partial \widetilde{t}} + \widetilde{v}\frac{\partial \widetilde{f}_1}{\partial \widetilde{z}} - \widetilde{E}(\widetilde{z},\widetilde{t})\frac{\partial \widetilde{f}_0}{\partial \widetilde{v}} = 0 \tag{2.12}$$

$$\frac{\partial \widetilde{E}(\widetilde{z},\widetilde{t})}{\partial \widetilde{z}} = -\int_{-\infty}^{+\infty} \widetilde{f}_1(\widetilde{z},\widetilde{v},\widetilde{t})d\widetilde{v}. \tag{2.13}$$

When dealing with a homogeneous system like this, it is useful to make a Fourier transformation in space. We use the convention:

$$\widehat{g}(k) = \frac{1}{\sqrt{2\pi}}\int_{-\infty}^{+\infty} g(z)e^{-ikz}dz \tag{2.14}$$

where $\widehat{g}(k)$ denotes the Fourier transform of $g(z)$. Since we have already normalized z, the k-variable appearing after the transformation is automatically normalized to the inverse of the Debye length. This way we get

$$\widehat{\widetilde{E}}(\widetilde{k},\widetilde{t}) = \frac{i}{\widetilde{k}} \int_{-\infty}^{+\infty} \widehat{\widetilde{f}}_1(\widetilde{k},\widetilde{v},\widetilde{t}) d\widetilde{v}. \tag{2.15}$$

Substituting this expression for the Fourier transform of the electric field in the differential equation for $\widetilde{f}_1$ leads to

$$i\frac{\partial \widehat{\widetilde{f}}_1(\widetilde{k},\widetilde{v},\widetilde{t})}{\partial \widetilde{t}} = \widetilde{k}\widetilde{v}\widehat{\widetilde{f}}_1(\widetilde{k},\widetilde{v},\widetilde{t}) - \frac{1}{\widetilde{k}}\frac{\partial \widetilde{f}_0}{\partial \widetilde{v}} \int_{-\infty}^{+\infty} \widehat{\widetilde{f}}_1(\widetilde{k},\widetilde{v},\widetilde{t}) d\widetilde{v}. \tag{2.16}$$

2.1 Approximative results

Before we approach the problem of solving (2.16) in a mathematically consistent way, it is useful to consider a simplified situation in which a damping effect arises. We will consider a simple model inspired by [9]. This will give us important physical insights about the nature of Landau damping. Let us look at a non-relativistic particle which is subject to a known electric field. For convenience, we assume the electric field to be a sinusoidal wave in the z-direction and that the initial velocity of the particle has also only a z-component, i.e., we reduce the situation to a one-dimensional problem. According to the approximations made, the equation of motion is

$$m\frac{dv}{dt} = qE\cos(kz - \omega t), \tag{2.17}$$

where m and q denote the mass and the charge of the particle, respectively. Without any loss of generality we can take the parameter k to be positive. Assuming that the electric field is of first order, we can treat it as a small perturbation of the zeroth order solution which is $z^{(0)}(t) = v_0 t + z_0$, where the subscript '0' denotes the initial values of the corresponding quantities. The first order velocity $v^{(1)}$ is determined by the equation of motion (2.17) when we substitute in it the zeroth order solution for $z(t)$:

$$m\frac{dv^{(1)}}{dt} = qE\cos(kz_0 + kv_0 t - \omega t). \tag{2.18}$$

With the initial condition $v^{(1)}(t=0) = 0$, one arrives at the result

$$v^{(1)} = \frac{qE}{m}\frac{(\sin(kz_0 + kv_0 t - \omega t) - \sin(kz_0))}{kv_0 - \omega}\,. \tag{2.19}$$

This allows us to determine the first order solution $z^{(1)}$ for the particle trajectory which reads

$$z^{(1)} = \int_0^t v^{(1)}(t')dt' = \frac{qE}{m}\left(\frac{-\cos(kz_0+pt)+\cos(kz_0)}{p^2} - \frac{t\sin(kz_0)}{p}\right), \tag{2.20}$$

where the new variable p is defined as $p := kv_0 - \omega$. Using $z^{(1)}(t)$ in the equation of motion, we can derive the second order velocity. The ultimate goal of this calculation is to find an approximate expression for the rate of change of the kinetic energy W of the particle. If we write the velocity as $v = v_0 + v^{(1)} + v^{(2)} + ...$, then up to second order we have

$$\frac{dW}{dt} = m(v_0 + v^{(1)} + v^{(2)} + ...)\frac{d}{dt}(v_0 + v^{(1)} + v^{(2)} + ...) \approx mv_0\frac{dv^{(1)}}{dt} + mv_0\frac{dv^{(2)}}{dt} + mv^{(1)}\frac{dv^{(1)}}{dt}. \tag{2.21}$$

The first order term in the above expression is proportional to the right-hand side of (2.18), which is a sine function with respect to z_0. Since we want to apply the results of this model to a plasma where particles have a variety of initial positions and velocities, we have to average dW/dt over all possible initial positions and velocities. If we average $mv_0 dv^{(1)}/dt$ over z_0, it gives zero. Therefore, we are left only with the second order terms. After calculating the second order velocity $v^{(2)}$ as explained above, the explicit form of dW/dt up to second order becomes

$$\begin{aligned}\frac{dW}{dt} \approx \frac{q^2E^2}{m}\left(\frac{\sin(kz_0+pt)-\sin(kz_0)}{p}\right)\cos(kz_0+pt) - \\ - \frac{kv_0q^2E^2}{m}\left(\frac{-\cos(kz_0+pt)+\cos(kz_0)}{p^2} - \frac{t\sin(kz_0)}{p}\right)\sin(kz_0+pt).\end{aligned} \tag{2.22}$$

First, we average the above quantity over all possible initial positions. Since we have a homogeneous plasma in mind, the average process is just an integral over z_0 from $-\infty$ to $+\infty$, i.e., the weight function is constant and equals one. This leads to

$$\left\langle \frac{dW}{dt} \right\rangle_{z_0} = \frac{q^2E^2}{2m}\left(-\omega\frac{\sin(pt)}{p^2} + t\cos(pt) + \omega t\frac{\cos(pt)}{p}\right). \tag{2.23}$$

The last step left is to average (2.23) over all possible initial velocities. However, one should bear in mind that not all velocities are equally probable. Therefore, the weight function for this averaging process is the equilibrium distribution function $f_0(v_0)$ which in the new notation is $f_0 = f_0((p+\omega)/k)$, i.e.,

$$\left\langle \frac{dW}{dt} \right\rangle_{z_0,v_0} = \frac{q^2E^2}{2mk}\int_{-\infty}^{+\infty}\left(-\omega\frac{\sin(pt)}{p^2} + t\cos(pt) + \omega t\frac{\cos(pt)}{p}\right) f_0((p+\omega)/k)dp. \tag{2.24}$$

One can show that the contribution to the final result from integrating the second and the third terms tends to zero when $t \to \infty$. It is noteworthy that the first term in the integrand

has a pole at $p = 0$ which is integrable since $\sin(pt)$ changes its sign at this point and f_0 does not. We can expand $f_0((p+\omega)/k)$ in Taylor series around $p = 0$. Since $\sin(pt)/p^2$ is an odd function of p, it is clear that only the odd terms of the Taylor series contribute to the integral. For a qualitatively good approximation, it is sufficient to consider only the first odd term. This gives

$$p.v. \int_{-\infty}^{+\infty} \frac{f_0((p+\omega)/k)\sin(pt)}{p^2} dp \approx \left.\frac{df_0}{dp}\right|_{p=0} p.v. \int_{-\infty}^{+\infty} \frac{\sin(pt)}{p} dp = \pi \left.\frac{df_0}{dp}\right|_{p=0} = \pi \left.\frac{df_0(v_0)}{dv_0}\right|_{v_0=\frac{\omega}{k}}. \tag{2.25}$$

From this follows

$$\left\langle \frac{dW}{dt} \right\rangle_{z_0,v_0} = -\frac{\pi q^2 E^2}{2mk} \left(\frac{\omega}{k}\right) \left.\frac{df_0(v_0)}{dv_0}\right|_{v_0=\frac{\omega}{k}}. \tag{2.26}$$

The above result shows that the sign of the averaged dW/dt depends on the derivative of the equilibrium distribution function with respect to velocity. A realistic f_0 would be a Maxwell distribution. The derivative of this function is positive when the argument is negative and vice versa. This means that the product $(\omega/k)(df_0/dv_0)|_{v_0=\omega/k}$ is always negative and therefore $\left\langle \frac{dW}{dt} \right\rangle_{z_0,v_0}$ is always positive. Recalling that the left-hand side of (2.26) is the rate of change of the kinetic energy of an average electron/ion in the plasma under the influence of a small sinusoidal electric field, one sees immediately that the plasma particles are going to gain energy from their interaction with the electrostatic wave. Because of energy conservation, the wave loses energy, i.e., it is damped.
Another interesting observation is that, to first order, not the whole equilibrium distribution influences the exchange of energy. The derivative of f_0 at the point $v_0 = \omega/k$ shows that the important particles are those that move with the same speed as the phase velocity of the wave. This is due to the fact that those particles are at rest with respect to the wave, i.e., they 'see' a constant electric field and, therefore, can interact with the wave much more effectively. The particles that are moving a little faster than the wave are decelerated, and those moving a little slower are accelerated. Strictly speaking, one should consider an infinitesimally small velocity interval of length $2dv$ around the point $v_0 = \omega/k$. If for positive ω, there are more electrons with initial velocity $v_0 \in [\omega/k - dv, \omega/k]$ than those with $v_0 \in [\omega/k, \omega/k + dv]$, the wave accelerates more particles than it decelerates and, thus, loses energy. The fact that the wave interacts most effectively with the particles that have the same velocity as its phase velocity is the reason that Landau damping is usually referred to as a resonant effect. Although the model we used in this subsection was greatly simplified, it still allowed us to gain useful physical insights into this kinetic effect and explains how an electrostatic wave in a plasma can be damped without collisions, which is not what one would expect intuitively.

2.2 Landau approach

The model that we used in the previous subsection was indeed sufficient for an introduction into the topic of Landau damping and allowed to gain of some useful physical insights, but it was not self-consistent. In this part, we are going to present a mathematically rigorous treatment of the problem of one-dimensional plasma waves.
One way to solve equation (2.16) is due to Landau [11] and involves a Laplace transform in time. This method has the advantage of easily incorporating the initial condition of the system which is essential for determining its time behaviour. Here we are going to present the same idea while using a slightly different notation in order to facilitate a comparison with later results. Let $g(t)$ be a function of time. We define a one-sided Fourier transform as follows:

$$\widehat{g}(\omega) = \frac{1}{\sqrt{2\pi}} \int_0^{+\infty} g(t) e^{i\omega t} dt \ . \tag{2.27}$$

For functions which are absolutely integrable, this integral is well defined at least in the upper $\widetilde{\omega}$-plane. The inverse transformation is then given by

$$g(t) = \frac{1}{\sqrt{2\pi}} \int_{-\infty+i\sigma}^{+\infty+i\sigma} \widehat{g}(\omega) e^{-i\omega t} d\omega \ , \tag{2.28}$$

where σ is a positive real number. Applying the transformation defined in (2.27) to equation (2.16), one arrives at

$$-\frac{i}{\sqrt{2\pi}} \widehat{\widetilde{f}}_1(\widetilde{k}, \widetilde{v}, \widetilde{t}=0) + \widetilde{\omega} \widehat{\widetilde{f}}_1(\widetilde{k}, \widetilde{v}, \widetilde{\omega}) = \widetilde{k}\widetilde{v} \widehat{\widetilde{f}}_1(\widetilde{k}, \widetilde{v}, \widetilde{\omega}) - \frac{1}{\widetilde{k}} \frac{\partial \widetilde{f}_0(\widetilde{v})}{\partial \widetilde{v}} \int_{-\infty}^{+\infty} \widehat{\widetilde{f}}_1(\widetilde{k}, \widetilde{v}, \widetilde{\omega}) d\widetilde{v} \ , \tag{2.29}$$

where the first term comes from integration by parts and we have used the property that $\widetilde{\omega}$ has some positive imaginary part, since this is the domain of definition of this transformation. Solving for $\widehat{\widetilde{f}}_1(\widetilde{k}, \widetilde{v}, \widetilde{\omega})$ and integrating over the velocity leads to

$$\int_{-\infty}^{+\infty} \widehat{\widetilde{f}}_1(\widetilde{k}, \widetilde{v'}, \widetilde{\omega}) d\widetilde{v'} \left(1 - \frac{1}{\widetilde{k}} \int_{-\infty}^{+\infty} \frac{1}{\widetilde{k}\widetilde{v} - \widetilde{\omega}} \frac{\partial \widetilde{f}_0(\widetilde{v})}{\partial \widetilde{v}} d\widetilde{v} \right) = \frac{i}{\sqrt{2\pi}} \int_{-\infty}^{+\infty} \frac{\widehat{\widetilde{f}}_1(\widetilde{k}, \widetilde{v}, \widetilde{t}=0)}{\widetilde{\omega} - \widetilde{k}\widetilde{v}} d\widetilde{v} \ . \tag{2.30}$$

If one recalls (2.15), one sees immediately that the first integral in the equation just derived is up to a factor of $i/\widetilde{k}$ the transformed (Fourier transformation in space and one-sided Fourier transformation in time) electric field. This eventually gives

$$\widehat{\widetilde{E}}(\widetilde{k},\widetilde{\omega}) = \frac{1}{\widetilde{k}\sqrt{2\pi}} \frac{\int_{-\infty}^{+\infty} \frac{\widehat{\widetilde{f}}_1(\widetilde{k},\widetilde{v},\widetilde{t}=0)}{\widetilde{k}\widetilde{v}-\widetilde{\omega}} d\widetilde{v}}{\left(1 - \frac{1}{\widetilde{k}} \int_{-\infty}^{+\infty} \frac{1}{\widetilde{k}\widetilde{v}-\widetilde{\omega}} \frac{\partial \widetilde{f}_0(\widetilde{v})}{\partial \widetilde{v}} d\widetilde{v}\right)} \ , \tag{2.31}$$

and this expression is defined in the upper half of the complex $\widetilde{\omega}$-plane. Since $\widetilde{k}$ is just a real parameter (that, without loss of generality, can be considered to be positive), there are no poles to be encountered while performing the velocity integrals. However, in order to perform a stability analysis of our system, we need to make sense of the integrals in (2.31) for $\widetilde{\omega}$ in the whole complex plane, i.e., we have to continue them analytically. Such a continuation will also help us to determine the long time behaviour of the electric field. When $\widetilde{\omega}$ has a positive imaginary part, one can do the velocity integrals in (2.31) along the real velocity axis, Figure 2.1 a. However, when $\widetilde{\omega}$ approaches the real axis and crosses it, the value of the integrals will jump by 2π which means that keeping the integration along the real $\widetilde{v}$-axis does not lead to a continuous function on the $\widetilde{\omega}$-plane. Therefore, in order to have an analytic continuation, one should deform the integration contour in such a way that the pole does not cross it. For real frequencies there is a pole on the integration path. In order to have an analytic continuation in this case, we have to deform the contour of integration such that the pole of the integrand at $\widetilde{v} = \widetilde{\omega}/\widetilde{k}$ does not lie on the integration path. One way to realise this, which also satisfies causality, is to make an infinitesimal semi-circle around the pole from below as shown in Figure 2.1 b. For $Im(\widetilde{\omega}) < 0$ we could, strictly speaking, perform the velocity integrals in (2.31) without any problem, since the integrand has no poles. However, this would not be an analytical continuation of the velocity integral. Therefore, the right contour in this case also encircles the pole as shown in Figure 2.1 c. We will refer to this way of deforming the integration contour in velocity space as the 'Landau prescription'. Now, when the transformed electric field is defined in the whole complex $\widetilde{\omega}$-plane (except at the points where $1 - \frac{1}{\widetilde{k}} \int_{-\infty}^{+\infty} \frac{1}{\widetilde{k}\widetilde{v}-\widetilde{\omega}} \frac{\partial \widetilde{f}_0(\widetilde{v})}{\partial \widetilde{v}} d\widetilde{v} = 0$), we can handle the inverse transformation of (2.31) in a more convenient way. Instead of performing the integration along a line that is parallel to the real line and crosses the imaginary axis in σ, we can now deform the integration contour by pushing it downwards by the value γ as shown in Figure 2.2 and by doing this the contour should still go around the poles from above.

A thorough mathematical analysis shows that for large times the dominant contribution to the electric field will come from the residues of $\widehat{\widetilde{E}}(\widetilde{k},\widetilde{\omega})e^{-i\widetilde{\omega}\widetilde{t}}$ when γ is large and the lines AB and CD are far away from the imaginary axis:

$$\widehat{\widetilde{E}}(\widetilde{k},\widetilde{t}) = \frac{1}{\sqrt{2\pi}} \int_{-\infty+i\sigma}^{+\infty+i\sigma} \widehat{\widetilde{E}}(\widetilde{k},\widetilde{\omega}) e^{-i\widetilde{\omega}\widetilde{t}} d\widetilde{\omega} \to -\sqrt{2\pi} i \sum Res\left(\widehat{\widetilde{E}}(\widetilde{k},\widetilde{\omega}) e^{-i\widetilde{\omega}\widetilde{t}}\right) \tag{2.32}$$

when $t \to +\infty$. Therefore it is crucial to determine the poles of $\widehat{\widetilde{E}}(\widetilde{k},\widetilde{\omega})$, i.e., the frequencies $\widetilde{\omega}_0$ for which the denominator of (2.31) is zero:

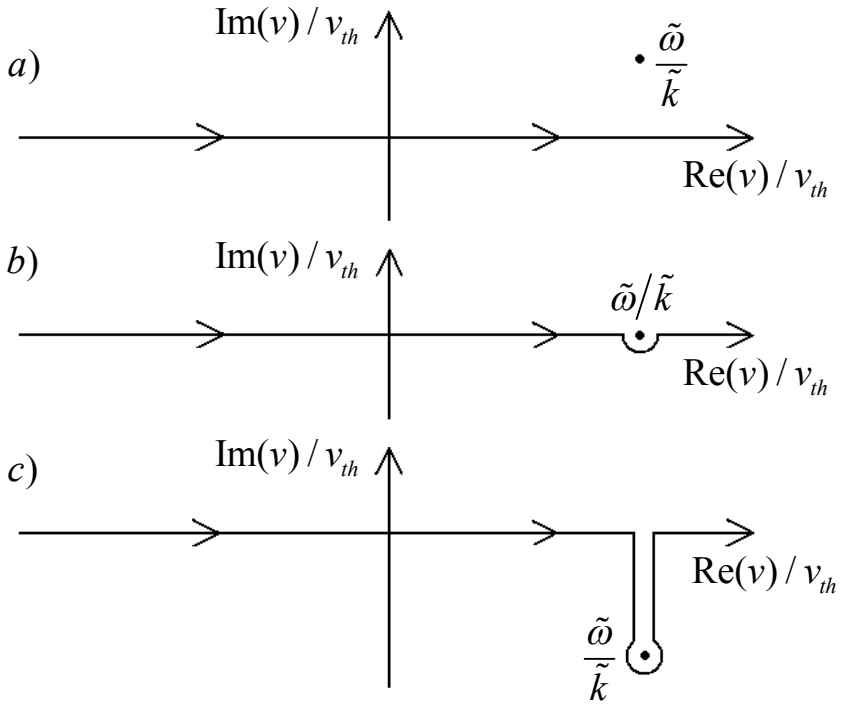

Figure 2.1: Landau contour for the analytical continuation.

$$1 - \frac{1}{\widetilde{k}^2} \int\limits_L \frac{1}{(\widetilde{v} - \widetilde{\omega}_0/\widetilde{k})} \frac{\partial \widetilde{f}_0}{\partial \widetilde{v}} d\widetilde{v} = 0. \tag{2.33}$$

Here, the L under the integral sign means that the integral is to be calculated along the 'Landau contour' as the analytic continuation of the integrals in (2.31) requires. In order to evaluate this expression explicitly, we need to know the function $f_0(v)$. Since the Maxwellian distribution corresponds to the state with the maximal entropy of the system, it is physically sound to assume that the equilibrium distribution of our system is also Maxwellian, i.e.,

$$f_0(v) = \frac{n_0}{\sqrt{2\pi k_B T_i/m_i}} \exp\left(-\frac{m_i v^2}{2k_B T_i}\right). \tag{2.34}$$

Using the normalization procedure outlined in (2.11), one easily sees that

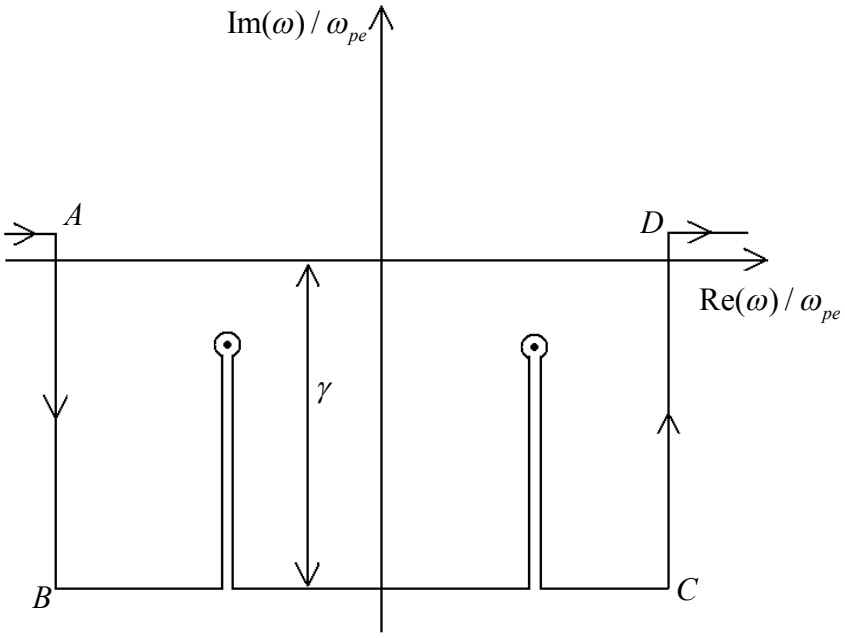

Figure 2.2: Path of integration for the analytic continuation of the electric field.

$$\widetilde{f}_0(\widetilde{v}) = \frac{1}{\sqrt{2\pi}} \exp\left(-\frac{1}{2}\widetilde{v}^2\right). \tag{2.35}$$

With this expression, equation (2.33) turns into

$$1 - \frac{1}{\sqrt{2\pi}\widetilde{k}^2} \int_L \frac{\widetilde{v} e^{-\widetilde{v}^2/2}}{(\widetilde{v} - \widetilde{\omega}_0/\widetilde{k})} d\widetilde{v} = 0 \ . \tag{2.36}$$

As outlined in the Appendix, the integral on the right-hand side can be expressed through the plasma dispersion function Z defined in [1] as:

$$\int_L \frac{\widetilde{v} e^{-\widetilde{v}^2/2}}{(\widetilde{v} - \widetilde{\omega}_0/\widetilde{k})} d\widetilde{v} = \sqrt{2\pi}\left(1 + \frac{\widetilde{\omega}_0}{\sqrt{2}\widetilde{k}} Z\left(\frac{\widetilde{\omega}_0}{\sqrt{2}\widetilde{k}}\right)\right). \tag{2.37}$$

Substituting this into (2.36) yields a dispersion relation of the form

$$1 + \widetilde{k}^2 + \frac{\widetilde{\omega}_0}{\sqrt{2}\widetilde{k}} Z\left(\frac{\widetilde{\omega}_0}{\sqrt{2}\widetilde{k}}\right) = 0 \ , \tag{2.38}$$

which is much easier to work with.

Basic properties of the dispersion relation

Before we evaluate (2.38) numerically, it is useful to analytically gain some insight into what the solutions of this equation look like. First, we define $x_0 := Re(\widetilde{\omega}_0)/(\sqrt{2}\widetilde{k})$ and $y_0 := Im(\widetilde{\omega}_0)/(\sqrt{2}\widetilde{k})$ and then split (2.38) into real and imaginary parts:

$$1 + \widetilde{k}^2 + x_0 ReZ(x_0, y_0) - y_0 ImZ(x_0, y_0) = 0 \tag{2.39}$$

$$x_0 ImZ(x_0, y_0) + y_0 ReZ(x_0, y_0) = 0. \tag{2.40}$$

Concerning the symmetry properties of Z, we know [1] that $ReZ(-x, y) = -ReZ(x, y)$ and $ImZ(-x, y) = ImZ(x, y)$. This means that if the pair (x_0, y_0) is a solution of the upper system of equations, so is the pair $(-x_0, y_0)$, i.e., the set of solutions of (2.38) is symmetric with respect to the imaginary $\widetilde{\omega}$-axis.
Next, we would like to prove analytically that (2.38) has only damped solutions, i.e., solutions that lie in the lower half of the complex $\widetilde{\omega}$-plane. At this point, one usually cites the Penrose criterion. However, for a Maxwellian equilibrium distribution there is also a straightforward proof of the non-existence of unstable or marginal solutions. First, we investigate if there are solutions on the real line (i.e., with $y_0 = 0$). In this case the last terms in (2.39) and (2.40) equal zero, so in (2.40) we are left with

$$x_0 \sqrt{\pi} e^{-x_0^2} = 0 \ ,$$

where we have used $ImZ(x, 0) = \sqrt{\pi} e^{-x^2}$ [1]. The upper equation has only one solution, namely $x_0 = 0$, but substituting this result in (2.39) leaves us with a left-hand side in the form $1 + \widetilde{k}^2$ that cannot equal zero, since $\widetilde{k}$ is real.
Now we consider the possibility that $x_0 = 0$, i.e., that there are solutions on the imaginary axis. In this case, (2.40) transforms into $y_0 ReZ(0, y_0) = 0$, which, however, gives us no condition, since $ReZ(0, y) \equiv 0$ for all y. We are thus left only with (2.39), which now reads $1 + \widetilde{k}^2 - y_0 ImZ(0, y_0) = 0$. For $y > 0$, we know that

$$y ImZ(0, y) = \frac{y^2}{\sqrt{\pi}} \int_{-\infty}^{+\infty} \frac{e^{t^2}}{t^2 + y^2} dt = \frac{1}{\sqrt{\pi}} \int_{-\infty}^{+\infty} \frac{e^{t^2}}{1 + \left(\frac{t}{y}\right)^2} dt < \frac{1}{\sqrt{\pi}} \int_{-\infty}^{+\infty} e^{t^2} dt = 1. \tag{2.41}$$

Since we have a strict inequality, we know that (for $x_0 = 0$ and $y_0 > 0$) the left-hand side of (2.39) is strictly positive, so there cannot be any solutions lying on the upper part of the imaginary $\widetilde{\omega}$-axis. Although our goal is merely to prove the non-existence of unstable solutions, for the sake of completeness, we also show that there are no solutions on the whole imaginary axis. If $x = 0$ and $y < 0$, we have that $Z(0, y) = Z^*(0, |y|) + 2i\sqrt{\pi} e^{y^2} = -iImZ(0, |y|) + 2i\sqrt{\pi} e^{y^2}$ [1]. From this it immediately follows that

$$\widetilde{k}^2 + 1 - y_0 ImZ(0, y_0) = \widetilde{k}^2 + \underbrace{1 - |y_0| ImZ(0, |y_0|)}_{>0} + 2\sqrt{\pi}|y_0|e^{|y_0|^2} > \\ > \widetilde{k}^2 + 2\sqrt{\pi}|y_0|e^{|y_0|^2} > 0. \quad (2.42)$$

Since we now know that there are no solutions on the axes and that the set of solutions is symmetric with respect to the imaginary $\widetilde{\omega}$-axis, it suffices to show that there are no solutions for $x_0 > 0$ and $y_0 > 0$ in order to prove the non-existence of unstable solutions. To do this, we recall the connection between the plasma dispersion function and its derivative, namely that $Z'(\xi) = -2(1+\xi Z(\xi))$ for all ξ [1]. Since Z is by definition an analytic function, we can write that

$$\frac{dZ(\xi)}{d\xi} = \frac{\partial ReZ(x,y)}{\partial x} + i\frac{\partial ImZ(x,y)}{\partial x} = \frac{\partial ImZ(x,y)}{\partial y} - i\frac{\partial ReZ(x,y)}{\partial y}. \quad (2.43)$$

Using these relations, one can rewrite (2.38) as

$$\frac{dZ(\xi)}{d\xi}|_{\xi=x_0+iy_0} = \frac{\partial ReZ(x,y_0)}{\partial x}|_{x=x_0} + i\frac{\partial ImZ(x,y_0)}{\partial x}|_{x=x_0} = 2\widetilde{k}^2. \quad (2.44)$$

Since the right-hand side of the last expression is real, a necessary condition for the existence of a solution is that the derivative of the imaginary part of Z with respect to x equals zero at the solution. For $y > 0$ $ImZ(x, y)$ reads as follows:

$$ImZ(x,y) = y\frac{1}{\sqrt{\pi}}\int_{-\infty}^{+\infty}\frac{e^{-t^2}}{(t-x)^2+y^2}dt. \quad (2.45)$$

A derivation of this relation is given in the Appendix. There we also prove that the integral commutes with a derivative with respect to x. Therefore, we can write that

$$\frac{\partial ImZ(x,y_0)}{\partial x}|_{x=x_0} = y_0\frac{2}{\sqrt{\pi}}\int_{-\infty}^{+\infty}\frac{(t-x_0)e^{-t^2}}{((t-x_0)^2+y_0^2)^2}dt. \quad (2.46)$$

Since we look for solutions in the area $\{y_0 > 0\}\bigcup\{x_0 > 0\}$, the last expression equals zero if and only if the integral part is zero, so we focus on this integral. A simple substitution $p := t - x$ leads to

$$\int_{-\infty}^{+\infty}\frac{(t-x_0)e^{-t^2}}{((t-x_0)^2+y_0^2)^2}dt = -e^{x_0^2}\int_0^{+\infty}\frac{pe^{-p^2}e^{2px_0}}{(p^2+y_0^2)^2} + e^{x_0^2}\int_0^{+\infty}\frac{pe^{-p^2}e^{-2px_0}}{(p^2+y_0^2)^2} = \\ = -2e^{-x_0^2}\int_0^{+\infty}\frac{pe^{-p^2}\sinh(2px_0)}{(p^2+y_0^2)^2}dp. \quad (2.47)$$

Looking at the last integral in (2.47), it is immediately clear that for $x_0 > 0$ the integrand is almost everywhere positive. Therefore, the partial derivative of $ImZ(x, y)$ with respect to x is negative in the second quadrant of the complex $\widetilde{\omega}$-plane. By this we have proved that there exist no unstable (and even no marginal, i.e., $Im\widetilde{\omega}_0 = 0$) solutions of (2.38).

Numerical solutions of the dispersion relation

Now we can focus on the implementation of this equation and solve it numerically. At first sight (2.38) looks simple, but the left-hand side is a complex valued function that takes also complex numbers as arguments, i.e., a full plot of the behaviour of this function will be four-dimensional, and thus difficult to work with. A way to simplify the problem without making any approximations is to note that (2.38) is true if and only if

$$\left| 1 + \widetilde{k}^2 + \frac{\widetilde{\omega}_0}{\sqrt{2\widetilde{k}}} Z\left(\frac{\widetilde{\omega}_0}{\sqrt{2\widetilde{k}}} \right) \right| = 0 \ . \tag{2.48}$$

On the left-hand side we now have a function that maps $\mathbb{C}$ onto $\mathbb{R}$, so the space of arguments and values of this function is three-dimensional. Since also the left hand side of (2.48) is by definition non-negative, the solutions of this equation will be the points where the surface defined by this function touches the complex $\widetilde{\omega}$-plane. A convenient way to find those points is to draw a contour plot in the $\widetilde{\omega}$-plane for some value of the parameter $\widetilde{k}$ (here $\widetilde{k} = 0.5$) as shown in Figure 2.3. This plot is produced using MATLAB, version R2009b, with the program *landau.m*, the code of which is shown in the Appendix. The left-hand side of (2.48) was evaluated on a quadratic grid in the $\widetilde{\omega}$-plane with the resolution of $\Delta\widetilde{\omega} = 0.001$ while the contours are drawn on equidistant 'heights' from 0 to 0.02 in steps of 0.001. One sees that all solutions lie in the lower part of the $\widetilde{\omega}$-plane, which in our notation corresponds to damping, as had to be expected in this simplified model of homogeneous plasma. Since these solutions are the poles of (2.31), they are going to determine the long time behaviour of the electric field produced by the perturbation $f_1(z, v, t)$, i.e., the electric field will decay exponentially and for $t \to \infty$ only the least damped solutions (closest to the real axis) will be important. This phenomenon is usually called 'Landau damping'. One also sees the symmetry of the solutions with respect to the imaginary axis which we derived analytically.

2.3 Van Kampen approach

In the literature, there is also another approach for solving (2.16) which is due to Van Kampen [12]. With this method, one looks for stationary solutions. Here, we are not going to follow all the steps described in [12]. Instead, we merely outline the ideas that lead to the result of Van Kampen and set the scene for the numerical computations to follow. In order to solve (2.16), we do a Fourier transformation of the equation in time,

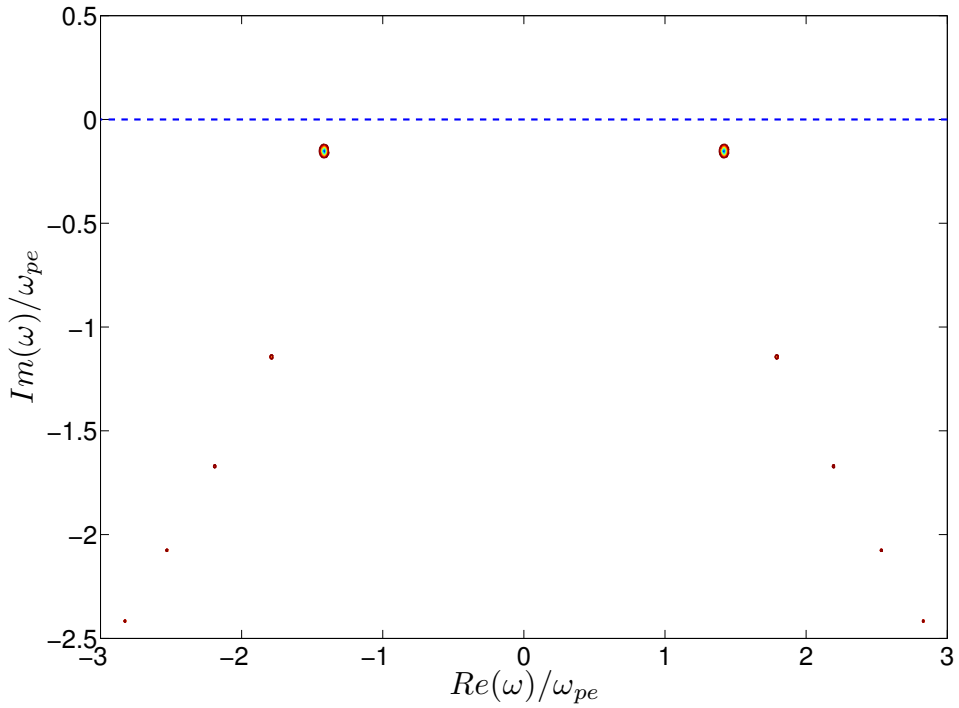

Figure 2.3: Landau solutions for $\widetilde{k} = 0.5$.

$$\widehat{\widetilde{f}}_1(\widetilde{k},\widetilde{v},\widetilde{\omega}) = \frac{1}{\sqrt{2\pi}} \int_{-\infty}^{+\infty} \widehat{\widetilde{f}}_1(\widetilde{k},\widetilde{v},\widetilde{t}) e^{i\widetilde{\omega}\widetilde{t}} d\widetilde{t} \; . \tag{2.49}$$

This definition is similar to (2.27)[1], which will make the comparison between the results of the two approaches easier. Applying this transformation on (2.16) gives

$$\widetilde{\omega}\widehat{\widetilde{f}}_1(\widetilde{k},\widetilde{v},\widetilde{\omega}) = \widetilde{k}\widetilde{v}\widehat{\widetilde{f}}_1(\widetilde{k},\widetilde{v},\widetilde{\omega}) - \frac{1}{\widetilde{k}}\frac{\partial \widetilde{f}_0}{\partial \widetilde{v}} \int_{-\infty}^{+\infty} \widehat{\widetilde{f}}_1(\widetilde{k},\widetilde{v},\widetilde{\omega}) d\widetilde{v}. \tag{2.50}$$

This is an integral equation for $\widehat{\widetilde{f}}_1(\widetilde{k},\widetilde{v},\widetilde{\omega})$, whose general solution is, as Van Kampen showed,

$$\widehat{\widetilde{f}}_{1,V}(\widetilde{k},\widetilde{v},\widetilde{\omega}) = p.v. \left(\frac{1}{\widetilde{k}} \frac{\partial \widetilde{f}_0(\widetilde{v})/\partial \widetilde{v}}{\widetilde{k}\widetilde{v} - \widetilde{\omega}} \right) + \delta(\widetilde{k}\widetilde{v} - \widetilde{\omega}) \left(\widetilde{k} - p.v. \int_{-\infty}^{+\infty} \frac{1}{\widetilde{k}\widetilde{v}' - \widetilde{\omega}} \frac{\partial \widetilde{f}_0(\widetilde{v}')}{\partial \widetilde{v}'} d\widetilde{v}' \right) , \tag{2.51}$$

[1] In this convention a negative imaginary part of $\widetilde{\omega}$ also corresponds to damping.

where δ denotes the Dirac delta function. One can verify that this solves (2.50) by explicitly substituting (2.51) into the equation. A subtlety one should account for is that $x\delta(x) = 0$, which follows from the theory of distributions. *p.v.* in front of the integral in (2.51) indicates that one should take the Cauchy principal value of the integral. There is also the abbreviation *p.v.* in front of the first expression in (2.51). It merely denotes that, if one happens to integrate this expression over $\widetilde{k}$, $\widetilde{v}$ or $\widetilde{\omega}$, the Cauchy principal value of the integral should be taken, but it does not influence algebraic manipulations. Clearly, for every real $\widetilde{\omega}$ there is a solution of (2.50) (a Case-Van Kampen mode), so the spectrum of frequencies, that the Van Kampen approach gives, is the whole real axis.
The Van Kampen modes are singular functions that do not represent a physically meaningful perturbation. Therefore, to study the time dependence of a physical initial perturbation, one should consider a superposition of uncountably infinitely many Van Kampen modes and then take their inverse Fourier transform with respect to time, i.e.,

$$\widehat{\widetilde{f}}_1(\widetilde{k},\widetilde{v},\widetilde{t}) = \int_{-\infty}^{+\infty} q(\widetilde{k},\widetilde{\omega})\,\widehat{\widetilde{f}}_{1,V}(\widetilde{k},\widetilde{v},\widetilde{\omega})\,e^{-i\widetilde{\omega}\widetilde{t}}\,d\widetilde{\omega}\ , \tag{2.52}$$

where the function $q(\widetilde{k},\widetilde{\omega})$ is chosen such that $\widehat{\widetilde{f}}_1$ fulfils the conditions discussed in more detail in chapter 3. After substituting (2.51) into the last expression, two integrals emerge. The first one reads

$$p.v.\int_{-\infty}^{+\infty} \frac{q(\widetilde{k},\widetilde{\omega})\,e^{-i\widetilde{\omega}\widetilde{t}}}{\widetilde{k}\widetilde{v}-\widetilde{\omega}}\,d\widetilde{\omega} = -e^{-i\widetilde{k}\widetilde{v}\widetilde{t}}\,p.v.\int_{-\infty}^{+\infty} \frac{q(\widetilde{k},\widetilde{k}\widetilde{v}-x)\,e^{ix\widetilde{t}}}{x}\,dx\ . \tag{2.53}$$

The integral on the right-hand side looks rather general, but for a large class of functions q one can show that it does not depend on time. We assume that $q(\widetilde{k},\widetilde{k}\widetilde{v}-x)$ has no singularities along the x-axis. In the case of an initial value problem, one considers the evolution of a perturbation whose value is prescribed at $t = 0$. Since we are interested in its behaviour for $t > 0$, we take an analytical continuation of q in the upper half of the complex plane and also demand that q does not increase faster than some polynomial of $|x|$ for $|x| \to \infty$. In this case, the integrands in (2.53) have at most one pole along the integration path. For evaluating the principal value integral we close the contour of integration by a semi-circle C_R of radius R in the upper half of the complex plane. The pole at $x = 0$ is circumvented from above by a semi-circle of an infinitesimal radius. Now, one can write

$$\oint \frac{q(\widetilde{k},\widetilde{k}\widetilde{v}-x)\,e^{ix\widetilde{t}}}{x}\,dx = p.v.\int_{-\infty}^{+\infty} \frac{q(\widetilde{k},\widetilde{k}\widetilde{v}-x)\,e^{ix\widetilde{t}}}{x}dx - i\pi Res\left(\frac{q(\widetilde{k},\widetilde{k}\widetilde{v}-x)\,e^{ix\widetilde{t}}}{x}\right)\Big|_{x=0} + \\ + \lim_{R\to\infty}\int_{C_R} \frac{q(\widetilde{k},\widetilde{k}\widetilde{v}-x)\,e^{ix\widetilde{t}}}{x}\,dx\ . \tag{2.54}$$

Since the integrand on the left-hand side is taken to be analytic in the upper half of the complex plane, the integration along the closed path we have chosen gives zero. The semi-circle C_R is parametrized as follows: $x = R\cos\phi + iR\sin\phi$; $\phi \in [0, \pi]$. Recalling that, if q goes to infinity for large R, it is not faster than some power of R, it immediately follows that the contribution from the semi-circle is zero, i.e.,

$$\int\limits_{C_R} \frac{q(\widetilde{k}, \widetilde{k}\widetilde{v} - x)\, e^{ix\widetilde{t}}}{x}\, dx = i \int\limits_0^{\pi} q(\widetilde{k}, \widetilde{k}\widetilde{v} - x)\, e^{iR\cos\phi\widetilde{t}}\, e^{-R\sin\phi\widetilde{t}}\, d\phi \sim R^N e^{-R} \to 0 \text{ for } R \to +\infty \ . \tag{2.55}$$

The second integral that emerges after a substitution of (2.51) into (2.52) involves a delta function and is therefore trivial. Taking this into account, as well as the fact that $Res(q(\widetilde{k}, \widetilde{k}\widetilde{v} - x)e^{ix\widetilde{t}}/x)|_{x=0} = q(\widetilde{k}, \widetilde{k}\widetilde{v})$, the entire expression for $\widehat{\widetilde{f}}_1(\widetilde{k}, \widetilde{v}, \widetilde{t})$ reads

$$\widehat{\widetilde{f}}_1(\widetilde{k}, \widetilde{v}, \widetilde{t}) = q(\widetilde{k}, \widetilde{k}\widetilde{v}) \left(-i\pi \frac{1}{\widetilde{k}} \frac{\partial \widetilde{f}_0(\widetilde{v})}{\partial \widetilde{v}} + \widetilde{k} - \right.$$
$$\left. - p.v. \int\limits_{-\infty}^{+\infty} \frac{1}{\widetilde{k}(\widetilde{v}' - \widetilde{v})} \frac{\partial \widetilde{f}_0(\widetilde{v}')}{\partial \widetilde{v}'} d\widetilde{v}' \right) e^{-i\widetilde{k}\widetilde{v}\widetilde{t}} =: g(\widetilde{k}, \widetilde{v})\, e^{-i\widetilde{k}\widetilde{v}\widetilde{t}} \ . \tag{2.56}$$

This shows explicitly that the entire time dependence of $\widehat{\widetilde{f}}_1(\widetilde{k}, \widetilde{v}, \widetilde{t})$ (and therefore also of $f_1(z, v, t)$) is in the exponential factor $e^{-i\widetilde{k}\widetilde{v}\widetilde{t}}$. Since $\widetilde{k}$, $\widetilde{v}$ and $\widetilde{t}$ are real variables, it is clear that this factor represents just oscillating behaviour in time with no growth or decay. We also make another observation in order to facilitate future comparison. Let us view $\widetilde{k}$ as a fixed parameter and look at this exponential factor at a given time $\widetilde{t}_0$. Now we study the behaviour of the real part[2] of the exponential factor in velocity space. This is a cosine function with $\widetilde{k}\widetilde{v}\widetilde{t}_0$ as an argument. Since the values of the cosine repeat when its argument equals $n2\pi$ where $n \in \mathbb{N}$, the same structure in velocity space will repeat after an interval of $\Delta\widetilde{v} = \frac{2\pi}{\widetilde{k}\widetilde{t}_0}$. If we make the same analysis at a later time, say $\widetilde{t} = \widetilde{t}_1 > \widetilde{t}_0$, the corresponding $\Delta\widetilde{v}$ will be even smaller, i.e., the oscillation of $\widehat{\widetilde{f}}_1$ with respect to velocity becomes more and more rapid with time. This allows us to make a statement about the Fourier transform in space of the electric field which by definition is an integral of $\widehat{\widetilde{f}}_1(\widetilde{k}, \widetilde{v}, \widetilde{t})$ over velocity, i.e.,

$$\widehat{\widetilde{E}}(\widetilde{k}, \widetilde{t}) = \frac{i}{\widetilde{k}} \int\limits_{-\infty}^{+\infty} g(\widetilde{k}, \widetilde{v})\, e^{-i\widetilde{k}\widetilde{v}\widetilde{t}}\, d\widetilde{v} \to 0 \text{ as } \widetilde{t} \to +\infty \ . \tag{2.57}$$

[2]The same conclusions also apply to the imaginary part.

The above result concerning the behaviour of the electric field in the limit for large t is a consequence of the Riemann-Lebesgue lemma. In order that this lemma can be applied in the present case, the function $g(\widetilde{k},\widetilde{v})$ should be absolutely integrable with respect to velocity. We choose q in such a way that this is true. Bearing in mind that $\widetilde{k}$, $\widetilde{v}$ and $\widetilde{t}$ are real, it can easily be seen that

$$\int_{-\infty}^{+\infty} |g(\widetilde{k},\widetilde{v})|\, d\widetilde{v} = \int_{-\infty}^{+\infty} |\widehat{\widetilde{f}}_1(\widetilde{k},\widetilde{v},\widetilde{\omega})\, e^{i\widetilde{k}\widetilde{v}\widetilde{t}}|\, d\widetilde{v} = \int_{-\infty}^{+\infty} |\widehat{\widetilde{f}}_1(\widetilde{k},\widetilde{v},\widetilde{\omega})|\, d\widetilde{v}\ . \tag{2.58}$$

In the next chapter, we will discuss in more detail the functional space to which $\widehat{\widetilde{f}}_1$ should belong in order that the above integral is finite and that the same applies also to all its velocity moments. This inevitably imposes similar conditions on q. Since in the Van Kampen approach there are only modes with real frequencies, (2.57) might look surprising at first sight. This time limit becomes intuitive if one views the integral over velocity in (2.57) as the surface enclosed under the integrand. If g is a continuous function with respect to velocity, which is a reasonable physical condition, the integrand becomes more oscillatory when time evolves and the variation of g during one period gets smaller, so the cancellation between the areas above and below the real axis becomes more accurate. The limit process in (2.57) is what one usually identifies with 'linear Landau damping' and is reproduced also by the Van Kampen method.

At first sight, it might look like the two approaches presented in this and the previous subsection, both solving (2.16) in a mathematically consistent way, lead to different results. However, this is not the case. It is important to note that Landau solved the initial value problem for the electric field which, in Fourier space, is proportional the 0th velocity moment of the distribution function, and there are uncountably infinitely many different distribution functions that give the same electric field after integration. On the other hand, Van Kampen solved (2.16) for the distribution function. Therefore, his result in terms of eigenfrequencies should not be directly compared to the Landau solutions. One first has to integrate over velocity in order to gain the electric field and, as we saw in (2.57), this electric field is damped also when using the Van Kampen solutions. In the literature, the integration over velocity is usually referred to as 'phase mixing'. This is due to the fact that for every fixed velocity, the integrand in (2.57) represents a harmonic oscillator. The velocity integration is the mathematical analogue to mixing uncountably infinitely many such oscillators where each of them has a different frequency.

Chapter 3

Mathematical considerations

One can view (2.50) as an integral equation determining $\widehat{\widetilde{f_1}}$. Solutions for this equation are the Case-Van Kampen modes which involve a delta function in velocity space. However, in this subsection we view (2.50) as an eigenvalue equation where the right-hand side is a linear operator acting on the Fourier transform of the perturbation $\widetilde{f_1}$. It should be clarified that these are merely two different perspectives and the solutions that arise in this way should be the same if one defines the operator appropriately. Since we are only interested in the eigenvalues of this operator, we are going to suppress for simplicity all unnecessary symbols accompanying $\widehat{\widetilde{f_1}}$ and also all arguments except v. The linear operator A, whose eigenvalues we want to find, is defined through its action on the perturbation of the electron distribution function, i.e., the right hand side of (2.50):

$$(Af)(v) := kvf(v) + \psi(v) \int_{-\infty}^{+\infty} f(v')dv' \tag{3.1}$$

where for the sake of generality we have written $\psi(v)$ in front of the integral. In the case of Langmuir waves, $\psi(v) = -\frac{1}{k}\frac{\partial f_0(v)}{\partial v}$. For a linear operator like A, we need not only a linear prescription like (3.1) that defines the action on a given function, but also the functional domain on which this operator is defined. The function f is the perturbation of the distribution function. From a physical point of view, one can impose on it the condition that all its velocity moments are finite, i.e.,

$$\left| \int_{-\infty}^{+\infty} v^n f(v)dv \right| < \infty \text{ for every } n \in \mathbb{N}_0. \tag{3.2}$$

This condition is fulfilled for every function in the Schwartz space S which, said figuratively, is defined as the functional space of all rapidly falling functions of a real argument that are infinitely many times continuously differentiable. However, for simplicity we take as a domain of definition of A, i.e. $D(A)$, the space

$$H := \{f(v) \in L^2 | vf(v) \in L^2\}. \tag{3.3}$$

As we will show in this chapter, for the functions in H one can only say with certainty that their 0th velocity moment is finite, i.e., the operator A be well defined. This is sufficient, since in this work we are not going to encounter any higher moments of f. It is also noteworthy that the Schwartz space is dense in H, i.e, S is a subspace of H and for every given function $f \in H$ there exist a sequence of functions $\{g_n\} \in S$ such that $\|g_n - f\| \to 0$. In other words, every function in H can be approximated with an arbitrary accuracy with a function in S. If we have defined the domain of A as S, then this would not have changed the important results of this chapter. It is useful to choose as a domain of A a Hilbert space. Neither S nor H are Hilbert spaces when equipped with the usual scalar product in L^2. However, with a new scalar product $\langle \cdot, \cdot \rangle_H$, defined as

$$\langle f, g \rangle_H := \int_{-\infty}^{+\infty} \overline{f(v)}(1 + |v|)^2 g(v) dv, \tag{3.4}$$

where $f, g \in H$, the space H can be turned into a Hilbert space.
In order that the operator A is well defined, the right-hand side of (3.1) (more precisely the integral) has to be finite for any f in the domain of A. This can be easily verified as follows:

$$\begin{aligned}\left| \int_{-\infty}^{+\infty} f(v) dv \right| &= \left| \int_{-\infty}^{+\infty} f(v) \frac{(1 + |v|)}{1 + |v|} dv \right| = \left| \left\langle (1 + |v|) f(v), \frac{1}{1 + |v|} \right\rangle_{L^2} \right| \leq \\ &\leq \|(1 + |v|) f(v)\|_{L^2} \cdot \underbrace{\| \frac{1}{1 + |v|} \|_{L^2}}_{=\sqrt{2}} = \sqrt{2} \|f(v) + |v| f(v)\|_{L^2} \leq \\ &\leq \sqrt{2} \|f(v)\|_{L^2} + \sqrt{2} \||v| f(v)\|_{L^2} < \infty. \end{aligned} \tag{3.5}$$

In the course of this work, we will see that the function $\psi(v)$ will always be a Gauss function times some polynomial which means that for the purpose of this work $\psi \in H$. In this case, the range of A is L^2, i.e.,

$$A : H \to L^2. \tag{3.6}$$

So far, we have only made some plausible definitions in order to express a physical problem in a more mathematical fashion, but we have not gained any further understanding. However, this more rigorous formulation of the problem will soon allow us to utilize some theorems from operator theory in order to make a more precise statement about the spectrum of A. First, one should note that A is a sum of two parts, A_0 and C, which we define as

$$(A_0 f)(v) := kvf(v) \quad ; \quad (Cf)(v) := \psi(v) \int_{-\infty}^{+\infty} f(v')dv'. \tag{3.7}$$

The domain of both operators we set as H. It is immediately seen that A_0 is (up to the real parameter k which is qualitatively not important) just a multiplication operator by v. A_0 is equivalent to the position operator in quantum mechanics which has been thoroughly studied. Defined as a map from H onto L^2, as in this case, it is known to be self-adjoint and to have only an essential[1] spectrum that consists of the entire real axis, i.e., $\sigma_{ess}(A) = \mathbb{R}$. Now we focus our attention on the second term, namely on C. From the definition of C, it is clear that this operator maps every function $f \in H$ to a function that is proportional to ψ where only the proportionality factor (in this case an integral over f which, for ease of notation, we will denote as γ_f) depends on f. In other words, C maps an infinite dimensional Hilbert space onto a finite dimensional space which is a subspace of L^2. Another important property of C is that it is a bounded operator which can be easily seen as follows. First, note that

$$\|Cf\|_{L^2} = \sqrt{\langle Cf, Cf\rangle_{L^2}} = |\gamma_f| \cdot \|\psi\|_{L^2}. \tag{3.8}$$

Recalling (3.5), we have

$$|\gamma_f| \leq \sqrt{2}\|(1+|v|)f(v)\|_{L^2} = \sqrt{2}\|f\|_H \tag{3.9}$$

which leads to

$$\frac{\|Cf\|_{L^2}}{\|f\|_H} = \frac{|\gamma_f| \cdot \|\psi\|_{L^2}}{\|f\|_H} \leq \frac{\sqrt{2}\|f\|_H \cdot \|\psi\|_{L^2}}{\|f\|_H} = \sqrt{2}\|\psi\|_{L^2} < \infty. \tag{3.10}$$

Since C is a bounded operator with a finite dimensional range, it follows that C is compact. We can now use this knowledge in order to apply a theorem due to Weyl [6, p. 113, Corollary 2] which in terms of our notation states the following:

Let A_0 be a self-adjoint operator and let C be a relative compact perturbation of A_0. Then:
a) $A = A_0 + C$ defined with $D(A) = D(A_0)$ is a closed operator.
b) If C is symmetric, A is self-adjoint.
c) $\sigma_{ess}(A) = \sigma_{ess}(A_0)$.

Thus, A also has an essential spectrum consisting of the entire real axis. The mathematical domain of definition for A, which we chose, reproduces the physical result. However, the aforementioned theorem does not state that this is the whole spectrum of A. It is possible, and here this is also the case, as we shall see, that the perturbation C has created some isolated eigenvalues. In order to show this, we have to determine the complete spectrum

[1] In this chapter we will often make use of the term 'essential' regarding the description of some part of a spectrum. In physics one usually calls this 'continuous' spectrum.

of the operator. It is noteworthy that, in our case, the operator C is indeed compact, but it is not symmetric with respect to the scalar products $\langle\cdot,\cdot\rangle_H$ or $\langle\cdot,\cdot\rangle_{L^2}$. Therefore, the operator A is not self-adjoint.
A convenient way to find the eigenvalues ω of A would be first to find the resolvent of $A-\omega$ and then to search for its poles. (More precisely, we should not speak about eigenvalues but rather about points of the spectrum, which is defined as the complement of the resolvent set. It can be, for example, that an operator has a non-empty spectrum but no eigenvalues in the mathematical sense of this word. However, from a physical point of view it is convenient to call every, in general complex, number ω that satisfies the equation $Af_\omega = \omega f_\omega$ an eigenvalue of A although this is an abuse of mathematical ideas.) One way to do that is to take the equation

$$\left((A-\omega)\,f\right)(v) = h(v), \tag{3.11}$$

where $h(v)$ is given and to try to solve it for $f(v)$. Using the definition of A, we find that

$$f(v) = \frac{h(v)}{kv-\omega} - \gamma_f \frac{\psi(v)}{kv-\omega}. \tag{3.12}$$

Integrating (3.12) over velocity space gives us an expression for γ_f which consists only of known functions. Substituting this expression into (3.12), we arrive at

$$f(v) = \frac{h(v)}{kv-\omega} - \frac{\psi(v)}{kv-\omega}\cdot\frac{1}{1+\int_{-\infty}^{+\infty}\frac{\psi(v')}{kv'-\omega}dv'}\int_{-\infty}^{+\infty}\frac{h(v')}{kv'-\omega}dv'. \tag{3.13}$$

One could view the right-hand side of (3.13) also as a linear operator acting on $h(v)$, namely as

$$f(v) = \left(R(\omega,A)h\right)(v), \tag{3.14}$$

where the operator $R(\omega,A)$ is the resolvent of $A-\omega$ and is given explicitly by

$$R(\omega,A) = \frac{1}{kv-\omega} - \frac{\psi(v)}{kv-\omega}\frac{1}{\left(1+\int_{-\infty}^{+\infty}\frac{\psi(v')}{kv'-\omega}dv'\right)}\int_{-\infty}^{+\infty}\frac{dv'}{kv'-\omega}. \tag{3.15}$$

Since k and v are real numbers, it is immediately clear that $R(\omega,A)$ has a pole for every real number. This is the essential spectrum of A, which corresponds to the solution of Van Kampen and also emerges in our mathematical analysis of A. However, from (3.15) one easily sees that this is not the entire spectrum, since $R(A-\omega,A)$ also has poles for frequencies which satisfy the relation

$$1+\int_{-\infty}^{+\infty}\frac{\psi(v)}{kv-\omega}dv = 0 \tag{3.16}$$

and which we will denote by ω_0. It is noteworthy that the pole in the integrand in the above expression makes it ambiguous. For the integral to have a definite value, it has to be specified how this pole is treated, and later on we will see that different treatments can yield completely different results.
One can easily verify by substitution that the eigenfunctions $f_\omega(v)$ of the operator A have the form

$$f_\omega(v) = -\frac{\psi(v)}{kv-\omega} + k\delta(kv-\omega)\left(1 + p.v.\int_{-\infty}^{+\infty}\frac{\psi(v)}{kv-\omega}dv\right). \tag{3.17}$$

In the case of a Maxwellian equilibrium distribution, this gives the same result as (2.51). Another observation that is straightforward to make is that, if $\psi(v)$ is an odd function, then the spectrum is symmetric with respect to zero, and for the corresponding eigenfunctions we have that $f_{-\omega}(v) = f_\omega(-v)$. At first sight, it might look disturbing that the eigenfunctions (3.17) do not belong to the functional space H which we used as a domain of A. However, since the functions $f_\omega(v)$ are integrable, we can technically apply A on them. Actually, this is a common situation in mathematics. For instance, the Laplace operator is usually defined as a quadratic form on the first Sobolev space, which is also dense in L^2, but its eigenfunctions are the plane waves that do not belong to L^2. Nevertheless, they are infinitely many times continuously differentiable and the Laplace operator can, technically, be applied on them. The situation with the operator A is completely analogous. Naively, one might have expected that the eigenfunctions $f_\omega(v)$ involve a delta function in velocity space. This comes from the fact that the Fourier transform with respect to velocity of the operator A_0 is proportional to the momentum operator known from quantum mechanics. The eigenfunctions of the momentum operator are the plane waves, and the inverse Fourier transform of a plane wave is a delta function. Of course, an arbitrary operator C added to A_0 could have altered the eigenfunctions profoundly, but in our case the influence of C on the eigenfunctions is merely change of the constant in front of the delta function (corresponding to the amplitude of the plane wave) and the addition of the first term in (3.17).

Next we would like to say something more about the solutions ω_0 in the case of Langmuir waves. For this we recall that $\psi(v) = -\frac{1}{k}\frac{\partial f_0(v)}{\partial v}$. As an equilibrium distribution function we take a centred normalized Maxwellian distribution which is given by

$$f_0(v) = \frac{1}{\sqrt{2\pi}}e^{-\frac{1}{2}v^2}. \tag{3.18}$$

Taking this into account and introducing the new variable a_0 defined as $a_0 := \omega_0/(\sqrt{2}k)$, we arrive at the equation

$$1 + \frac{1}{\sqrt{\pi}k^2}\int_{-\infty}^{+\infty}\frac{xe^{-x^2}}{x-a_0}dx = 0 \tag{3.19}$$

where the new integration variable x is related to the velocity via $x = v/\sqrt{2}$. The problem with this integral is that its value is ambiguous if $Im(a_0) = 0$, since in this case there is a pole on the integration path for $x = Re(a_0)$ and the value of the integral depends on how we treat this pole. One option, which corresponds to the solution of Van Kampen, would be to take the Cauchy principal value (denoted in this thesis by $p.v.$ in front of the integral). We will show in the rest of this subsection that this treatment of the pole leads to solutions of (3.19) which are real.
First, we divide a_0 into real and imaginary parts as $a_0 = Re(a_0) + iIm(a_0) =: a_{0r} + ia_{0i}$. This allows us to split also the integral $\int_{-\infty}^{+\infty} \frac{xe^{-x^2}}{x-a_0} dx$, which one can view as a complex valued function of a_0, into a real and an imaginary part. Substituting this result in (3.19), gives us the following system of two equations

$$1 + \frac{1}{\sqrt{\pi}k^2} p.v. \int_{-\infty}^{+\infty} \frac{x(x-a_{0r})e^{-x^2}}{(x-a_{0r})^2 + a_{0i}^2} dx = 0 \tag{3.20}$$

$$\frac{1}{\sqrt{\pi}k^2} a_{0i} p.v. \int_{-\infty}^{+\infty} \frac{xe^{-x^2}}{(x-a_{0r})^2 + a_{0i}^2} dx = 0. \tag{3.21}$$

If $a_{0i} \neq 0$, the notation $p.v.$ can, of course, be omitted, since there is no ambiguity regarding the value of the integral. However, we will keep it for convenience. There are three cases in which the second equation is satisfied: $a_{0i} = 0$, the integral is zero, or both a_{0i} and the integral equal zero. Since the third case is fulfilled if and only if the other two are, it suffices to consider only the first two cases.

Case 1: $a_{0i} = 0$
If this is the case, then we have only real solutions which was what we wanted to prove.

Case 2: $p.v. \int_{-\infty}^{+\infty} \frac{xe^{-x^2}}{(x-a_{0r})^2+a_{0i}^2} dx = 0$
Substituting this relation into the first equation of system (3.20) leads to

$$1 + \frac{1}{\sqrt{\pi}k^2} \int_{-\infty}^{+\infty} \frac{x^2 e^{-x^2}}{(x-a_{0r})^2 + a_{0i}^2} dx = 0. \tag{3.22}$$

The integral which appears in (3.22) is clearly positive, so (3.22) has no solutions (k is real by definition), i.e., the condition that determines **Case 2** is never fulfilled.
However, the system of equations (3.20), whose solution is by definition a_0, must hold which means that $a_{0i} = 0$, i.e., $a_0 \in \mathbb{R}$.
Since we now know that (3.19) has only real solutions, we can easily show that $\omega_{0r} p.v. \int_{-\infty}^{+\infty} \frac{e^{-x^2}}{x-\omega_{0r}/(\sqrt{2}k)} dx$ is an even function of ω_{0r} which means that, if ω_{0r} is a solution of

$$-\frac{\omega_{0r}}{\sqrt{2}k}\frac{1}{\sqrt{\pi}}p.v.\int_{-\infty}^{+\infty}\frac{e^{-x^2}}{x-\frac{\omega_{0r}}{\sqrt{2}k}}dx = 1+k^2, \tag{3.23}$$

then so is $-\omega_{0r}$. ((3.23) is equivalent to (3.19).) For a real argument, like in this case, one can easily show that the integral in the upper equation is proportional to the real part of the plasma dispersion function and the whole left hand side reads $aReZ(a)$, where a is defined as $a := \omega/(2k)$. Since a is real, $aReZ(a)$ is a real valued function and this allows us to easily plot the left-hand side of (3.23), as done in Figure 3.1. The solutions a_{0r}, that are proportional to ω_{0r}, are the values of the argument for which the function crosses the horizontal line given by $1+k^2$. The solid blue line represents the left-hand side of (3.23), and the red dashed line stands for its right hand side. It is evident that the number of solutions (i.e., discrete eigenvalues of A in the case of Langmuir waves) depends on the value of $\widetilde{k}$. Since k is real and non-zero (finite length scales), the left-hand side of (3.23) is always bigger than 1. One sees also that the blue line approaches asymptotically 1 when $\omega \to \pm\infty$. This means that for small k there are four solutions of (3.23), i.e., discrete Van Kampen eigenvalues, each with multiplicity 1. When the dashed line touches the two maxima of the blue curve (approximately for $k = 0.534$), we have only two discrete Van Kampen eigenvalues but each with multiplicity 2. For k bigger than this critical value there are no solutions of (3.23) and the whole Van Kampen spectrum is continuous.

Since the result of Van Kampen, who derived a continuous spectrum of A along the entire real line, has been well known for decades, one could wonder if it was necessary to look on the problem from the perspective of operator theory. The different prospective that we chose has some advantages which should be discussed here. First, in our opinion it is always preferable to formulate the problem in a mathematically rigorous way, which we did by defining the operator and thus its eigenvalue equation on a physically reasonable domain. Second, it should be noted that this gave us not just more certainty in the correctness of the results derived but also the opportunity to gain further insights into the problem. Now we know for sure that the whole spectrum of A is not continuous but that it can also have some discrete part consisting of isolated eigenvalues. In the last part of this subsection we showed that in the case of spatially homogeneous plasma with constant temperature these discrete eigenvalues also lie on the real axis and therefore usually remain unnoticed in a numerical evaluation as in chapter 4. However, this part of the spectrum will appear to be of great importance in further parts of this work. For example, instabilities can arise in the case of a background distribution $f_0(v)$ that is not Maxwellian (like the so called 'bump-on-tail' distribution) or in the presence of temperature gradients. We will see that in such cases only isolated frequencies do not lie on the real axis and, apart from these exceptions, the rest of the eigenvalues are real. Observing these numerical results, an important question arises: If the whole Van Kampen spectrum were continuous, then how could a continuous change of some parameters (for example, varying the temperature gradient from zero to some small value) alter the spectrum in such a non-continuous way, i.e., that only finitely

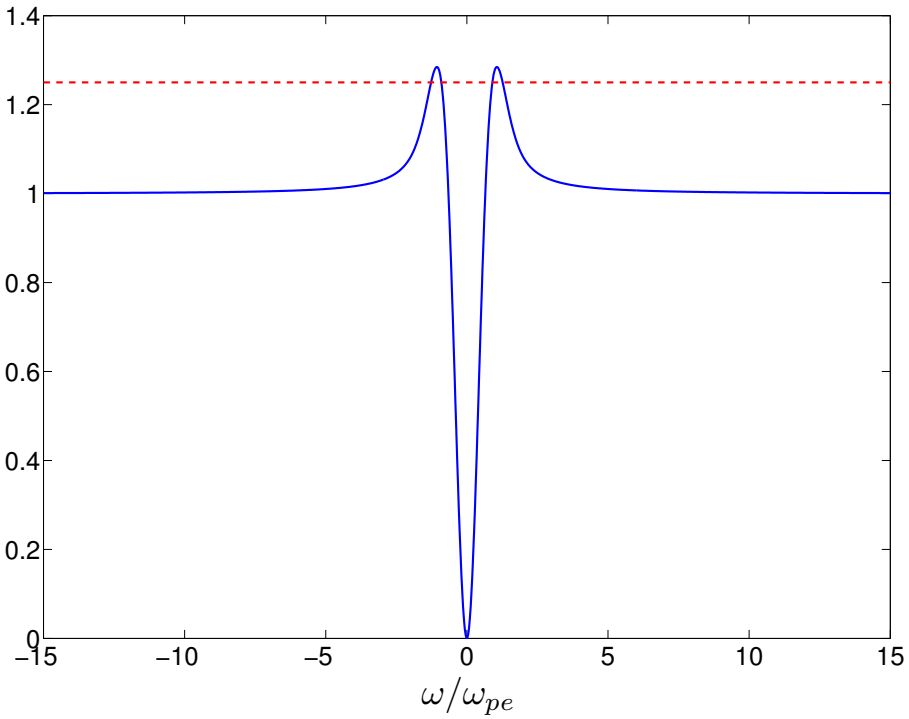

Figure 3.1: Plot of the left and right-hand side of equation (3.23) for $k = 0.5$. The discrete eigenvalues of A are the values of ω for which the blue solid line crosses the red dashed line.

many points gain a non-zero imaginary part and not some small interval consisting of uncountably infinitely many points? The answer to this question is, and we will see this explicitly on the equations later on, that the continuous part of the Van Kampen spectrum remains unchanged if we take a non Maxwellian $f_0(v)$ or introduce a temperature gradient. The eigenvalues that are perturbed by such changes are exactly the discrete eigenvalues that, in the case of Langmuir waves with a Maxwellian background, remain hidden among the continuous spectrum located on the real line. From a mathematical point of view, in such cases we will get a different function $\psi(v)$ and this will result in solutions of (3.16) which will not always be real.

Another thing we would like to note in this section is the similarity of (3.19) and (2.36). (Recall the definitions of a_0 and x.) Strictly speaking, (3.19) is ambiguous, because of the pole in the integrand, until we explicitly define an integration path in the complex plane that treats this pole in a mathematically rigorous way. If one takes the Cauchy principle value of the integral, then the left hand side of (3.19) is not an analytic function of ω and one obtains the discrete part of the Van Kampen spectrum that is the important one in the analysis of the ITG and 'bump-on-tail' instability. If for the sake of analyticity the integration in (3.19) is done along the Landau contour, then (3.19) reduces to (2.36) and this gives the Landau solutions. For this reason, in more complicated examples that we

will study, we are not going to undertake the complicated analysis of contour deformation as in section 2.2. Instead, we will derive the corresponding resolvent operator, separate its discrete part and treat the ambiguity differently (Cauchy principle value or Landau prescription) which will give us the discrete part of the Van Kampen spectrum and the Landau solutions respectively.
At this point, we would like to make a few comments regarding the classic paper [13] of Case about one-dimensional electrostatic electron oscillations in a plasma with immobile ions viewed in the framework of linear theory. The notation used in this paper is similar to that which is used here, except that in [13] $\eta(v)$ is what we here called $\psi(v)$ and the eigenvalues are denoted by ν, and are related to ours via the simple formula $\nu = \omega/k$. In his paper (on page 353), Case summarizes his results by claiming that: 'We have a continuum of solutions for all real ν such that not simultaneously

$$\eta(\nu_i) = 0 = \lambda(\nu_i) \equiv 1 + \int_{-\infty}^{+\infty} \frac{\eta(v)dv}{v - \nu_i}.' \tag{3.24}$$

Considering the rest of the paper, most probably the Cauchy principle value of the integral in the expression above is meant. However, in this part of our work we showed that this cannot be true. Let us take a Maxwell distribution for the form of $f_0(v)$. In this case, η equals zero only when its argument also equals zero, so the first condition of (3.24) cannot produce a continuous spectrum consisting of the entire real line. The second condition, involving λ, is the same as (3.16) with the Cauchy principle value prescription, and we saw in this subsection that this expression is directly related to the real part of the plasma dispersion function, because the argument (here ν_i) is taken to be real. Since $ReZ(x, 0)$ is not proportional to $1/x$, $\lambda(\nu_i)$ cannot have the same value for all real ν_i. From this, it follows that the conditions given in (3.24) cannot reproduce the known continuous Van Kampen spectrum which, as we know for certain, exists when f_0 is a Maxwell distribution. There is also a more general argument for that. Our mathematical analysis showed that even the multiplication operator A_0 alone has a continuous spectrum situated on the entire real line. We also proved, using a general mathematical theorem of Weyl, that the addition of the operator C does not change anything about the continuous spectrum of A_0, since C is compact. The function $\eta(v)$, however, is present only in C. Therefore, one can conclude that presence of the continuous part of the spectrum cannot be influenced by any condition that involves $\eta(v)$, which is the case for both conditions in (3.24). The continuous Van Kampen spectrum is a remnant of the operator A_0 and, therefore, has nothing to do with the particular form of $\eta(v)$.
Further, we would also like to discuss the discrete part of the spectrum. In his paper, Case notes that also discrete sets of eigenvalues can exist:
"We have a discrete set of solutions for ν_i such that either ν_i is complex and

$$\int_{-\infty}^{+\infty} \frac{\eta(v)dv}{v - \nu_i} = 1 \tag{3.25}$$

or ν_i is real with $\eta(\nu_i) = \lambda(\nu_i) = 0$.'
As we already noted, $\eta(v)$ is the same as $\psi(v)$ in our notation, so condition (3.25) is similar to (3.16). The two conditions would have been the same if the right-hand side of (3.25) were -1 instead of 1. We think that this discrepancy is due to a typing error. However, the conditions regarding the discrete set of real eigenvalues also do not agree with our results. As we found, there exist isolated eigenvalues given by (3.16) where one should take the Cauchy principle value of the integral. In the notation of Case, (3.16) corresponds to $\lambda(\nu_i) = 0$. However, $\eta(\nu_i) = 0$ does not need to be fulfilled. For example, in the case of a Maxwell background electron distribution $\eta(\nu_i) = 0$ is true only for $\nu_i = 0$ but, as we saw, in this case (3.16) is satisfied also for values of $\widetilde{\omega}_0$ different from zero. By applying A on the eigenfunction corresponding to these real non-zero eigenvalues one sees that they still fulfil the eigenvalue equation even though $\eta(\nu_i) \neq 0$.

Chapter 4

Numerical description of Langmuir waves

4.1 Collisionless case

4.1.1 Maxwellian background

In the previous chapter we set the basis for a better qualitative mathematical understanding of the spectrum of the operator A. However, such a qualitative understanding is not completely satisfactory. Instead, we would like to have some quantitative results that describe the system under consideration. Even in the collision free case, the equations are complicated enough such that the results we are interested in cannot be expressed in a closed form using elementary functions, i.e., we cannot derive an analytic solution. Therefore, we are going to undertake a numerical approach. In subsequent parts of our study, when we include also complicated collision operators, e.g., the Lenard-Bernstein collision operator, we will have to rely almost exclusively on numerical results. In section 2.2 we have already used numerics to find the solutions of (2.48). In this part we model numerically the Van Kampen approach. For this we are going to discretize the velocity axis which turns the distribution function into a vector in a high but finite dimensional space (dimension equals the number of points in velocity space), i.e.,

$$v \in (-\infty, +\infty) \to \{v_j\}_{j=1,2,\ldots,N+1} \Longrightarrow \widehat{\widetilde{f}}_1(\widetilde{k}, \widetilde{v}, \widetilde{\omega}) \to F(\widetilde{k}, \widetilde{v}_j, \widetilde{\omega}) =: F_j, \tag{4.1}$$

where F_j stands for the jth component of the vector $\vec{F}$ representing the Fourier transformed perturbation of the distribution function in velocity space. We shall also use a set of points in velocity space that is symmetric with respect to 0. The derivative of the equilibrium distribution function with respect to v is also expressed by a vector which will be denoted by $\vec{G}$:

$$G_j := \frac{\partial \widetilde{f}_0}{\partial \widetilde{v}}(\widetilde{v}_j). \tag{4.2}$$

With this notation (2.50) becomes

$$\widetilde{\omega}F_j = \widetilde{k}\widetilde{v}_j F_j - \frac{1}{\widetilde{k}} G_j \cdot \underbrace{\sum_{i=1}^{N+1} F_i \Delta\widetilde{v}}_{\leftrightarrow \int_{-\infty}^{+\infty} \widehat{\widetilde{f}}_1(\widetilde{k},\widetilde{v},\widetilde{\omega})d\widetilde{v}} \quad , \tag{4.3}$$

where $\Delta\widetilde{v}$ is the distance between two neighbouring points on an equidistant grid in velocity space and the integral over velocity has been transformed into a finite sum. We want to express the right-hand side of (4.3) as matrix acting on the vector $\vec{F}$. Mathematically, this means that we approximate the continuous operator on the right-hand side of (2.50), i.e., A, through a matrix. Naively thinking, one could expect that, if one takes more and more points on the velocity axis, i.e., one makes the matrix bigger, then the approximation should get better and better. This, however, is not straightforward. Since A, defined on the Hilbert space H, is not a compact operator, we can be certain that there does not exist a sequence of matrices, i.e., finite rank operators, that converges to A in the operator norm [7, p. 135, Satz 3.8 d)]. In our case this means that increasing the rank of the matrices, i.e., making the resolution in velocity space better, does not necessarily make the numerical results more correct. Therefore, we are going to test our numerical approximation against some known qualitative results which have been derived analytically. If we are able to reproduce these results, then this will give us some confidence in the methods we use.
First, we make the discretisation of the velocity axis more precise. When the index j runs from 1 to $N+1$, the velocity points will vary from $-\widetilde{v}_{max}$ to $\widetilde{v}_{max}$, where the latter is defined as the maximal velocity in the set and corresponds to $j = N+1$. This leads to

$$\widetilde{v}_j = -\widetilde{v}_{max} + (j-1)\Delta\widetilde{v} = -\widetilde{v}_{max} + \frac{2\widetilde{v}_{max}}{N}(j-1). \tag{4.4}$$

According to this we have for the first term on the right-hand side in (4.3):

$$\widetilde{k}\widetilde{v}_j F_j = -\widetilde{k}(\widetilde{v}_{max} + \Delta\widetilde{v})F_j + \widetilde{k}\Delta\widetilde{v} j F_j \tag{4.5}$$

and jF_j is the jth component of the vector given by the product

$$\begin{pmatrix} 1 & 0 & 0 & \cdots & 0 \\ 0 & 2 & 0 & \cdots & 0 \\ 0 & 0 & 3 & \cdots & 0 \\ \vdots & \vdots & \vdots & \ddots & \vdots \\ 0 & 0 & 0 & \cdots & N+1 \end{pmatrix} \begin{pmatrix} F_1 \\ F_2 \\ F_3 \\ \vdots \\ F_{N+1} \end{pmatrix} =: B \cdot \vec{F}. \tag{4.6}$$

If we define a $(N+1)$-dimensional row-vector $\vec{b}$ as $\vec{b} := (1, 1, 1, ..., 1)$, then the second term on the right in (4.3) can be rewritten as follows:

$$-\frac{\Delta\widetilde{v}}{\widetilde{k}} \left\{ G_j \sum_{j=1}^{N+1} F_i \right\} = -\frac{\Delta\widetilde{v}}{\widetilde{k}} \vec{G} \left(\vec{b} \cdot \vec{F} \right) = -\frac{\Delta\widetilde{v}}{\widetilde{k}} \left(\vec{G} \otimes \vec{b} \right) \cdot \vec{F}. \tag{4.7}$$

This way we can rewrite (4.3) in a more convenient form, namely as a matrix eigenvalue equation:

$$\widetilde{\omega}\vec{F} = M \cdot \vec{F}, \tag{4.8}$$

where the matrix M is given by

$$M = -\widetilde{k}\widetilde{v}_{max}\frac{(N+2)}{N}I + \widetilde{k}\Delta\widetilde{v}B - \frac{\Delta\widetilde{v}}{\widetilde{k}}\vec{G}\otimes\vec{b}. \tag{4.9}$$

and I represents the identity matrix of rank $N+1$. For a numerical evaluation we have to specify the vector $\vec{G}$. Since we want to reproduce the Van Kampen spectrum of Langmuir waves that corresponds to the set of Landau solutions which we already derived in section 2.2, we take also in this case a normalized and centred Maxwellian as an equilibrium distribution given in (3.18). This means that

$$G(\widetilde{v}) = -\frac{\widetilde{v}}{\sqrt{2\pi}}e^{-\widetilde{v}^2/2}. \tag{4.10}$$

Now we can easily evaluate (4.8) by writing a simple routine in MATLAB (shown in the Appendix under the name *eigenvalue.m*) that diagonalizes M and plots its eigenvalues. Such a plot for $\widetilde{v}_{max} = 6$, $\widetilde{k} = 0.5$ and 51 points in velocity space is shown in Figure 4.1, where the crosses represent the position of the calculated eigenvalues.
It is evident that the program produces only real eigenvalues which is consistent with our expectation based on the mathematical analysis in chapter 3. The largest deviation of an eigenvalue from the imaginary axis is of the order of 10^{-15}. Since in this example the numerical precision was set to *double*, this deviation is due to numerical 'noise'. Another interesting observation that one can make and on which we are going to elaborate further later on, is that the density of the eigenvalues on the real line (inverse proportional to the distance between two neighbouring eigenvalues) is not constant. We have plotted this spectral density (solid blue line) in Figure 4.2 where for convenience it is normalized through a multiplication by $\Delta\widetilde{v}$. The horizontal black dashed line represents the constant function of 2.
A comparison with Figure 2.1 shows that the position of the two peaks coincides with the projection of the least damped Landau solutions onto the real axis (represented here via the two vertical red dashed lines). In other words, the Van Kampen eigenvalues somehow sense the presence of the most important Landau solutions. It is noteworthy that the spectral density has noticeable variations only in the central part of the frequency interval while for frequencies considerably greater than the real part of the least damped Landau solution it quickly approaches the value of 2. In order to understand this behaviour and the meaning of the constant line, we recall the resolvent operator of A that is given explicitly by (3.15). The first part of this operator is $1/(\widetilde{k}\widetilde{v} - \widetilde{\omega})$ and it is responsible for the continuous part of the spectrum. If this were the whole resolvent operator, then in a discretized velocity space also the continuous spectrum becomes discrete with eigenvalues that are given by $\widetilde{\omega}_j = \widetilde{k}\widetilde{v}_j$. This leads to equidistant points that are separated by $\Delta\widetilde{\omega} = \widetilde{k}\Delta\widetilde{v}$. In this case,

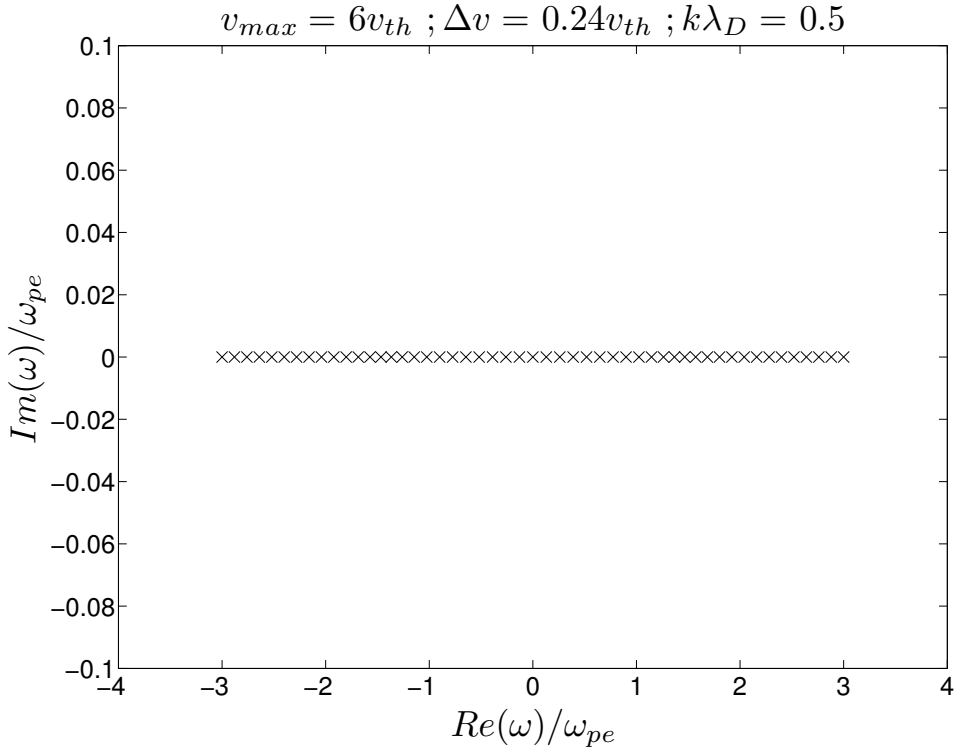

Figure 4.1: Collisionless Van Kampen spectrum for $\widetilde{k} = 0.5$.

the spectral density according to our definition would have been $\Delta\widetilde{v}/\Delta\widetilde{\omega} = 1/\widetilde{k} = 2$ which corresponds to the black dashed line. However, the whole spectral density is not given by a constant function. From this, it follows that the non-trivial behaviour of the density of the eigenvalues is determined by the second part of the resolvent operator which is due to the operator C that arises from the Poisson equation in our model. In front of the integral in the expression for C there is the derivative of the equilibrium distribution which we represented by a Maxwell distribution centred around zero. This means that $\partial f_0(v)/\partial v$ falls rapidly when velocity increase. Since the velocity is related to the frequency by $v = \omega/k$, this can explain why for large ω the operator C has practically no influence on the spectral density.

Another qualitative test of our numerical approach is to reproduce Landau damping. Since damping is a phenomenon concerning the time behaviour of the quantity in view, we will therefore turn to equation (2.16). In order to prevent further complication of the notation, the discretised version of $\widehat{\widetilde{f}}_1(\widetilde{k}, \widetilde{v}, \widetilde{t})$ is also going to be denoted by $\vec{F}$. Bearing this in mind, the discretised version of (2.16) can be written as

$$i\frac{\partial \vec{F}(\widetilde{t})}{\partial \widetilde{t}} = M \cdot \vec{F}(\widetilde{t}), \tag{4.11}$$

which is a first order differential equation in time. Since the matrix M depends neither on

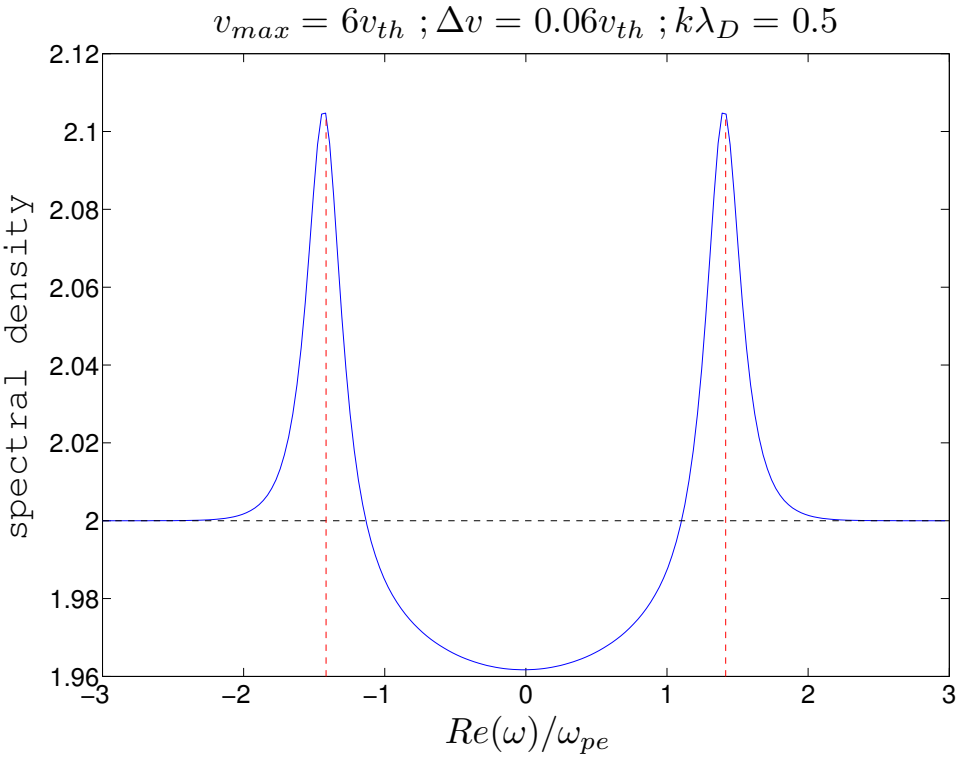

Figure 4.2: Spectral density of the collisionless Van Kampen spectrum ($\widetilde{k} = 0.5$).

time nor on the vector $\vec{F}$, we can write the solution of this equation immediately as

$$\vec{F}(\widetilde{t}) = e^{-iM\widetilde{t}} \cdot \vec{F}_0, \tag{4.12}$$

where $\vec{F}_0$ represents the value of $\vec{F}$ at $\widetilde{t} = 0$ which is regarded as given. Equation (4.12) can be easily implemented numerically which we have done with the program *initial_value.m* given in the Appendix. Using this program (combined with *distribution.m*), one can produce the plot shown in Figure 4.3. As an initial condition we have taken a normalized Gauss curve centred at 0 with the width of 2. At first sight this could be confusing since we have used the same function also for the equilibrium distribution. However, (4.11) is linear, so we can multiply its solution with an arbitrary number (in order to satisfy the smallness condition that the perturbation f_1 has to fulfil) and it will still be a solution. A physically more reasonable initial condition would be a shifted Gauss function with a different width which corresponds to a population of particles that moves with respect to the ion background and has a different temperature than the majority of the electrons. Nevertheless, such an initial condition produces qualitatively the same result as the one we have used in order to show the increasing oscillation of f_1 with time.
One observes exactly the oscillation behaviour with respect to velocity which gets more and more rapid when time increases as we expected, as shown in Figure 4.3.
The last test of our numerical scheme is to reproduce the exact value of the damping

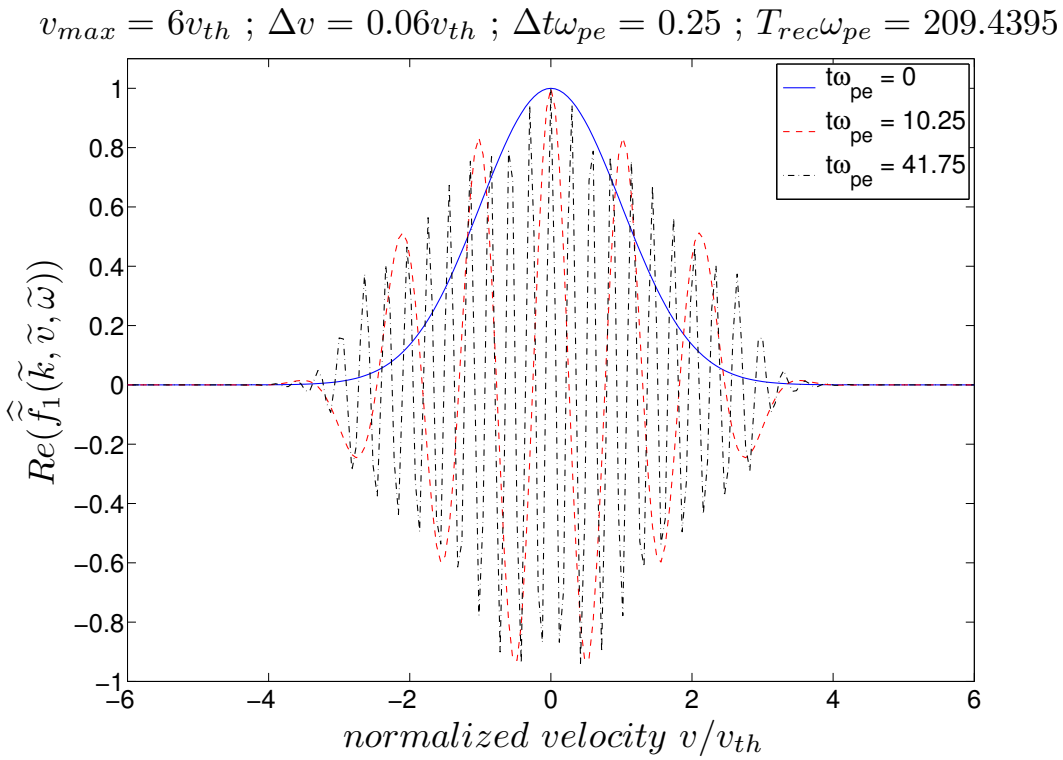

Figure 4.3: Enhancement of the oscillatory character of $\widehat{\widetilde{f}}_1(\widetilde{k},\widetilde{v},\widetilde{t})$ in velocity space when time evolves.

rate. Since we already have the whole discretised distribution function for all times, we just have to do the velocity integration, which is trivial. This is done by the program *electric_field.m* (to be found in the Appendix) and the corresponding output is shown in Figure 4.4.

One sees indeed some oscillatory behaviour that corresponds to the oscillations of the perturbation f_1, since it produces the electric field, but the amplitude of these oscillations decreases. For a better display of the phenomenon that we want to emphasize, we have plotted not $Re(\widetilde{E}(\widetilde{k},\widetilde{t}))$ but the natural logarithm of its absolute value. After some small transient time one observes an exponential decay in the amplitude of $Re(\widetilde{E}(\widetilde{k},\widetilde{t}))$ which is consistent with the analysis in section 2.2. We verify this assumption also in a quantitatively more precise way. If one takes the local maxima of $\ln|Re(\widetilde{E})|$ for the interval of time for which we have exponential decay (in this case for $\widetilde{t} \lesssim 100$) and plots them, then one gets a line, the slope of which equals about -0.1536. On the other hand, the imaginary part of the least damped Landau solution, which is the one responsible for the long time behaviour of the electric field as we saw in section 2.2, can be computed numerically from (2.38) with a great precision and equals approximatively -0.1534. The comparison between these two results shows a good agreement.

Apart from the exponential decay of the electric field, one also notices two other distinctive

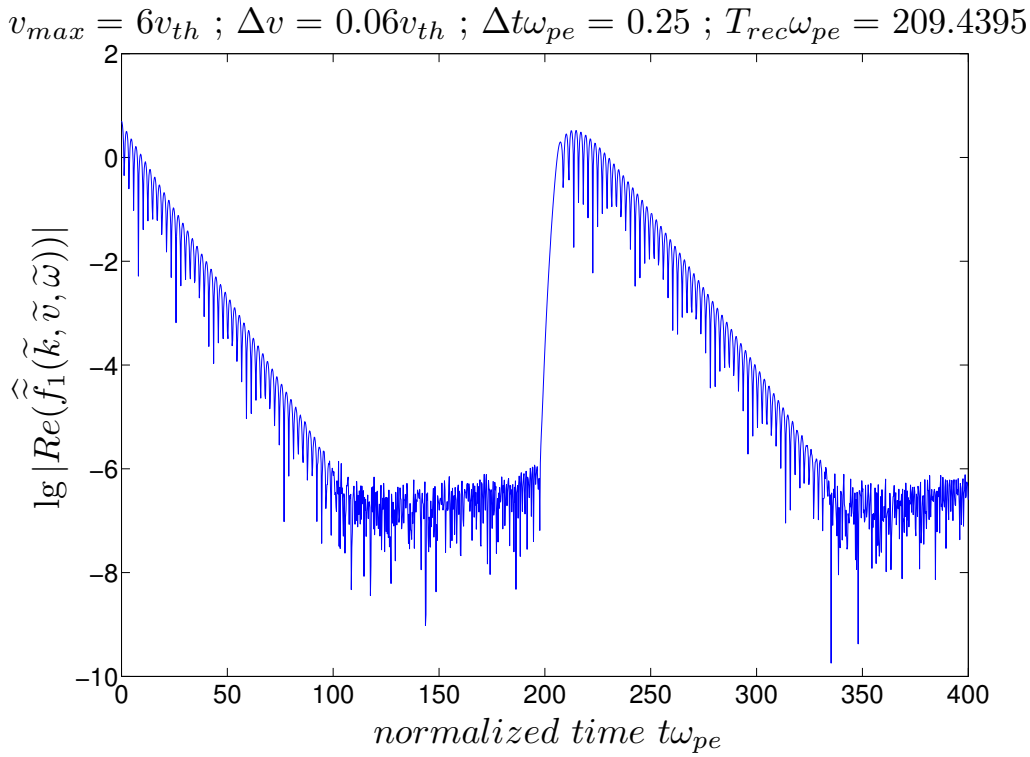

Figure 4.4: Time dependence of the Fourier transform of the electric field.

features in Figure 4.4. First, all structures seem to repeat periodically. This is not a physical effect but is due to our discretisation of velocity space. Once we have set the length of the velocity interval $[-\widetilde{v}_{max}, \widetilde{v}_{max}]$ and the number of points it is to be represented with, the minimal distance of points $\Delta\widetilde{v}$ is determined. This is the resolution in velocity space. If one recalls the exponential factor in (2.56), then it is clear that a non-zero $\Delta\widetilde{v}$ leads to finite time $\widetilde{T}_{rec}$ (which we will call recurrence time) given by $\widetilde{T}_{rec} = \frac{2\pi}{\widetilde{k}\Delta\widetilde{v}}$ after which the phase ϕ can be related to the phases from previous times as $\phi(\widetilde{t}) = \phi(\widetilde{t} - \widetilde{T}_{rec}) + 2\pi$ which, of course, leads to the same value of the exponent, i.e., this periodic behaviour is a consequence of our numerical treatment and does not represent real physics, so results for $\widetilde{t} > \widetilde{T}_{rec}$ should be ignored. The other effect is what appears to be a saturation effect just before recurrence occurs. In a linear theory such a saturation effect does not exist and the electric field should be damped to zero. However, every computer has a certain numerical precision and the electric field cannot be damped under this precision which in our case produces the effect observed. In Figure 2.15 the numerical saturation occurs at values of the electric field of the order of 10^{-7}. The reason for this is that in our program there were objects defined with the computer precision *single*. Therefore, this is also the precision of the end result.

Now, after we have successfully tested our numerical approach, we would like to use it to gain more information about the system under consideration. As we already observed in

Figure 4.2, the Van Kampen eigenvalues, although bound to the real axis, seem to sense the position of the least damped Landau solutions by increasing their density just above these Landau roots. This hints at the importance of the Van Kampen modes that correspond to these eigenvalues. In the Landau approach of solving the collisionless linearised Vlasov equation one solves for the electric field E and one discovers that it is damped exponentially. However, as we already explained, the distribution function is not damped. It just oscillates more rapidly in velocity space as time increases. It is not straightforward to connect the Van Kampen modes with Landau damping, since the electric field is proportional to the 0th velocity moment of the distribution function and there are uncountably infinitely many distribution functions that reproduce a damped electric field with a given damping rate. Therefore, we are going to use our numerical scheme to investigate this matter. Since we took a finite interval on the velocity axis and discretized it, the continuous operator A turned into a matrix and the eigenvectors of this matrix, which we will denote by $\vec{e}_\ell$, correspond to the Van Kampen modes. Every vector $\vec{e}_\ell$ is a function of velocity in the sense that every component of the $(N+1)$-dimensional vector is the value of this function at the corresponding point in velocity space. Integration of this function over velocity translates into the sum of all components of $\vec{e}_\ell$ multiplied by the grid resolution $\Delta\widetilde{v}$. As eigenvectors of the matrix M, defined in (4.9), $\{\vec{e}_\ell\}_{\ell=1,2,...,N+1}$ form a basis in the space of $(N+1)$-dimensional vectors. The vectors of this basis are normalized by MATLAB but they are not orthogonal. In order to make the further analysis more convenient, we introduce the so called left eigenvectors $\vec{g}_\ell$ of M that are defined by a similar eigenvalue equation, namely $\vec{g}_\ell^T \cdot M = \widetilde{\omega}_\ell \vec{g}_\ell^T$. A well known result from Linear Algebra is that for non-degenerate eigenvalues $\vec{e}_m \cdot \vec{g}_n = 0$ when $n \neq m$. At this point a remark has to be made. The eigenvectors are normalized to one with respect to the usual norm of finite dimensional vectors. However, this is going to make a comparison between analytical and numerical results harder. The reason for this is that this scalar product of finite dimensional vectors corresponds to the L^2 scalar product of functions. The numerical eigenvectors have to represent the analytical eigenfunctions that we found and that are not square integrable. In the literature the eigenfunctions are, therefore, usually 'normalized' such that their integral over velocity is one[1]. A possible solution of this problem is to normalize the numerical eigenvectors such that the sum of their components is one, i.e., that

$$\Delta\widetilde{v} \sum_{m=1}^{N+1} e_{\ell m} = 1 \text{ for every } \ell \in \{1, 2, ..., N+1\}. \tag{4.13}$$

This can be easily done by merely rescaling every component the vector e_ℓ in the appropriate way. A plot of one of the numerical eigenvectors (the one that corresponds to the eigenvalue closest to $\sqrt{2}$) is shown in Figure 4.5 as a solid blue line.
It is seen how the function peaks at the position $\widetilde{v} = \sqrt{2}/\widetilde{k}$, where in this case the normalized wave number equals 0.5. This feature hints at the fact that the analytical eigenfunction

[1]We put the word 'normalized' in quotation marks because this prescription does not represent a norm in the mathematical sense of this word.

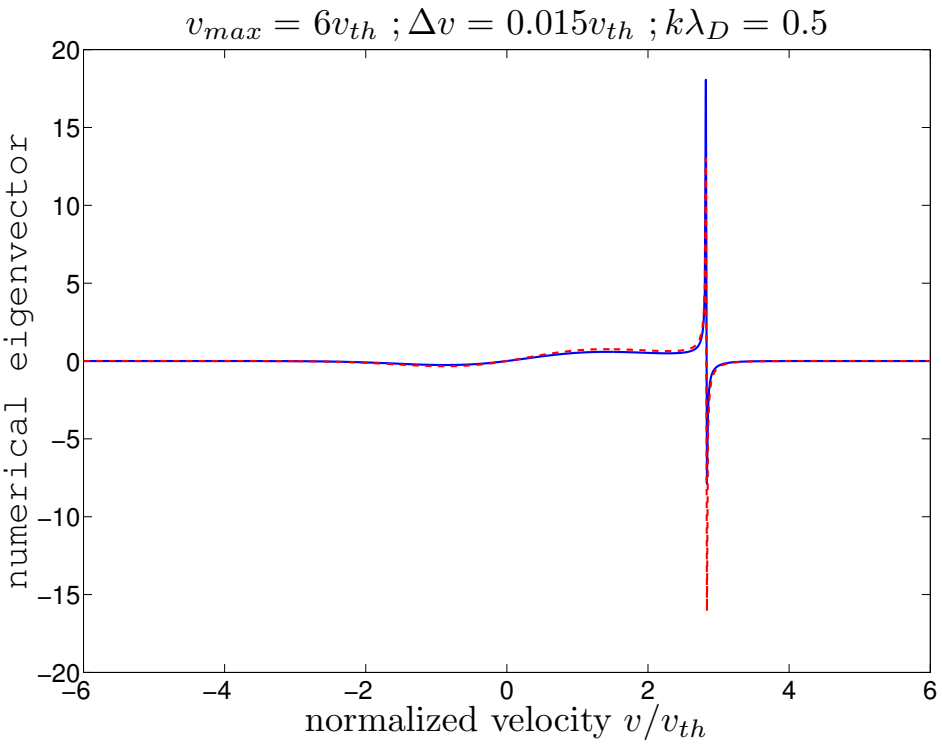

Figure 4.5: One of the numerical eigenvectors (blue) compared to the first term of the corresponding analytical eigenfunction (red).

has a singularity at this point. However, both terms in (2.51) exhibit such a singularity. In order to clarify this issue, on the same plot also the first part of the eigenfunction is shown (red dashed line). It has been normalized such that the principal value of its velocity integral equals one. Both lines coincide almost exactly which implies that with our velocity discretization the second part of the eigenfunction that involves a delta function cannot be resolved numerically, as it should be expected.
Since the set $\{\vec{e}_\ell\}_{\ell=1,2,\ldots,N+1}$ is a complete basis in the space of $(N+1)$-dimensional vectors, we can decompose the vector $\vec{F}$, i.e., the discretized distribution function, with respect to it:

$$\vec{F}(t) = \sum_{\ell=1}^{N+1} c_\ell \vec{e}_\ell, \tag{4.14}$$

where $\{c_\ell\}$ is the corresponding set of coefficients. Recalling the solution (4.12) of the discretized version of the differential equation that determines the time evolution of the distribution function, one can reason that the components of $\vec{F}$ at an arbitrary moment of time $t_0 > 0$ will be complex. Since the Van Kampen modes are real functions, all components of $\vec{e}_\ell$ for every ℓ are real. Therefore, in order that the upper decomposition holds, the coefficients c_ℓ should be complex. Because of the aforementioned relation regarding

the scalar product between left and right eigenvectors and the new normalization we can write that

$$c_\ell(t) = \frac{\vec{g}_\ell \cdot \vec{F}(t)}{\vec{g}_\ell \cdot \vec{e}_\ell}. \tag{4.15}$$

Here we have written the coefficients as functions of time, which they are. However, the real and imaginary part of every coefficient change in such a way that, at least in the case of Langmuir waves, $|c_\ell|$ is constant in time. Recalling (4.12), one can write

$$\begin{aligned}(\vec{g}_\ell \cdot \vec{e}_\ell)c_\ell(\widetilde{t}) = \vec{g}_\ell^T \cdot \left(e^{-iM\widetilde{t}} \cdot \vec{F}_0\right) = \left(\vec{g}_\ell^T \cdot e^{-iM\widetilde{t}}\right) \cdot \vec{F}_0 = \\ = \left(\sum_{n=1}^{\infty} \frac{(-it)^n}{n!} \underbrace{\vec{g}_\ell^T \cdot M^n}_{=\widetilde{\omega}_\ell^n \vec{g}_\ell^T}\right) \cdot \vec{F}_0 = e^{-i\widetilde{\omega}_\ell \widetilde{t}} \underbrace{\vec{g}_\ell^T \cdot \vec{F}_0}_{\propto c_\ell(\widetilde{t}=0)} = (\vec{g}_\ell \cdot \vec{e}_\ell)c_\ell(\widetilde{t}=0)e^{-i\widetilde{\omega}_\ell \widetilde{t}}.\end{aligned} \tag{4.16}$$

Since, as we proved, in the case of Langmuir waves all eigenfrequencies are real, it is obvious that $|c_\ell(\widetilde{t})| = |c_\ell(\widetilde{t}=0)| = const.$ One sees immediately that the absolute value of the coefficients depends entirely on the initial value $\vec{F}_0$ of the discretized perturbation of the electron distribution function. In Figure 4.6 we have shown $|c_\ell|$ as a function of ℓ (i.e., $\widetilde{\omega}_\ell$) for two different initial perturbations. The solid blue line corresponds to $\widehat{\widetilde{f}}_1(\widetilde{k} = 0.5, \widetilde{v}, \widetilde{t} = 0) = e^{-\widetilde{v}^2/2}$ and the black dashed line stands for an initial condition of the form $\widehat{\widetilde{f}}_1(\widetilde{k} = 0.5, \widetilde{v}, \widetilde{t} = 0) = e^{-(\widetilde{v}-1)^2/2}$. The projections of the least damped Landau solutions onto the real axis are indicated by the red dashed lines that help to compare their position with the position of the peaks. For the initial condition that is symmetric with respect to $\widetilde{v} = 0$ one sees that the largest coefficients lie around the projections of the least damped Landau solutions. This hints at the importance of these Van Kampen modes. Qualitatively, the same behaviour is observed also in the case of an initial condition in the form of a Gauss curve centred at $\widetilde{v} = 1$ (corresponding here to $\widetilde{\omega} = 0.5$). However, this time the structure is not symmetric with respect to zero, as has to be expected.
From this plot it is evident that the Van Kampen modes that lie directly above the least damped Landau roots are of vital importance for a successful description of the Langmuir waves. This is the same conjecture that we arrived at after the investigation of the density of eigenvalues shown in Figure 4.2. However, it is evident that also the Van Kampen modes around zero have non-vanishing coefficients and should not be neglected. One can check the relative importance of the Van Kampen modes by removing parts of the initial condition and then testing if the correct damping rate of the electric field is reproduced. One way to do this is to decompose the initial condition into Van Kampen modes and then to construct a new initial condition as as a sum of only some part of the Van Kampen modes (including coefficients). For instance, we choose a centred Gauss curve as an initial condition and divide the $\widetilde{\omega}$-axis in Figure 4.6 in five parts. The first part is from -3 to -2 and at first sight it should not be important since the the coefficients corresponding to

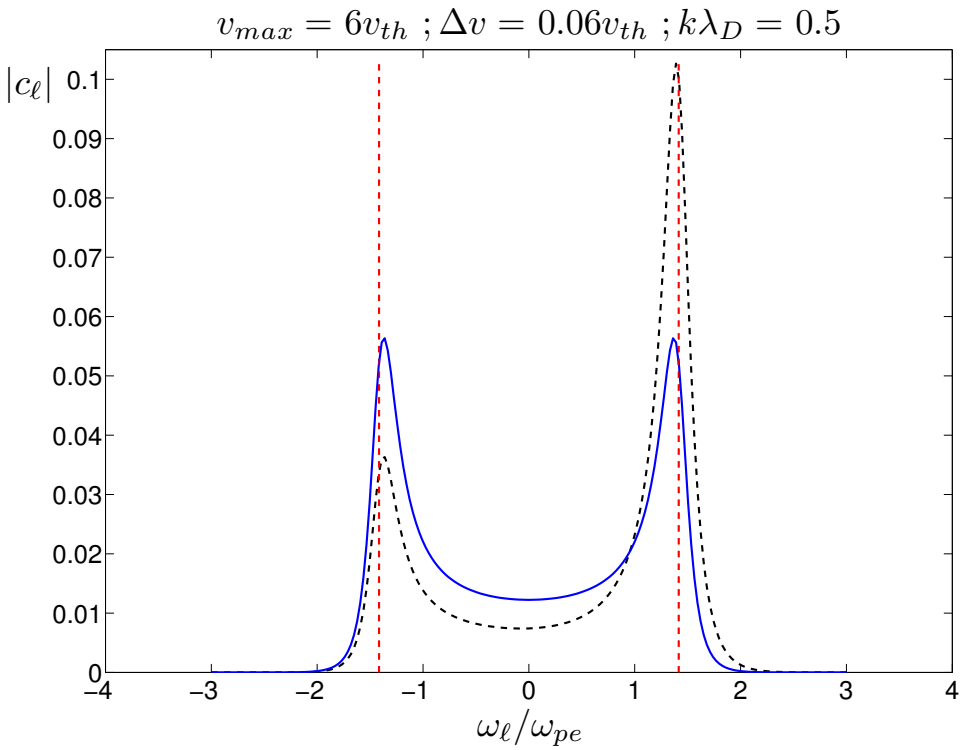

Figure 4.6: Coefficients corresponding to the decomposition of the perturbation of the electron distribution function into (discrete) Van Kampen modes.

these modes are negligible. The next two parts are the areas $\widetilde{\omega} \in (-2, -1)$ and $\widetilde{\omega} \in (1, 2)$ which enclose the peaks and lie above the least damped Landau solutions. Last, there is the middle part for $\widetilde{\omega} \in (-1, 1)$ where the coefficients are considerably smaller than those at the two peaks but still not negligible. The last part is equivalent to the first one but for positive $\widetilde{\omega}$. Let $\vec{F}_0$ be the full initial condition. Then we decompose it into Van Kampen modes. The modified initial condition $\vec{F}_{0,new}$, e.g., for the middle part of the $\widetilde{\omega}$-axis is built as

$$\vec{F}_{0,new} = \sum_{\widetilde{\omega}\in(-1,1)} c_\ell \vec{e}_\ell. \tag{4.17}$$

In the above expression, the sum is performed along those indices that correspond to the normalized frequencies in $(-1, 1)$. Figure 4.7 represents different modified initial conditions. From the form of the coefficients one could expect that an initial condition consisting of the Van Kampen modes with big coefficients should successfully reproduce the Landau damping at least qualitatively. However, in Figure 4.7 a it is clear that in this case there is no exponential damping which means that the modes which we eliminated are important. The plot in Figure 4.7 b makes clear that even the Van Kampen modes around the two least damped Landau solutions put together cannot reproduce the Landau damping. For

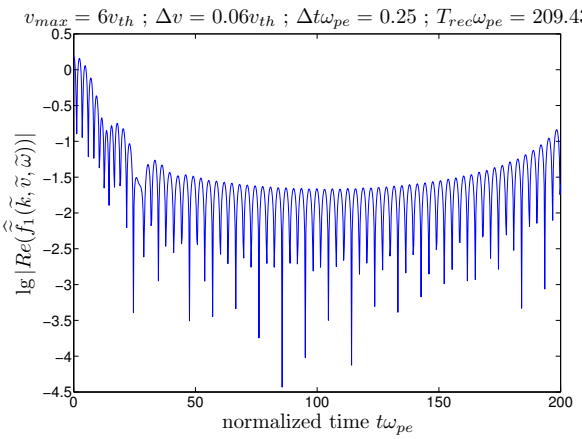

(a) Van Kampen modes with $\widetilde{\omega} \in (1, 2)$.

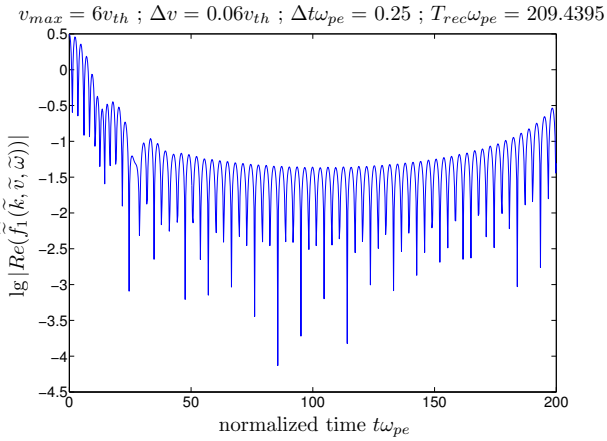

(b) Van Kampen modes with $\widetilde{\omega} \in (-2, -1) \cup (1, 2)$.

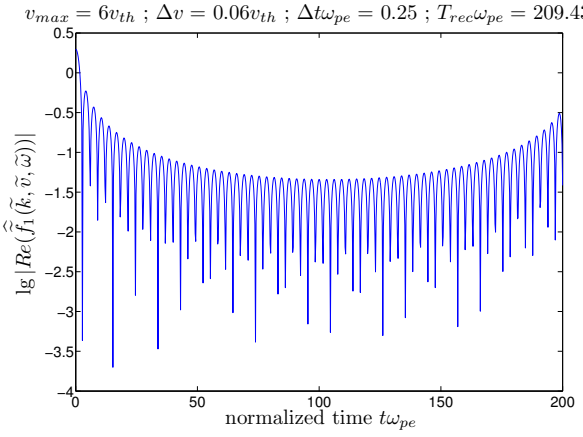

(c) Van Kampen modes with $\widetilde{\omega} \in (-1, 1)$.

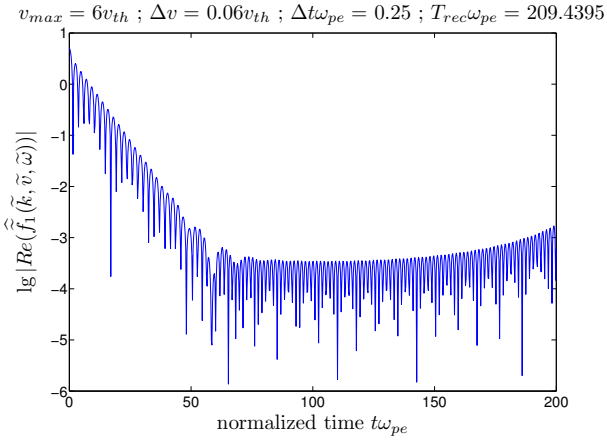

(d) Van Kampen modes with $\widetilde{\omega} \in (-2, 2)$.

Figure 4.7: Electric field produced by different reduced initial conditions.

an exponential decay all Van Kampen modes with non-negligible coefficients (in the frequency interval $(-2, 2)$) have to be taken into account as in Figure 4.7 d. However, even the Van Kampen modes in $(-2, 2)$ fail to reproduce the exact behaviour of the electric field for $\widetilde{t} > 50$ which leads us to the surprising result that one should include even the modes with negligible coefficients if one wants to have an exact result for the electric field for large $\widetilde{t}$. The slope in the area of exponential decay in Figure 4.7 d is approximatively -0.1537 which is almost the same result as in the case of the full initial condition.
Next we would like to focus on another physically meaningful quantity, namely the entropy. Since we have decomposed the whole electron distribution function into an equilibrium background distribution $\widetilde{f}_0(\widetilde{v})$ and a perturbation $\widetilde{f}_1(\widetilde{v})$, we have mathematically divided the electrons into two populations: electrons corresponding to the background and those that represent the perturbation. Both of these electron populations have their own internal entropy and by δS we will denote the entropy of the perturbed electron population. Since

we have agreed to use a Maxwell distribution as $f_0(v)$, then for a fixed k δS reads [19]

$$\delta S = \frac{1}{2}\int_{-\infty}^{+\infty} \frac{|\widehat{\widetilde{f}}_1(\widetilde{k},\widetilde{v},\widetilde{t})|^2}{\widetilde{f}_0(\widetilde{v})} d\widetilde{v}. \tag{4.18}$$

If one denotes the vector corresponding to the discretized Maxwell distribution by $\vec{F}^{(M)}$, then the last equation translates into

$$\delta S = \frac{\Delta\widetilde{v}}{2}\sum_{n=1}^{N+1}\frac{|F_n|^2}{F_n^{(M)}} = \frac{\Delta\widetilde{v}}{2}\sum_{n=1}^{N+1}\left|\sum_{\ell=1}^{N+1} c_\ell e_{\ell,n}\right|^2 \frac{1}{F_n^{(M)}} = \\ = \sum_{\ell=1}^{N+1} \underbrace{\frac{\Delta\widetilde{v}}{2}|c_\ell|^2 \sum_{n=1}^{N+1}\frac{|e_{\ell,n}|^2}{F_n^{(M)}}}_{=:\delta S_\ell} + R = \sum_{\ell=1}^{N+1}\delta S_\ell + R, \tag{4.19}$$

where $e_{\ell,n}$ is the nth component of $\vec{e}_\ell$. In this expression we have defined by δS_ℓ the quantity that represents the entropy corresponding to the jth Van Kampen mode and R stands for the contribution of the cross-terms that arise when $|\sum c_\ell e_{\ell,n}|^2$ is expanded. If one wants to approximate the whole entropy of the disturbed electron population via the sum of all δS_j, then this leads to an error that equals R, which is the reason why we would like to call R an error term. If one plots δS_ℓ with respect to the normalized frequency $\widetilde{\omega}$, one sees that the picture is qualitatively the same as in Figure 4.6. There are two large peaks above the least damped Landau solutions and the other Van Kampen modes have much smaller entropy. However, one should note that the error term R is of considerable amplitude. This is a consequence of the non-orthogonality of the Van Kampen modes with respect to the usual L^2 scalar product. This issue of orthogonality is what we focus on next. In [8] the claim is stated that with respect to the prescription

$$\langle f(v), g(v)\rangle_{f_0} := \int_{-\infty}^{+\infty} \frac{\overline{f(v)}g(v)}{f_0} dv \tag{4.20}$$

the Van Kampen modes corresponding to different frequencies are orthogonal to each other. It is straightforward to prove explicitly that the prescription introduced in (4.20) defines a proper scalar product when $f_0(v)$ is positive definite, as in the case of a Maxwell distribution.

We are going to test this conjecture and also compute the scalar product of the eigenmodes with the usual L^2 scalar product. For a Maxwellian background distribution the Van Kampen eigenmodes are given by (2.51). Then we have for the two scalar products:

case 1) normal L^2 scalar product, $\widetilde{\omega}_1 \neq \widetilde{\omega}_2$:

$$\left\langle \widehat{\widetilde{f}}_{1,V}(\widetilde{k},\widetilde{v},\widetilde{\omega}_1), \widehat{\widetilde{f}}_{1,V}(\widetilde{k},\widetilde{v},\widetilde{\omega}_2) \right\rangle_{L^2} := \int_{-\infty}^{+\infty} \widehat{\widetilde{f}}_{1,V}(\widetilde{k},\widetilde{v},\widetilde{\omega}_1)\widehat{\widetilde{f}}_{1,V}(\widetilde{k},\widetilde{v},\widetilde{\omega}_2)d\widetilde{v} =$$

$$= \frac{1}{2\pi\widetilde{k}^2} p.v. \int_{-\infty}^{+\infty} \frac{\widetilde{v}^2 e^{-\widetilde{v}^2}}{(\widetilde{k}\widetilde{v}-\widetilde{\omega}_1)(\widetilde{k}\widetilde{v}-\widetilde{\omega}_2)} d\widetilde{v} + \frac{C_2}{\sqrt{2\pi}\widetilde{k}} p.v. \int_{-\infty}^{+\infty} \frac{(-\widetilde{v})e^{-\widetilde{v}^2/2}}{\widetilde{k}\widetilde{v}-\widetilde{\omega}_1}\delta(\widetilde{k}\widetilde{v}-\widetilde{\omega}_2)d\widetilde{v} +$$

$$+ \frac{C_1}{\sqrt{2\pi}\widetilde{k}} p.v. \int_{-\infty}^{+\infty} \frac{(-\widetilde{v})e^{-\widetilde{v}^2/2}}{\widetilde{k}\widetilde{v}-\widetilde{\omega}_2}\delta(\widetilde{k}\widetilde{v}-\widetilde{\omega}_1)d\widetilde{v} + C_1C_2 \underbrace{\int_{-\infty}^{+\infty} \delta(\widetilde{k}\widetilde{v}-\widetilde{\omega}_1)\delta(\widetilde{k}\widetilde{v}-\widetilde{\omega}_2)d\widetilde{v}}_{\propto\delta(\widetilde{\omega}_1-\widetilde{\omega}_2)=0 \text{ , since } \widetilde{\omega}_1\neq\widetilde{\omega}_2} =$$

$$= \frac{1}{2\pi\widetilde{k}^4} p.v. \int_{-\infty}^{+\infty} \frac{\widetilde{v}^2 e^{-\widetilde{v}^2}}{(\widetilde{v}-\frac{\widetilde{\omega}_1}{\widetilde{k}})(\widetilde{v}-\frac{\widetilde{\omega}_2}{\widetilde{k}})} d\widetilde{v} + \frac{1}{\sqrt{2\pi}\widetilde{k}^2(\widetilde{\omega}_1-\widetilde{\omega}_2)} \left(C_2\widetilde{\omega}_2 e^{\widetilde{\omega}_2^2/(2\widetilde{k}^2)} - C_1\widetilde{\omega}_1 e^{\widetilde{\omega}_1^2/(2\widetilde{k}^2)} \right) \neq 0,$$

where C_i is defined as the velocity independent expression that multiplies the delta function in the second term of $\widehat{\widetilde{f}}_{i,V}$ as given in (2.51).

case 2) entropy scalar product, $\widetilde{\omega}_1 \neq \widetilde{\omega}_2$:

$$\left\langle \widehat{\widetilde{f}}_{1,V}(\widetilde{k},\widetilde{v},\widetilde{\omega}_1), \widehat{\widetilde{f}}_{1,V}(\widetilde{k},\widetilde{v},\widetilde{\omega}_2) \right\rangle_{f_0} := \int_{-\infty}^{+\infty} \frac{\widehat{\widetilde{f}}_{1,V}(\widetilde{k},\widetilde{v},\widetilde{\omega}_1)\widehat{\widetilde{f}}_{1,V}(\widetilde{k},\widetilde{v},\widetilde{\omega}_2)}{\widetilde{f}_0(\widetilde{v})} d\widetilde{v} =$$

$$= \frac{1}{2\pi\widetilde{k}^2} p.v. \int_{-\infty}^{+\infty} \frac{\widetilde{v}^2 e^{-\widetilde{v}^2/2}}{(\widetilde{k}\widetilde{v}-\widetilde{\omega}_1)(\widetilde{k}\widetilde{v}-\widetilde{\omega}_2)} d\widetilde{v} + \frac{C_2}{\sqrt{2\pi}\widetilde{k}} p.v. \int_{-\infty}^{+\infty} \frac{(-\widetilde{v})}{\widetilde{k}\widetilde{v}-\widetilde{\omega}_1}\delta(\widetilde{k}\widetilde{v}-\widetilde{\omega}_2)d\widetilde{v} +$$

$$+ \frac{C_1}{\sqrt{2\pi}\widetilde{k}} p.v. \int_{-\infty}^{+\infty} \frac{(-\widetilde{v})}{\widetilde{k}\widetilde{v}-\widetilde{\omega}_2}\delta(\widetilde{k}\widetilde{v}-\widetilde{\omega}_1)d\widetilde{v} + C_1C_2 \underbrace{\int_{-\infty}^{+\infty} \frac{\delta(\widetilde{k}\widetilde{v}-\widetilde{\omega}_1)\delta(\widetilde{k}\widetilde{v}-\widetilde{\omega}_2)}{e^{-\widetilde{v}^2/2}} d\widetilde{v}}_{\propto\delta(\widetilde{\omega}_1-\widetilde{\omega}_2)=0 \text{ , since } \widetilde{\omega}_1\neq\widetilde{\omega}_2} =$$

$$= \frac{1}{\sqrt{2\pi}\widetilde{k}^4} p.v. \int_{-\infty}^{+\infty} \frac{\widetilde{v}^2 e^{-\widetilde{v}^2}}{(\widetilde{v}-\frac{\widetilde{\omega}_1}{\widetilde{k}})(\widetilde{v}-\frac{\widetilde{\omega}_2}{\widetilde{k}})} d\widetilde{v} + \frac{1}{\widetilde{k}^2(\widetilde{\omega}_1-\widetilde{\omega}_2)} \left(C_2\widetilde{\omega}_2 - C_1\widetilde{\omega}_1 \right) = -\frac{1}{\widetilde{k}^2} \neq 0.$$

Although this straightforward computation is not the most elegant way to make this point clear, it is sufficient to show that the statement in [8] regarding the orthogonality of the eigenfunctions that correspond to different frequencies is apparently wrong. This means that the operator A, that we studied in chapter 3, is not symmetric also with respect to the modified entropy scalar product. We can confirm our computation numerically. If normalized correctly, the 'entropy' scalar product of any two different numerical eigenvectors

should give nearly 4 for $\widetilde{k} = 0.5$ which the program *eigenvalue.m* yields. For different values of the wave number the numerical results are also in agreement with the analytical computation.
At this point, it is useful to make a comment regarding the matrix M defined in (4.9). As it is known from Linear Algebra, one can find a scalar product under which the eigenvectors of the matrix M corresponding to different eigenvalues are orthogonal if and only if M is normal, i.e., if $M \cdot M^* - M^* \cdot M = 0$, where the star denotes transposition and complex conjugation. In the collisionless case, the matrix has only real elements, so one simply needs to transpose it. If one computes $P = M \cdot M^* - M^* \cdot M$ and searches for the element of P with the greatest absolute value, i.e., takes the supremum norm $\|P\|_\infty$ of P, then one sees that the elements of P get smaller when the resolution in velocity space gets better. It is easy to see numerically, as well analytically, that $\|P\|_\infty$ scales linearly with $\Delta\widetilde{v}$. At first sight, one would conclude that the matrix M gets closer to normality when the velocity resolution increases, and in the continuous limit, it should become normal, from which it follows that its eigenvectors are going to be orthogonal in this limit with respect to some scalar product. However, in our numerical examination of the 'entropy' scalar product between different eigenmodes there was no such scaling dependence on $\Delta\widetilde{v}$. In order to solve this puzzle, one should take into account the fact that the size of the matrix depends linearly on N. Thus, when velocity resolution is halved, the biggest element in P will also halve but, on the other hand, M, and therefore also P, will have four times more elements. To take into account this fact, one should consider another norm of P which include all matrix elements. An example of such a prescription is the 'trace norm', $\|P\|_{tr}^2 := tr(P^* \cdot P)$. Practically, this is the sum of the absolute value squared of all elements of P. The numerical computation for the case of Langmuir waves gives that $\|P\|_{tr}$, having nearly the value of 14 for $\widetilde{k} = 0.5$, stays constant and does not scale with $\Delta\widetilde{v}$ in any way. Thus, even in the continuous limit the matrix M is not going to be normal. In this example one sees that if the limit process requires changing the size of the matrix, i.e., changing the operator, then the limit is by far not straightforward. We are going to encounter a similar problem later on in this work when dealing with the Lenard-Bernstein collision operator in subsection 4.2.2.

4.1.2 'Bump-on-tail' instability

Now, after we have tested our numerical scheme for reproducing known qualitative and quantitative results and gained confidence in its applicability to real problems in plasma physics, we will use this method to study the so called 'bump-on-tail' instability. In the case of Langmuir waves in homogeneous collisionless plasma in global thermal equilibrium we used as a background electron distribution a Maxwell distribution in velocity. Here, this assumption is going to be modified by adding a second Maxwellian to it that corresponds to a different temperature and average velocity. Physically, this means that we have two different electron populations in our plasma and they have different temperatures. From basic thermodynamics we know, of course, that in such cases both electron populations are going to interact with each other in such a way that a global thermal equilibrium is achieved,

since this is the state with the greatest entropy. However, this thermal equilibration means increase of entropy and is therefore possible only through collisions. In our analysis so far we neglected the influence of collisions under the assumption that we focus on processes that develop on time scales that are much smaller than the inverse collision frequency. Hence, since the change of the background electron distribution occurs on time scales comparable to the inverse collision frequency, we can view it as stationary in the analysis that follows.
In mathematical terms, we write f_0 as

$$f_0(v) = C_a \frac{n_0}{\sqrt{2\pi k_B T_a/m_e}} \exp\left(\frac{mv^2}{2k_B T_a}\right) + \\ + (1-C_a)\frac{n_0}{\sqrt{2\pi k_B T_b/m_e}} \exp\left(\frac{m(v-v_b)^2}{2k_B T_b}\right), \quad (4.21)$$

where T_a and T_b denote the corresponding temperatures of the two electron populations, v_b is the average velocity of the second one with respect to the first and C_a is a normalization constant (between 0 and 1) such that the density n_0 is again defined via (2.4).Normalization of this expression where the thermal velocity is taken as $\sqrt{k_B T_a/m_e}$ gives

$$\widetilde{f}_0(\widetilde{v}) = C_a \frac{1}{2\pi} e^{-\frac{1}{2}\widetilde{v}^2} + (1-C_a)\frac{\sqrt{\tau}}{2\pi} e^{-\tau\frac{1}{2}(\widetilde{v}-\widetilde{v}_b)^2}, \quad (4.22)$$

where τ is defined as T_a/T_b. In this case the eigenfrequencies of the system are given by exactly the same eigenvalue equation as (2.50). The only difference is that now $\widetilde{f}_0$ has a different form but the analysis still applies, since it is again a function of velocity only. As outlined in chapter 3, the spectrum consists of a continuous part which lies again on the real line, because it comes from the first term of the resolvent operator in (3.15) which is not influenced by the form of $f_0(v)$, and a discrete part that is determined by f_0 and satisfies equation (3.16). In the case under current consideration the only difference consists in the exact form of $\psi(\widetilde{v})$ which now is given by

$$\psi(\widetilde{v}) := -\frac{1}{\widetilde{k}}\frac{\partial \widetilde{f}_0}{\partial \widetilde{v}} = -C_a \frac{\widetilde{v}}{\sqrt{2\pi}} e^{-\widetilde{v}^2/2} - (1-C_a)\frac{\tau^{3/2}(\widetilde{v}-\widetilde{v}_b)}{\sqrt{2\pi}} e^{-\tau(\widetilde{v}-\widetilde{v}_b)^2/2}. \quad (4.23)$$

In chapter 3 we also realised that (3.16) is ill defined in the sense that its value is ambiguous and that for the discrete part of the Van Kampen spectrum the Cauchy principle value of the integral should be taken. Taking into account (4.22) leads to

$$1 + \frac{C_a}{\widetilde{k}\sqrt{2\pi}} p.v. \int_{-\infty}^{+\infty} \frac{\widetilde{v} e^{-\widetilde{v}^2/2}}{\widetilde{k}\widetilde{v} - \widetilde{\omega}_V} d\widetilde{v} + \frac{(1-C_a)\tau^{3/2}}{\widetilde{k}\sqrt{2\pi}} p.v. \int_{-\infty}^{+\infty} \frac{(\widetilde{v}-\widetilde{v}_b) e^{-\tau(\widetilde{v}-\widetilde{v}_b)^2/2}}{\widetilde{k}\widetilde{v} - \widetilde{\omega}_V} d\widetilde{v} = 0, \quad (4.24)$$

where the subscript V, by which the frequencies are denoted, indicates that they are attained by the principal value prescription and are therefore part of the Van Kampen

spectrum. On the other hand, in chapter 3 we derived that interpreting the integral in (3.16) as done along the Landau contour ('Landau prescription') gives the Landau solutions, denoted by $\widetilde{\omega}_L$, that correspond to the $t \to +\infty$ limit of the initial value problem, so now we simply write

$$1 + \frac{C_a}{\widetilde{k}\sqrt{2\pi}} \int\limits_L \frac{\widetilde{v} e^{-\widetilde{v}^2/2}}{\widetilde{k}\widetilde{v} - \widetilde{\omega}_L} d\widetilde{v} + \frac{(1-C_a)\tau^{3/2}}{\widetilde{k}\sqrt{2\pi}} \int\limits_L \frac{(\widetilde{v} - \widetilde{v}_b) e^{-\tau(\widetilde{v}-\widetilde{v}_b)^2/2}}{\widetilde{k}\widetilde{v} - \widetilde{\omega}_L} d\widetilde{v} = 0 \tag{4.25}$$

without undertaking the cumbersome analysis done previously in section 2.2. We will focus our attention first on the last expression and transform it into a form that is more convenient to work with. Recalling the relations derived in the Appendix between the type of integrals in the last equation and the plasma dispersion function, we note that

$$\int\limits_L \frac{\widetilde{v} e^{-\widetilde{v}^2/2}}{\widetilde{k}\widetilde{v} - \widetilde{\omega}_L} d\widetilde{v} = \frac{\sqrt{2\pi}}{\widetilde{k}} + \frac{\sqrt{2\pi}}{\widetilde{k}} \frac{\widetilde{\omega}_L}{\widetilde{k}\sqrt{2}} Z\left(\frac{\widetilde{\omega}_L}{\widetilde{k}\sqrt{2}}\right) \ ; \tag{4.26}$$

$$\int\limits_L \frac{(\widetilde{v} - \widetilde{v}_b) e^{-\tau(\widetilde{v}-\widetilde{v}_b)^2/2}}{\widetilde{k}\widetilde{v} - \widetilde{\omega}_L} d\widetilde{v} = \frac{\sqrt{2\pi}}{\widetilde{k}\sqrt{\tau}} + \frac{\sqrt{2\pi}}{\widetilde{k}} \left(\frac{\widetilde{\omega}_L}{\widetilde{k}\sqrt{2}} - \frac{\widetilde{v}_b}{\sqrt{2}}\right) Z\left(\sqrt{\frac{\tau}{2}}\left(\frac{\widetilde{\omega}_L}{\widetilde{k}\sqrt{2}} - \frac{\widetilde{v}_b}{\sqrt{2}}\right)\right), \tag{4.27}$$

which eventually leads to the following dispersion relation:

$$\widetilde{k}^2 + \tau + C_a(1-\tau) + C_a \frac{\widetilde{\omega}_L}{\widetilde{k}\sqrt{2}} Z\left(\frac{\widetilde{\omega}_L}{\widetilde{k}\sqrt{2}}\right) + \\ + (1-C_a)\tau\sqrt{\frac{\tau}{2}}\left(\frac{\widetilde{\omega}_L}{\widetilde{k}} - \widetilde{v}_b\right) Z\left(\sqrt{\frac{\tau}{2}}\left(\frac{\widetilde{\omega}_L}{\widetilde{k}} - \widetilde{v}_b\right)\right) = 0. \tag{4.28}$$

Equation (4.28) is analogous to (2.38), which appeared in the study of Langmuir waves, and, as we shall see, the similarity in not only in the appearance but they also produce similar sets of (countably infinitely many) solutions. The difference is that, because of the term involving $\widetilde{v}_b$, the set of solutions of (4.28) is not symmetric with respect to the imaginary axis and that for some values of the parameters C_a, τ, and $\widetilde{v}_b$, (4.28) can have one unstable solution, while, as we already know, all solutions of (2.38) lie in the lower half of the complex $\widetilde{\omega}$-plane. One easy way to find the solutions of (4.28) would be to proceed as in section 2.2 and to draw a contour plot of the absolute value of the function on the left-hand side, which we will do later in this subsection.

Before this we elaborate a little more on (4.24). The principal value integral can be viewed as a complex valued function of the complex argument $\widetilde{\omega}_V$ and we will split it into real and imaginary part in order to gain some insights into this mathematical expression. Since the two integrals are of the same type, we treat only the first one:

$$g(\widetilde{\omega}_V) := p.v. \int_{-\infty}^{+\infty} \frac{\widetilde{v}e^{-\widetilde{v}^2/2}}{\widetilde{v} - \widetilde{\omega}_V/\widetilde{k}} d\widetilde{v} = p.v. \int_{-\infty}^{+\infty} \frac{\widetilde{v}(\widetilde{v} - \widetilde{\omega}_V^*/\widetilde{k})e^{-\widetilde{v}^2/2}}{|\widetilde{v} - \widetilde{\omega}_V/\widetilde{k}|^2} d\widetilde{v} =$$

$$= p.v. \int_{-\infty}^{+\infty} \frac{\widetilde{v}(\widetilde{v} - \widetilde{\omega}_{Vr}/\widetilde{k})e^{-\widetilde{v}^2/2}}{|\widetilde{v} - \widetilde{\omega}_V/\widetilde{k}|^2} d\widetilde{v} + i\frac{\widetilde{\omega}_{Vi}}{\widetilde{k}} p.v. \int_{-\infty}^{+\infty} \frac{\widetilde{v}e^{-\widetilde{v}^2/2}}{|\widetilde{v} - \widetilde{\omega}_V/\widetilde{k}|^2} d\widetilde{v}, \quad (4.29)$$

where the asterisk denotes complex conjugation and $\widetilde{\omega}_{Vr,i}$ denote the real and imaginary part of $\widetilde{\omega}$, respectively. From the above computation it follows immediately that $g^*(\widetilde{\omega}_V) = g(\widetilde{\omega}_V^*)$. At this point we may tend to think that the above conclusion was obvious. However, it is noteworthy that at first sight such a simple relation seems obvious also when we do the integral in question along the Landau contour but such a conclusion would be wrong. In the case of the Landau prescription the integral is related to the plasma dispersion function via (4.26) and Z does not have this simple property when complex conjugated but instead $Z(\xi^*) = -Z^*(-\xi)$ [1]. A completely analogous computation leads to the same result for the second integral, which we will denote by $g_\tau(\widetilde{\omega}_V)$, namely that $g_\tau^*(\widetilde{\omega}_V) = g_\tau(\widetilde{\omega}_V^*)$. In terms of this notation (4.24) can be rewritten as

$$\widetilde{k}\sqrt{2\pi} + C_a g(\widetilde{\omega}_V) + (1 - C_a)\tau^{3/2} g_\tau(\widetilde{\omega}_V) = 0. \quad (4.30)$$

Taking the complex conjugate of both sides and using the relations we just derived, we arrive at

$$\widetilde{k}\sqrt{2\pi} + C_a g(\widetilde{\omega}_V^*) + (1 - C_a)\tau^{3/2} g_\tau(\widetilde{\omega}_V^*) = 0, \quad (4.31)$$

which means that, if $\widetilde{\omega}_V$ is a solution of (4.24), then so is $\widetilde{\omega}_V^*$. In other words, the discrete part of the Van Kampen spectrum possesses a mirror symmetry with respect to the real axis. Since the whole spectrum consists of the union of the continuous part situated on the real line and the discrete part given by (4.24), then this mirror symmetry applies to the whole Van Kampen spectrum but is absent for the set of Landau solutions $\widetilde{\omega}_L$.

Last, we derive analytically another interesting property of the solutions of (4.24) and (4.28). For this we go back to the definition of the Landau contour. It is constructed in such a way that the integration path goes from $-\infty$ to $+\infty$ and encircles the poles of the integrand in the anticlockwise direction if they lie on the real line or in the lower half plane as shown in Figure 2.1. In the problem under consideration, the integrands in (4.24) and (4.28) have only one pole, namely $\widetilde{v} = \frac{\widetilde{\omega}_{V,L}}{\widetilde{k}}$. If there are solutions of the equations with positive imaginary part (that in our convention corresponds to instability), then both the Cauchy principal value and the Landau contour reduce to a normal integration along the real line, since in that case the position of the pole resolves all ambiguities. From this, it follows immediately that the unstable solutions of (4.24) and (4.28) are the same.

For a numerical evaluation of (4.28) we use the same idea as outlined in section 2.2 (implemented in MATLAB with the program *bump_landau.m* shown in the Appendix) which

gives us a contour plot of the absolute value of the left-hand side of the equation. Here the corresponding function was also evaluated on a quadratic grid with the resolution of $\Delta\widetilde{\omega} = 0.001$ and 5 contours have been drawn on equidistant heights from 0 to 0.02.
For numerical reproduction of the Van Kampen spectrum we again discretize the velocity axis as described extensively in subsection 4.1.1. The only difference here lies in the form of G, namely

$$G(\widetilde{v}) = -\frac{C_a\widetilde{v}}{\sqrt{2\pi}}e^{-\widetilde{v}^2/2} - \frac{(1-C_a)\tau^{3/2}(\widetilde{v}-\widetilde{v}_b)}{\sqrt{2\pi}}e^{-\tau(\widetilde{v}-\widetilde{v}_b)^2/2}. \tag{4.32}$$

The corresponding spectrum is shown in Figure 4.8 (produced with the programs *bump.m* and *landau_bump.m* that can be found in the Appendix) together with a contour plot of the Landau solutions and the numerical parameters ($\widetilde{k}$, $\widetilde{v}_{max}$, $\Delta\widetilde{v}$, C_a, $\widetilde{v}_b$ and τ) needed to reproduce them. The Van Kampen eigenvalues are indicated by blue crosses.

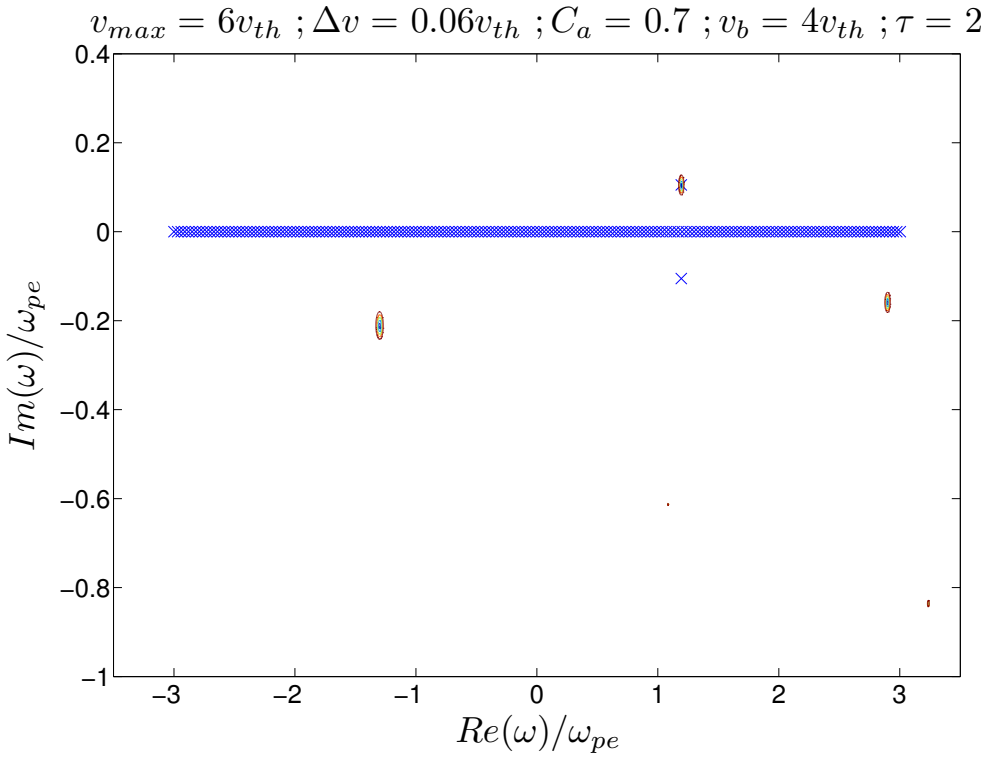

Figure 4.8: Landau solutions and Van Kampen spectrum for the case of 'bump-on-tail' instability ($\widetilde{k} = 0.5$).

One sees immediately that our numerical scheme preserves the symmetry of the spectrum, which we derived analytically. This fact can be understood easily. For this one should recall the form of the matrix M defined in (4.9). The first two terms represent the multiplication operator A_0 analysed in chapter 3 and all the parameters in front of the matrices I and B are, of course, real. By the transition from Langmuir waves to the 'bump-on-tail'

distribution only the last term has changed its particular form but, as a derivative of the real function $\widetilde{f}_0(\widetilde{v})$, it is still real. Therefore, all elements in M are real numbers. The eigenvalues of M, the set of which is intended to serve as an approximation of the Van Kampen spectrum, are determined as solutions of the polynomial equation

$$\det(M - \widetilde{\omega}_V I) = 0. \tag{4.33}$$

Since all elements of M are real, it follows that also all coefficients in the polynomial $\det(M - \widetilde{\omega} I)$ (formed via multiplications and additions/subtractions of elements of M) are real. In this case it is clear that, if $\widetilde{\omega}_V$ is a solution of (4.33), then so is $\widetilde{\omega}_V^*$. In other words, our numerical scheme, based on discretization of the velocity axis, preserves the symmetry of the continuous equations, that we are trying to approximate. Since this is not always the case in numerics, this observation help us gain even more confidence in our approach. Another feature of our numerical evaluation, that is clearly seen in Figure 4.8, is that the position of the unstable Van Kampen eigenvalues seem to coincide with the position of the unstable Landau solutions as we already predicted analytically. This result can be verified more precisely. Since we have already computed the exact position of the unstable Van Kampen eigenvalue, we only need the exact position of the unstable Landau solution on the complex plane. From the contour plot we can derive the value of $\widetilde{\omega}_L$ with practically arbitrary precision (up to the computer limit, of course). For the unstable solution one finds numerically

$$\widetilde{\omega}_V \approx 1.194 + 0.105i \quad ; \quad \widetilde{\omega}_L \approx 1.194 + 0.104i. \tag{4.34}$$

These frequencies have been computed with almost the same parameters as those used to produce Figure 4.8. The only change, that has been made, was that for the sake of better precision the number of points on the velocity axis was set to 2000. This comparison demonstrates that our numerical analysis reproduces the analytical results quite well. The minor difference in the imaginary parts of the two solutions, which is on the order of 10^{-3}, is most probably due to the numerical resolution in velocity space which is good but nevertheless finite.

After this quick mathematical analysis of the 'bump-on-tail' instability, it is worth to elaborate on its physical meaning. In section 2.1 we discussed a simplified model of the interaction between an electrostatic wave and a plasma. We discovered that the collisionless damping is a resonant effect and that it depends on the slope of $\widetilde{f}_0(\widetilde{v})$ at the point that corresponds to the wave frequency. For a centred Gauss curve it was not possible to have an energy transfer from the particles to the wave because the derivative of the Gauss function has always the opposite sign of the argument for which it is taken and, therefore, the product $v_0 \, \partial f_0/\partial v|_{v=v_0}$ is always negative. However, in the case of two combined Maxwell distributions, like here, there can be some set of parameters for which this product is positive. Such a situation is shown in Figure 4.9. In the interval between the two red dashed lines the derivative of the function and its argument at the corresponding point have the same signs which is a necessary condition for an instability. If there is an electrostatic wave in the plasma with frequency and wave number such that $\widetilde{\omega}/\widetilde{k}$ lie in the interval

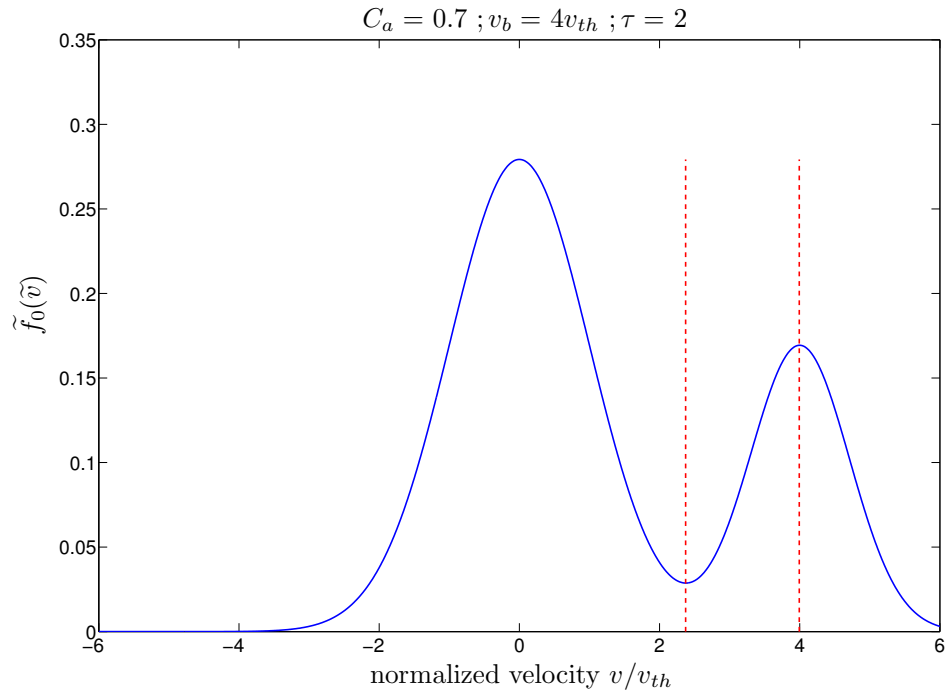

Figure 4.9: Background distribution function $\widetilde{f}_0(\widetilde{v})$ in the case of 'bump-on-tail' instability.

limited by the red lines, then the wave decelerates more particles than is accelerates and, thus, gains energy which is equivalent to an instability. For these parameters the frequency of the instability in Figure 4.8 corresponds to a phase velocity that is at the beginning of this interval.

4.2 Introducing collision operators

In this section we go one step further toward a better physical model by introducing collisions into our system. Since we are working with a one dimensional system, there are not many choices available. The reason for this is that only few collision operators can be formulated in one dimension.

4.2.1 Krook model

The first collision operator which we introduce is the so called Bhatnagar-Gross-Krook collision operator introduced in [17] which in mathematical terms is given by

$$\left(\frac{\partial f}{\partial t}\right)_{col} = -\nu(f(z,v,t) - f_0(v)), \tag{4.35}$$

where ν is the collision frequency. This is a very simple and minimalistic model for collisions. One can easily see (by computing the 0th, 1st and 2nd velocity moment of (4.35)) that this collision operator satisfies neither particle, nor momentum, nor energy conservation which are fundamental physical constraints. However, because of its simple form, it is widely used in plasma physics and especially in fluid theory and often allows physical insights into the role of collisions. Therefore, we are going to use it and see how it alters our system.
Recalling (2.3), it is immediately clear that this collision operator is proportional to $f_1(z, v, t)$. A natural normalization for ν would be the plasma frequency ω_{pe}. With this, the normalized and linearised Boltzmann equation reads

$$\frac{\partial \widetilde{f}_1}{\partial \widetilde{t}} + \widetilde{v}\frac{\partial \widetilde{f}_1}{\partial \widetilde{z}} - \widetilde{E}(\widetilde{z}, \widetilde{t})\frac{\partial \widetilde{f}_0}{\partial \widetilde{v}} = -\widetilde{\nu}\widetilde{f}_1(z, v, t), \tag{4.36}$$

where the electric field is again determined by (2.13). In order to solve this equation together with (2.13) we make a Fourier transform of both equations in space and in time by using the same conventions as in (2.14) and (2.49). This leads to

$$(\widetilde{\omega} - i\widetilde{\nu})\widehat{\widetilde{f}}_1(\widetilde{k}, \widetilde{v}, \widetilde{\omega}) = \widetilde{k}\widetilde{v}\widehat{\widetilde{f}}_1(\widetilde{k}, \widetilde{v}, \widetilde{\omega}) - \frac{1}{\widetilde{k}}\frac{\partial \widetilde{f}_0}{\partial \widetilde{v}}\int_{-\infty}^{+\infty} \widehat{\widetilde{f}}_1(\widetilde{k}, \widetilde{v}, \widetilde{\omega})d\widetilde{v}. \tag{4.37}$$

This is an eigenvalue equation from the same type as (2.50). The only difference is that the normalized frequency on the right is modified by the term $i\widetilde{\nu}$. Nevertheless, the mathematical problem consists in finding the eigenvalues of the linear operator on the right-hand side of (4.37) and this operator is the same as in (2.50), so we already know that its spectrum is the entire real line, i.e., $\widetilde{\omega}^* := \widetilde{\omega} + i\widetilde{\nu}$ is real. This immediately leads to the conclusion that the imaginary part of $\widetilde{\omega}$ equals $-i\widetilde{\nu}$. In other words, the effect of the Bhatnagar-Gross-Krook collision operator on our simple system was to shift the whole Van Kampen spectrum shown in Figure 4.1 downwards by $\widetilde{\nu}$. This means that now all Van Kampen modes are individually damped by a damping rate of $\widetilde{\nu}$ which adds to the Landau damping. One can also easily compute the electric field in this model and produce a plot that is analogous to the one in Figure 4.4. The only difference will be that the collision frequency will accelerate the damping such that the new growth rate will be $Im(\widetilde{\omega}_L) - \widetilde{\nu}$.

4.2.2 Lenard-Bernstein model

In this subsection, we consider another type of collision operator named after A. Lenard and I. B. Bernstein that can also be formulated in a one-dimensional velocity space. To the best of our knowledge it has been applied to one-dimensional Langmuir waves for first time in [18]. However, this subsection was inspired primarily by [15] where the authors show that in this model the Van Kampen spectrum is altered profoundly. In this subsection this claim is tested with a different numerical scheme and after confirming their result we make and additional step and investigate which part of the collision operator is responsible for

the qualitative changes observed.
The linearised Lenard-Bernstein collision operator is given by

$$\left(\frac{\partial f}{\partial t}\right)_{col,1} = \nu f_1(z,v,t) + \nu v \frac{\partial f_1(z,v,t)}{\partial v} + \nu v_{th}^2 \frac{\partial^2 f_1(z,v,t)}{\partial v^2}, \tag{4.38}$$

where ν is again the collision frequency which in this model is taken to be independent of the particle velocity. The collision operator introduced in (4.38) has important advantages from a physical point of view compared to (4.35). It conserves the number of particles, satisfies the H theorem, and preserves the velocity space diffusion which also characterizes the more comprehensive Fokker-Planck collision operator. This model of introducing collisional effects in our system fulfils some fundamental physical constraints and is therefore much more realistic than the one considered in subsection 4.2.1. The normalization of (4.38) using the quantities defined in (2.11) is straightforward and one arrives at

$$\frac{\partial \widetilde{f}_1}{\partial \widetilde{t}} + \widetilde{v}\frac{\partial \widetilde{f}_1}{\partial \widetilde{z}} - \widetilde{E}(\widetilde{z},\widetilde{t})\frac{\partial \widetilde{f}_0}{\partial \widetilde{v}} = \widetilde{\nu}\left(\widetilde{f}_1(\widetilde{z},\widetilde{v},\widetilde{t}) + \widetilde{v}\frac{\partial \widetilde{f}_1(\widetilde{z},\widetilde{v},\widetilde{t})}{\partial \widetilde{v}} + \frac{\partial^2 \widetilde{f}_1(\widetilde{z},\widetilde{v},\widetilde{t})}{\partial \widetilde{v}^2}\right) \tag{4.39a}$$

$$\frac{\partial \widetilde{E}(\widetilde{z},\widetilde{t})}{\partial \widetilde{z}} = -\int_{-\infty}^{+\infty} \widetilde{f}_1(\widetilde{z},\widetilde{v},\widetilde{t})d\widetilde{v}. \tag{4.39b}$$

We approach this system of equations in the same way as we did in the previous cases: through a Fourier transformation in space and time according to (2.14) and (2.49). This allows us to substitute the transformed second equation into the first one, so we are left with

$$\widetilde{\omega}\widehat{\widetilde{f}}_1 = \widetilde{k}\widetilde{v}\widehat{\widetilde{f}}_1 - \frac{1}{\widetilde{k}}\frac{\partial \widetilde{f}_0}{\partial \widetilde{v}}\int_{-\infty}^{+\infty} \widehat{\widetilde{f}}_1(...,\widetilde{v},...)d\widetilde{v} + i\widetilde{\nu}\left(\widehat{\widetilde{f}}_1 + \widetilde{v}\frac{\partial \widehat{\widetilde{f}}_1}{\partial \widetilde{v}} + \frac{\partial^2 \widehat{\widetilde{f}}_1}{\partial \widetilde{v}^2}\right). \tag{4.40}$$

This equation can also be viewed as an eigenvalue equation where the right-hand side of (4.40) represents a linear operator acting on $\widehat{\widetilde{f}}_1(\widetilde{k},\widetilde{v},\widetilde{\omega})$. The first part of this operator is the one defined in (3.1) as A which we already analysed thoroughly in 3. The second part, proportional to the collision frequency, can be viewed as a perturbation of A which we will denote by $i\widetilde{\nu}P$. With this notation (4.40) can be written as

$$\widetilde{\omega}\widehat{\widetilde{f}}_1(\widetilde{k},\widetilde{v},\widetilde{\omega}) = ((A + i\widetilde{\nu}P)\widehat{\widetilde{f}}_1)(\widetilde{k},\widetilde{v},\widetilde{\omega}). \tag{4.41}$$

In order to solve the problem via the Van Kampen approach we have to find the spectrum of the perturbed operator $A+i\widetilde{\nu}P$. In principle, we can try to find the corresponding resolvent operator $R(\widetilde{\omega}, A+i\widetilde{\nu}P)$ and then search for its poles. When we have the poles, we can then study how the spectrum changes in the limit $\widetilde{\nu} \to 0$. However, because of the complicated form of the operator which involves a multiplication, integral and differential operators,

such an approach is not straightforward in this case. Instead, we will approach the problem numerically by again discretizing the velocity axis which will turn the continuous operator into a matrix and then find the eigenvalues, the set of which is the Van Kampen spectrum, of this matrix numerically. At first sight, it might look obvious that in the limit $\widetilde{\nu} \to 0$ one should recover the usual continuous Van Kampen spectrum consisting of the entire real line. Nevertheless, this naive way of thinking would be correct only if the resolvent $R(\widetilde{\omega}, A + i\widetilde{\nu}P)$ is a continuous function of $\widetilde{\nu}$ (or at least continuous in some small interval around $\widetilde{\nu} = 0$). We cannot be certain of that, since we do not know how $R(\widetilde{\omega}, A + i\widetilde{\nu}P)$ looks like. Our numerical evaluation will show that indeed the limit $\widetilde{\nu} \to 0$ is non-trivial which suggests a discontinuity of the resolvent operator at $\widetilde{\nu} = 0$. From a physical point of view this means that collisions, no matter how small the collision frequency, alter the system profoundly (at least when modelled using the Lenard-Bernstein collision operator). Since we already derived a matrix approximation for A, we now have to consider only the perturbation P. The first part of it is just the identity operator, for which we use, of course, the identity matrix. For a discrete implementation of the first and second derivatives we use a centred scheme given by

$$\left(\frac{\partial \widehat{\widetilde{f}}_1}{\partial \widetilde{v}}\right)_j = \frac{F_{j+1} - F_{j-1}}{2\Delta\widetilde{v}} \; ; \; \left(\frac{\partial^2 \widehat{\widetilde{f}}_1}{\partial \widetilde{v}^2}\right)_j = \frac{F_{j+1} - 2F_j + F_{j-1}}{\Delta\widetilde{v}^2}, \tag{4.42}$$

where the vector $\vec{F}$ is the discrete representation of $\widehat{\widetilde{f}}_1(\widetilde{k}, \widetilde{v}, \widetilde{\omega})$ when $\widetilde{v} \to \widetilde{v}_j$ and is defined in subsection 4.1.1. The vector $\{F_{j+1}\}$ can be produced from $\vec{F}$ by shifting its components one position upwards:

$$X_{+1} \cdot \vec{F} := \begin{pmatrix} 0 & 1 & 0 & \cdots & 0 \\ 0 & 0 & 1 & \cdots & 0 \\ \vdots & \vdots & \vdots & \ddots & \vdots \\ 0 & 0 & 0 & \cdots & 1 \\ 0 & 0 & 0 & \cdots & 0 \end{pmatrix} \begin{pmatrix} F_1 \\ F_2 \\ F_3 \\ \vdots \\ F_{N+1} \end{pmatrix} = \begin{pmatrix} F_2 \\ F_3 \\ \vdots \\ F_{N+1} \\ 0 \end{pmatrix}, \tag{4.43}$$

where we have erased F_1. It is noteworthy that the last component of the new vector is set to zero. From a physical point of view, however, it is clear that $\widehat{\widetilde{f}}_1$ does not fall to zero for $\widetilde{v} > \widetilde{v}_{max}$ but from our previous analysis we know that $\widehat{\widetilde{f}}_1 \to 0$ for $|\widetilde{v}| \to +\infty$ since the integral $\int_{-\infty}^{+\infty} |\widehat{\widetilde{f}}_1| d\widetilde{v}$ has to converge. For this to be true $\widehat{\widetilde{f}}_1$ has to decrease rapidly enough when $\widetilde{v}$ increases. In order to make our statements a little more precise we write the discrete form of the previous integral but this time with 0 and $+\infty$ as limits of integration, which does not influence the conclusions we are about to make:

$$\int_0^{+\infty} |\widehat{\widetilde{f}}_1| d\widetilde{v} \to \Delta\widetilde{v} \sum_{j=1}^{\infty} |F_j| < \infty. \tag{4.44}$$

For this to be true the condition $\lim_{j\to\infty} \frac{|F_{j+1}|}{|F_j|} < 1$ must hold which implies that, for j sufficiently large, $|F_{j+1}| < |F_j|$. Recalling (4.42), it also follows that for large j

$$\left| \left(\frac{\partial \widehat{\widetilde{f}}_1}{\partial \widetilde{v}} \right)_j \right| = \frac{|F_{j+1} - F_{j-1}|}{2\Delta\widetilde{v}} \leq \frac{|F_{j-1}|}{\Delta\widetilde{v}}, \tag{4.45}$$

which means that our centred equidistant derivative should fall for large $\widetilde{v}$ at least as rapidly as $\widehat{\widetilde{f}}_1$. This means that setting the last component in the vector on the right-hand side of (4.43) to zero is a small mistake if N is sufficiently large. Thus, the discretized derivatives in matrix notation can be written as

$$\frac{\partial \widehat{\widetilde{f}}_1}{\partial \widetilde{v}} \to \frac{1}{2\Delta\widetilde{v}}(X_{+1} - X_{-1}) \cdot \vec{F} \; ; \tag{4.46}$$

$$\frac{\partial^2 \widehat{\widetilde{f}}_1}{\partial \widetilde{v}^2} \to \frac{1}{\Delta\widetilde{v}^2}(X_{+1} - 2I + X_{-1}) \cdot \vec{F} \; , \tag{4.47}$$

where I is the identity matrix of dimension $N+1$ and X_{-1} is defined as

$$X_{-1} := \begin{pmatrix} 0 & 0 & \cdots & 0 & 0 \\ 1 & 0 & \cdots & 0 & 0 \\ 0 & 1 & \cdots & 0 & 0 \\ \vdots & \vdots & \ddots & \vdots & \vdots \\ 0 & 0 & \cdots & 1 & 0 \end{pmatrix}. \tag{4.48}$$

The first derivative in the expression for P is multiplied by $\widetilde{v}$. In subsection 4.1.1 we saw that in the discrete case this is achieved by a multiplication with the matrix $-\widetilde{v}_{max}\frac{(N+2)}{N}I + \Delta\widetilde{v}B$ with B defined as in the corresponding subsection. Therefore, the matrix approximation of (4.41) can be written as

$$\widetilde{\omega}\vec{F} = \left[M + i\widetilde{\nu} \left(I + \frac{1}{2\Delta\widetilde{v}} \left(-\widetilde{v}_{max}\frac{(N+2)}{N}I + \Delta\widetilde{v}B \right) \cdot (X_{+1} - X_{-1}) + \right. \right.$$
$$\left. \left. + \frac{1}{\Delta\widetilde{v}^2}(X_{+1} - 2I + X_{-1}) \right) \right] \cdot \vec{F} =: M_\nu \cdot \vec{F}, \tag{4.49}$$

where M is defined in (4.9). This matrix eigenvalue equation can be implemented easily using MATLAB. Four results of such an implementation for $\widetilde{\nu} = 0.01$, achieved with the program *Lenard_Bernstein.m* which can be found in the Appendix, are shown in Figure 4.11. One sees that all Van Kampen modes (represented by blue crosses) lie in the lower half of the complex $\widetilde{\omega}$-plane, i.e., they are damped. If we try to investigate the limit $\widetilde{\nu} \to 0$ by just computing this spectrum for smaller and smaller $\widetilde{\nu}$ without changing the size of the matrix on the right-hand side of (4.49), then the result would be that all eigenvalues

of the collisional spectrum will tend to the real axis. This can be easily understood as follows. The numerical Van Kampen eigenvalues are defined as the solutions of the equation $\det(M_\nu - \widetilde{\omega} I) = 0$. From the definition of M_ν in (4.49) it is clear that all elements of this matrix are analytic functions of $\widetilde{\nu}$ which implies that also all coefficients of the polynomial $\det(M_\nu - \widetilde{\omega} I)$ are analytic functions of the collision frequency. In this case one can be certain [6, p. 4, Theorem XII.2] that the position of the eigenvalues is a continuous function of $\widetilde{\nu}$. More precise, if for a given value $\widetilde{\nu}_0$ there is an eigenvalue, say $\widetilde{\omega}_0$, with multiplicity m, then for $\widetilde{\nu}_1$ close to $\widetilde{\nu}_0$ there are going to be eigenvalues in the immediate vicinity of $\widetilde{\omega}_0$ and the sum of their multiplicity is m. However, such a limit, although reasonable from a mathematical point of view, does not reproduce the right physics. We already know that the Van Kampen modes in the collision free case involve a delta function in velocity space. This means that for $\widetilde{\nu} = 0$ there exist arbitrary small structures in velocity space.

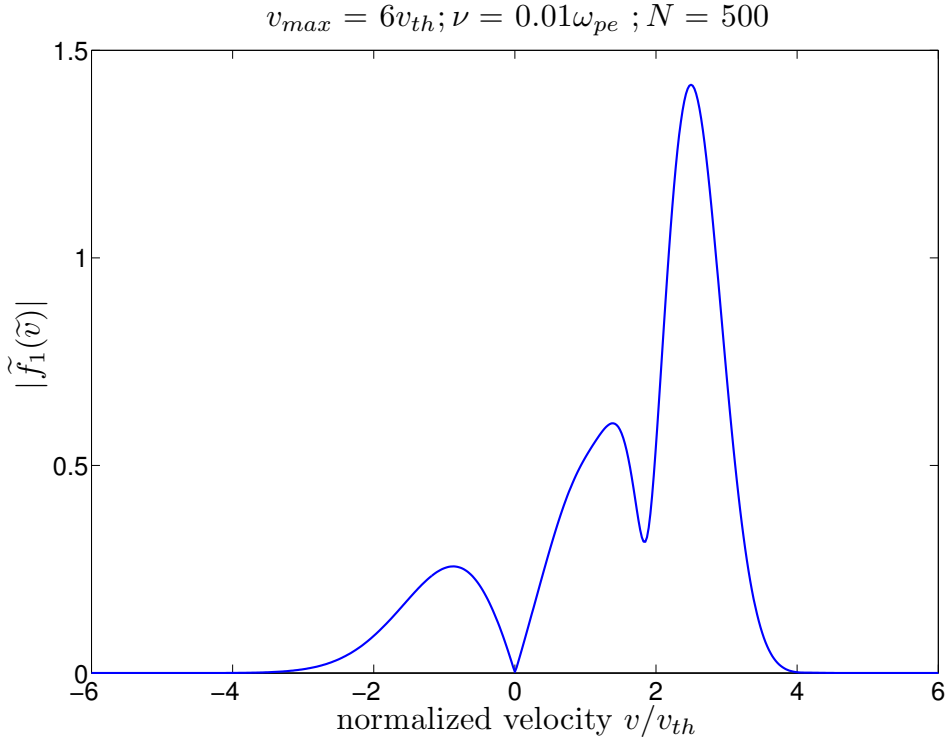

Figure 4.10: Typical eigenvector corresponding to the discretized form of $A + i\widetilde{\nu}P$.

If collisions are present in our model, they make the eigenfunctions smooth with respect to the velocity [16]. When the collision frequency tends to zero, the structures in velocity space get smaller. In order to make physically meaningful conclusions, we must be able to resolve these structures, i.e., we must increase the numerical resolution in velocity space (i.e., number of points in the interval $[-v_{max}, v_{max}]$) when we decrease $\widetilde{\nu}$. Therefore, one should always change the operator while performing the limit $\widetilde{\nu} \to 0$. This has to be done in such a way that the resolution is always sufficiently high. First we should give 'sufficiently high' a more precise explanation. As already mentioned, for $\widetilde{\nu} = 0$ the eigenfunction of the

corresponding continuous operator consist of a delta function. When collisions are included into the system, they tend to 'smear' out the delta functions and make the eigenfunctions smooth. So instead of a singularity at a particular $\widetilde{v}$, we have smooth peaks, as shown in Figure 4.10, that get sharper when the collision frequency tends to zero. A reasonable condition for sufficient resolution, to which we shall from now on adhere, would be to always have at least 10 points under the sharpest peak of the eigenfunction.

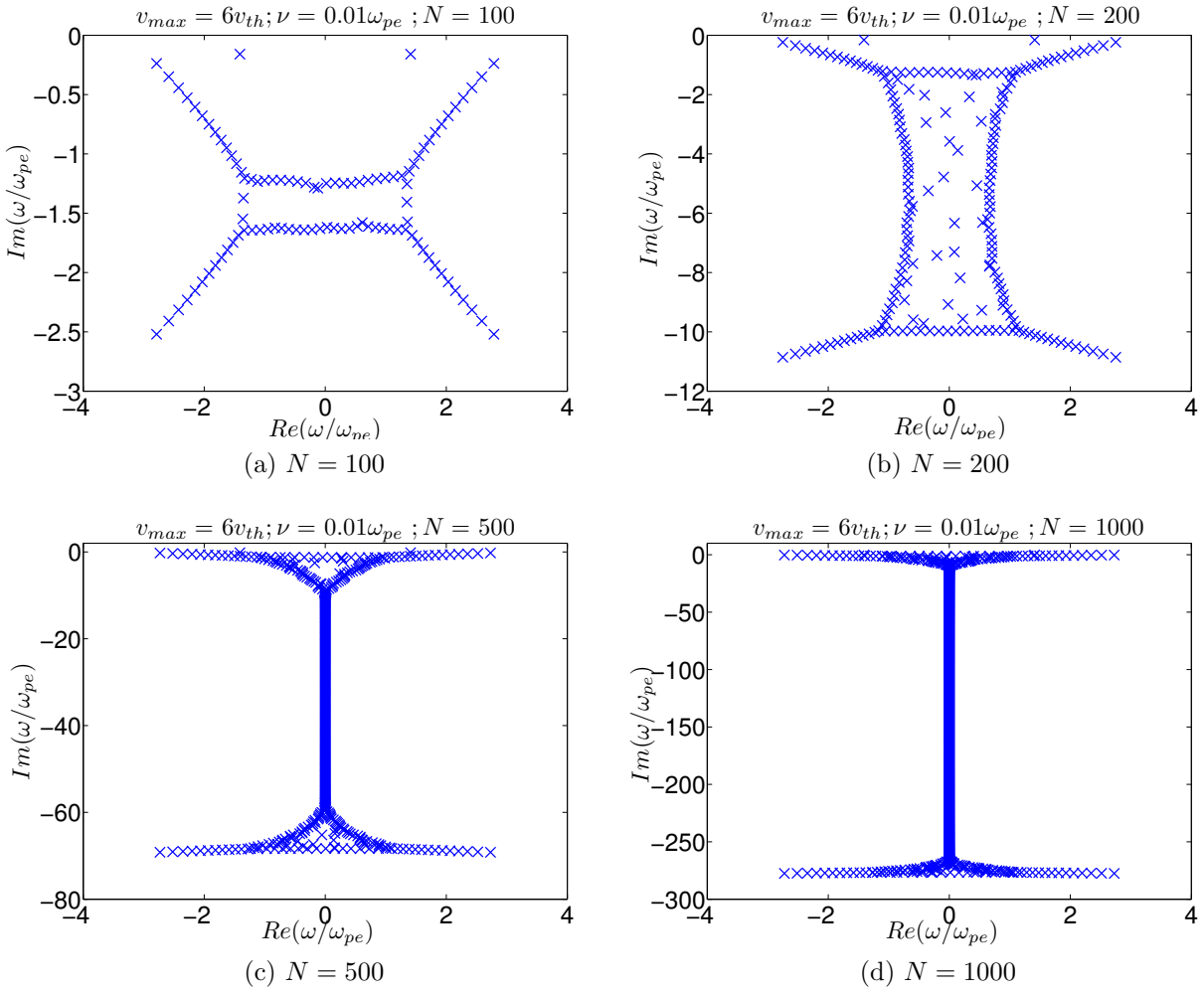

(a) $N = 100$ (b) $N = 200$

(c) $N = 500$ (d) $N = 1000$

Figure 4.11: Van Kampen spectrum with collisions for fixed collision frequency ($\widetilde{\nu} = 0.01$) and different velocity resolution.

Although we are interested in the limit $\widetilde{\nu} \to 0$, it is still useful to see what happens numerically if we fix the collision frequency to some small value and start increasing the resolution in velocity space. Thereby, one gets a global overview of the spectrum of M_ν and also gains some insight into what should happen in the continuous limit which has to reproduce the real operator $A + i\widetilde{\nu}P$. Part of such a limit process is shown on the four plots in Figure 4.11. On the first plot ($N = 100$), one can hardly identify some particular

structure of the spectrum. However, as the resolution is increased, it becomes apparent that the spectrum consists of three different parts. Some of the eigenvalues form two lines which are parallel to the real line. The first such line is just below the real axis and the second one is on the other side of the spectrum and its imaginary part increases nearly quadratically with N. The rest of the eigenvalues form a line on the imaginary $\widetilde{\omega}$-axis that connects the other two groups of eigenvalues. From this global overview of the spectrum, we see also two other distinctive features. First, there are points that separate from the rest of the spectrum and their position appears to be in the vicinity of the two least damped Landau solutions that are shown in Figure 2.3. This foreshadows the correctness of the statement that in the $\nu \to 0$ limit these Van Kampen eigenvalues will tend to the least damped Landau solutions.
Looking at Figure 4.11, one also notices that for fixed resolution, there is always some area in the spectrum where the eigenvalues are distributed stochastically. From the theoretical model it is known [16] that, if $\widetilde{\omega}_r + i\widetilde{\omega}_i$ is an eigenvalue, then so is $-\widetilde{\omega}_r + i\widetilde{\omega}_i$. However, this symmetry is not observed in the central area of the first two plots which leads us to the conjecture that the distribution of eigenvalues there is not physical but is rather due to some numerical effect. Increasing the resolution, this area shrinks and divides into two parts when some of the eigenvalues align on the imaginary axis. When we investigate the limit process of decreasing collision frequency later on, we will ensure that all Landau solutions lie outside this area of stochasticity in order to be certain that no Van Kampen eigenvalues approach a Landau solution randomly. This imposes a lower limit on the resolution in velocity space that is stricter than the one we determined while discussing the form of the eigenfunctions.

Numerical limit $\widetilde{\nu} \to 0$

Now, after we have made ourselves familiar with some general properties of the discretized Van Kampen spectrum, we focus on the issue of the $\nu \to 0$ limit. In order to gain some insight into what happens qualitatively, we have shown in Figure 4.12 the same part of the complex $\widetilde{\omega}$-plane for different collision frequencies. Here the resolution in velocity space has been chosen to satisfy the last convergence condition discussed above. It should be noted also that these plots are produced for $\widetilde{k} = 0.5$. The blue crosses represent again the Van Kampen eigenvalues and the red circles denote the Landau solutions for collisionless plasma. In order to achieve better resolution in velocity space while having the same matrix size, we have taken a smaller interval in velocity space, namely $-4 < \widetilde{v} < 4$. This will be useful when taking the limit $\widetilde{\nu} \to 0$, since it allows us to go to smaller values of the collision frequency with the same computational power.
One sees clearly how two of the Van Kampen eigenvalues get closer and closer to the least damped Landau solutions when the collision frequency decreases. In order to validate this assumption and to make it mathematically more precise, one can compute the absolute value of the difference $\widetilde{\omega}$ between one of the least damped Landau solution (here the one with positive real part) and the corresponding Van Kampen eigenvalue for a set of collision frequencies. The results of such a computation (the blue stars) are shown in

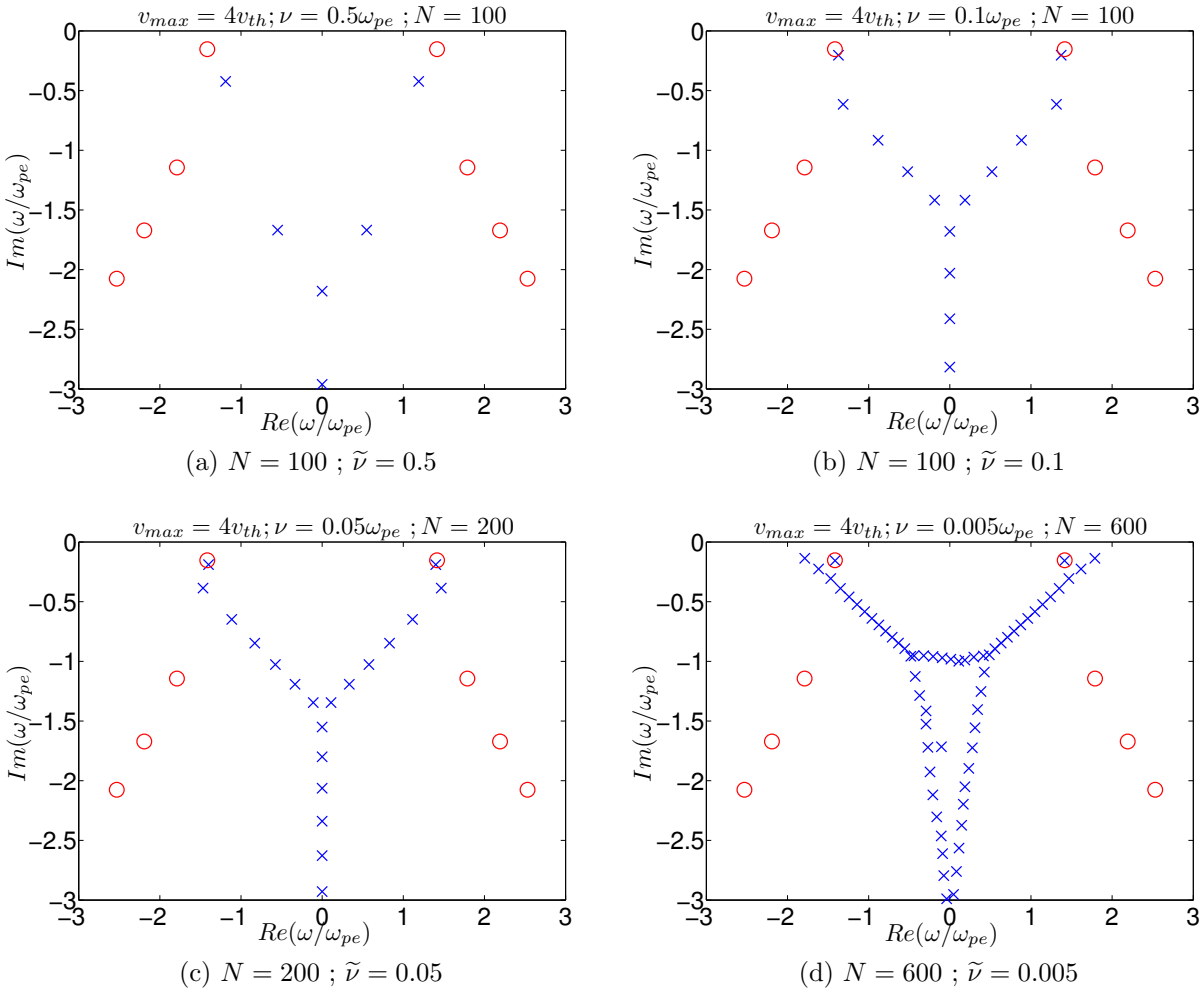

(a) $N = 100$; $\widetilde{\nu} = 0.5$ (b) $N = 100$; $\widetilde{\nu} = 0.1$

(c) $N = 200$; $\widetilde{\nu} = 0.05$ (d) $N = 600$; $\widetilde{\nu} = 0.005$

Figure 4.12: Convergence of Van Kampen eigenvalues (blue crosses) to the two least damped Landau solutions (red circles).

Figure 4.13. From this plot one could suppose a linear dependence of $\Delta\widetilde{\omega}$ on $\widetilde{\nu}$ and this is represented by the dashed blue line which is the linear function $\Delta\widetilde{\omega} = a\widetilde{\nu}$. We have omitted the free term in this parametrization because we want to test the conjecture that two of the Van Kampen eigenvalues tend to the two least damped Landau solutions. With the method of least squares one easily computes that the best such fit corresponds to a slope of $a \approx 0.6801$. However, this conjecture is merely a hypothesis and as such one should also make a mathematically more precise statement about how probable this hypothesis is. A typical choice in this case would be the χ^2-test which here leads to $\chi^2 \approx 6.7 \cdot 10^{-4}$. Such a small value for χ^2 gives us the confidence that for small collision frequencies the Van Kampen eigenvalues tend linearly to the least damped Landau solutions.

Now, after we are convinced that at least for the two least damped collisionless Landau solutions there exist two Van Kampen eigenvalues that tend to those solutions when one

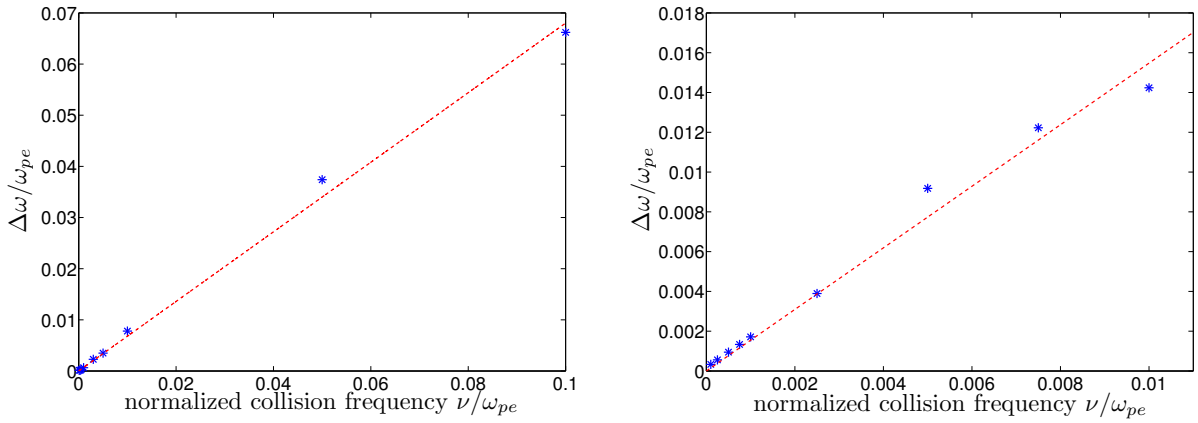

(a) Lenard-Bernstein operator (b) reduced Lenard-Bernstein operator

Figure 4.13: Distance between one of the least damped Landau solutions and the corresponding Van Kampen eigenvalue as a function of collision frequency for the complete (a) and reduced (b) Lenard-Bernstein operator.

decreases the collision frequency, it is interesting to test if some Van Kampen eigenvalues approach also the other Landau solutions. For this we first investigate the same plots like in Figure 4.11 but this time we focus just on the upper part of the complex $\widetilde{\omega}$-plane and plot also the eight least damped Landau solutions for $\widetilde{\nu} = 0$. Such a situation is shown in Figures 4.14. There we have taken a normalized collision frequency of 0.001 because one should expect that the behaviour of interest appears at low $\widetilde{\nu}$. However, the two plots appear to be the same. There is no Van Kampen eigenvalue that approaches the second least damped Landau solution, so, if this is the case, then it should happen at much lower collision frequency. Unfortunately, going to much smaller values of $\widetilde{\nu}$ is numerically expensive and could not be done in the framework of this work. On these two plots it is also evident why we called certain parts of the spectrum areas of stochasticity. One can see an example of such an area in the middle of every plot in the figures. First, there is no particular symmetry in the position of the eigenvalues there. Second, it is noticeable that, although the position of the eigenvalues outside this area does not change, i.e., they have converged, the eigenvalues in the rectangular area in the middle change their position abruptly with changing of N without leaving the area. This observation verifies the correctness of our decision to claim convergence for the purposes of the $\widetilde{\nu} \to 0$ limit process only when all Landau solutions lie outside this area of stochasticity.

Our observations so far seem to verify the statement, to our best knowledge first made in [18], that collisions (at least when modelled using the Lenard-Bernstein collision operator in one dimension) alter the kinetic model profoundly. In chapter 3 we already saw that for Langmuir waves the operator A, that corresponds to a collisionless system, has a spectrum that consists of a continuous part on the entire real line plus (for some values of the parameter $\widetilde{k}$) finitely many discrete eigenvalues, which, however are also real. Af-

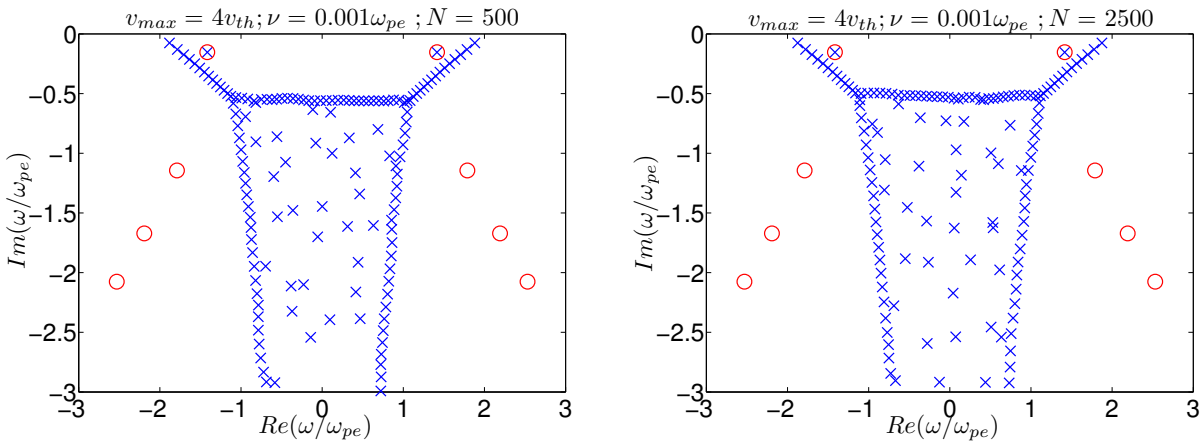

(a) $N = 500$ (b) $N = 2500$

Figure 4.14: Comparison of Van Kampen spectra for fixed collision frequency $\widetilde{\nu} = 0.001$ and different velocity resolution.

ter introducing the collision operator considered in this subsection there are only damped eigenmodes. As we saw in Figure 4.11 the spectrum tends to spread in the lower half of the complex $\widetilde{\omega}$-plane. For fixed collision frequency the most damped eigenvalues have an imaginary part that is proportional to N^2, where N is the number of points in velocity space, so for the continuous case one can assume that there are eigenvalues with arbitrary large damping rate. With the programs that we used to validate the conjecture that two of the Van Kampen eigenvalues tend to the two least damped Landau roots with decreasing collision frequency one can also show that this behaviour is qualitatively independent of the value of $\widetilde{k}$. The same tendency is observed, for example, for $\widetilde{k} = 0.7$, although in this case, as we saw in chapter 3, there is no discrete Van Kampen eigenvalues. This means that it is not the discrete part of the Van Kampen spectrum that approaches the Landau roots. Therefore, one could feel tempted to conjecture that introduction of collisions makes the whole Van Kampen spectrum discrete.

The analysis done so far reinforces the claim that the limit $\widetilde{\nu} \to 0$ is non-trivial and even a small collision frequency alters the Van Kampen spectrum completely. Now one has to find the reason for this surprising behaviour of the eigenvalues. It could be conjectured that some eigenmodes have such a structure that they evolve a sharp peak when collision frequency decreases such that the product of the second derivative of the eigenmodes and the collision frequency (the third term in (4.38)) remains constant. For this to happen the second derivative should scale like $1/\widetilde{\nu}$. We will test this conjecture on three different modes: the one that goes to the least damped Landau solution, one in the upper left corner that approaches the real $\widetilde{\omega}$-axis when velocity resolution is increased and one mode from the line of eigenvalues on the lower half of the imaginary axis. Since the second derivative of the eigenvectors is again a vector that also has complex arguments, we are going to

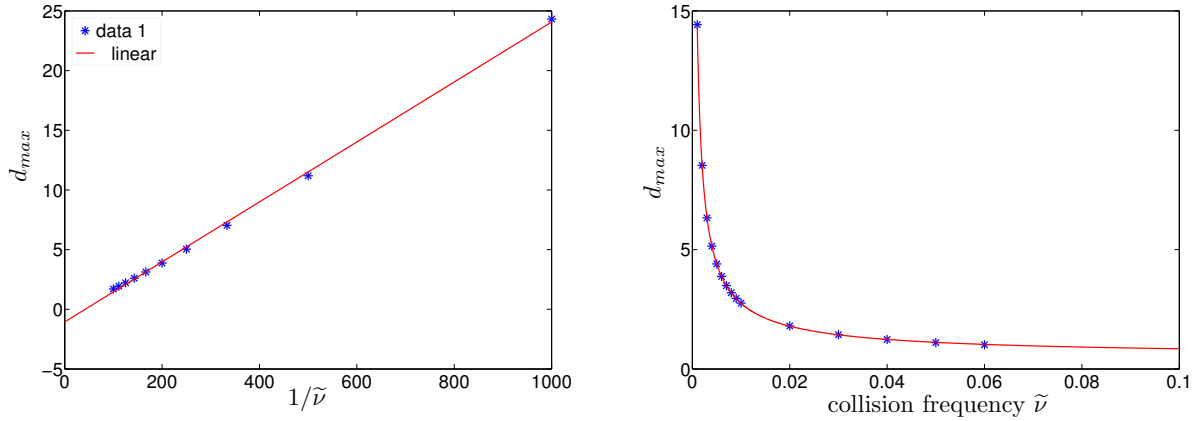

(a) Mode closest to the least damped Landau solution. (b) Mode in the upper left corner of the spectrum.

Figure 4.15: Scaling of the second derivative of different modes with respect to collision frequency.

consider its component with the largest absolute value. If one makes this computation, one notes that the result (the maximum of the absolute value of second derivative, which we will call d_{max} for convenience) depends on the resolution in velocity space. However, this dependence is such that d_{max} approaches exponentially a constant value. Therefore, we compute d_{max} for 10 different velocity resolutions ($N = 400, 500, 600, ..., 1300$) and then fit the results on a curve parametrized by $d_{max} + e^{-x_1 N + x_2}$. The results that we achieved this way are displayed in Figure 4.15. It is immediately seen that the second derivative of the Van Kampen mode that corresponds to the eigenvalue which tends to one of the least damped Landau solutions scales like $1/\widetilde{\nu}$. For the other mode such a linear approximation did not yield a good result so we fitted the results shown in Figure 4.15 b the function $y_1(1/\widetilde{\nu})^{y_2} + y_3$. The best fit produced the value $y_2 = -0.788$. This means that for this mode the product $\widetilde{\nu} d_{max}$ scales like $\widetilde{\nu}^{0.212}$ and, therefore, goes to zero when $\widetilde{\nu} \to 0$. For the mode on the imaginary axis we could not determine a definitive scaling. This might be due to the difficulty to distinguish individual modes in that part of the spectrum.

Reduced Lenard-Bernstein collision operator

Since we are now certain about the results of the $\widetilde{\nu} \to 0$ limit process, the next question we would like to answer is which part of the Lenard-Bernstein collision operator is responsible for the behaviour observed. The first term in (4.38) is (up to a sign) the Bhatnagar-Gross-Krook collision operator that we have already studied. In subsection 4.2.1 we showed that this operator only shifts the whole Van Kampen spectrum (continuous and discrete part) in the lower half of the complex $\widetilde{\omega}$-plane such that the imaginary part of all new eigenvalues equals $-\widetilde{\nu}$. Therefore, the profound change of the spectrum that we observed should be due to the two other terms in (4.38). However, it is not clear if the given combination of

both terms is necessary to produce such a behaviour of the spectrum in the $\nu \to 0$ limit or if only one of these terms plays an essential role. Our presumption is that the third part of the collision operator, the one involving a second derivative with respect to velocity, is responsible for the abrupt change of the spectrum. In order to test this hypothesis, we remove the second term in (4.38). The discretized version of this reduced Lenard-Bernstein collision operator is given by a matrix (denoted by $M_{\nu,2}$) similar to M_ν that reads

$$M_{\nu,2} := M + i\widetilde{\nu}\left(I + \frac{1}{\Delta\widetilde{v}^2}(X_{+1} - 2I + X_{-1})\right). \tag{4.50}$$

The MATLAB routine that computes and plots the eigenvalues of $M_{\nu,2}$ can be found in the Appendix under the name *Lenard_Bernstein_2*. With it one can produce analogous plots to those in Figure 4.11. This way one sees that the spectrum of $M_{\nu,2}$ shows the same qualitative behaviour as the one of the full matrix M_ν, and this observation is a hint that our conjecture was correct. In order to verify this, we focus on the part of the Van Kampen spectrum that lies in the vicinity of the collisionless Landau roots. Computing the spectrum of $M_{\nu,2}$ for different collision frequencies and resolutions in velocity space, one can note that in this case convergence of the spectrum is achieved at lower resolution than with M_ν. For a collision frequency of 0.01, the spectrum converges already for 501 points on the velocity axis. In Figure 4.16 we show the spectrum of $M_{\nu,2}$ for two different values of the collision frequency but, for the ease of comparison, at the same velocity resolution.

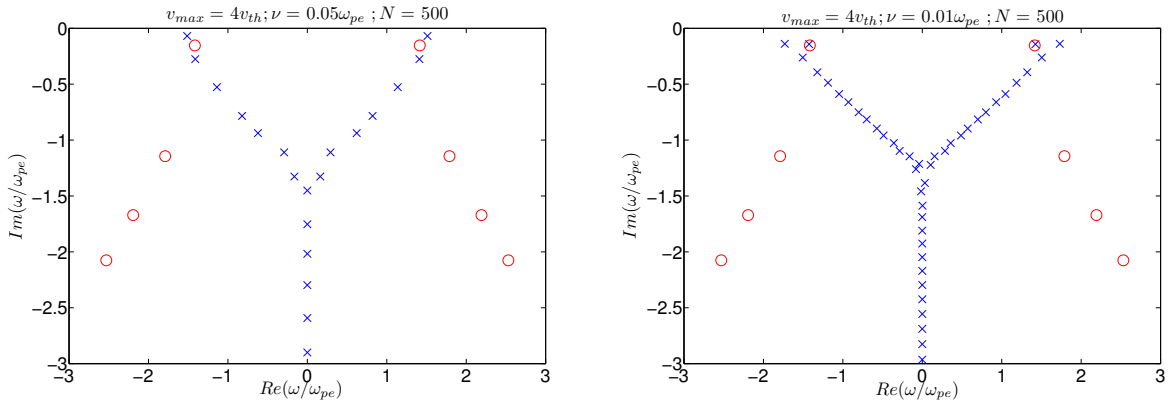

(a) $\widetilde{\nu} = 0.05$ (b) $\widetilde{\nu} = 0.01$

Figure 4.16: Spectrum of $M_{\nu,2}$ for $N = 500$.

One notes that on the second plot we have two Van Kampen eigenvalues that are very close to the two least damped Landau roots which is what we have expected. However, compared to the previous case, this time not the first (viewed from the real line) Van Kampen eigenvalue goes to the Landau root but the second one. In order to make this more clear we show in Figure 4.17 the same part of the spectrum of $M_{\nu,2}$ for different collision frequencies. The resolution is kept fixed ($N = 500$) which means that the number of eigenvalues in the whole spectrum is fixed. Therefore, any changes in the upper part of

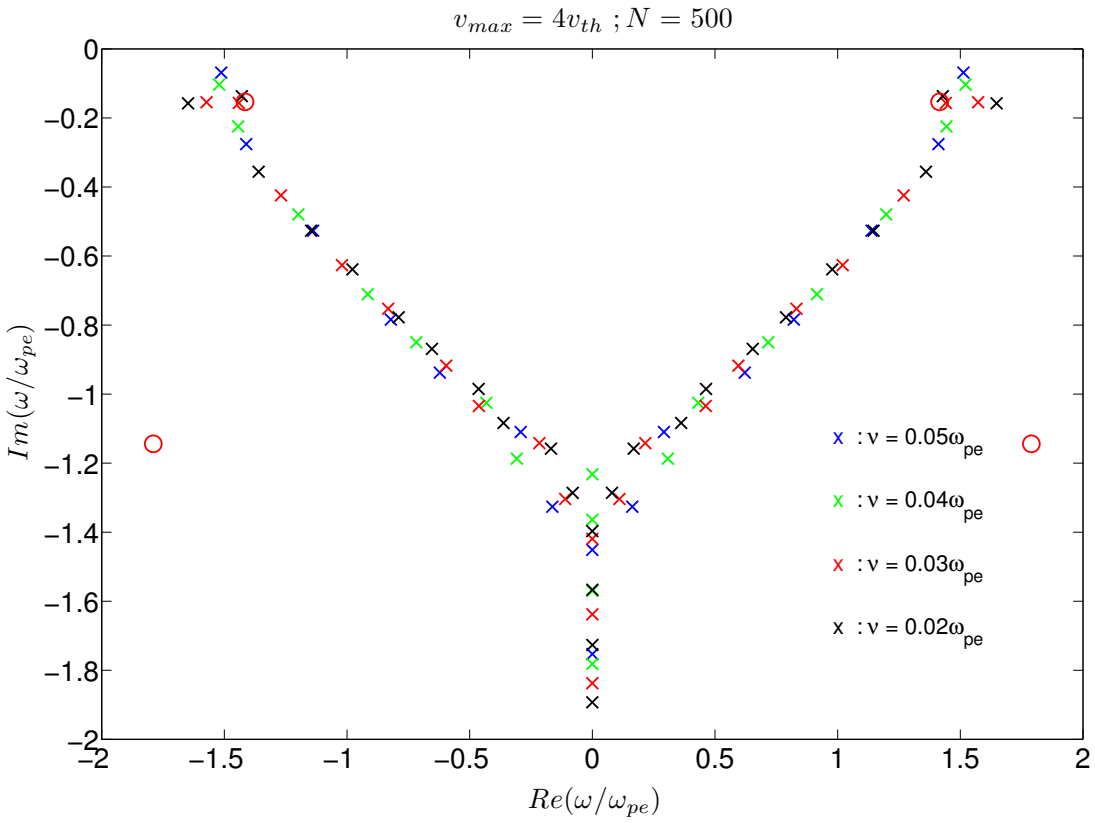

Figure 4.17: Spectrum of $M_{\nu,2}$ for fixed resolution ($N = 500$) and different collision frequencies.

the spectrum are due to movement of the eigenvalues and not to the appearance of new ones. In order to keep track of the development of the spectrum, we have also used different colours for different frequencies. In the beginning ($\widetilde{\nu} = 0.05$) the two least damped Van Kampen eigenvalues are equally far away from the Landau root. By decreasing the collision frequency the imaginary part of the least damped eigenvalues decreases while in the same time they migrate to the outside. On the other hand, the second least damped eigenvalue comes closer to the real line and approaches the least damped Landau root. For mathematically more precise conclusions one can again compute the distance $\Delta\widetilde{\omega}$ between the least damped Landau solution and the Van Kampen eigenvalue that is next to it. As in the previous case, this evaluation should be done when the spectrum has converged and we will use the same definition of convergence like the one used for producing Figure 4.13. This gives us the plot shown in Figure 4.13 b. It is apparent that a linear dependence $\Delta\widetilde{\omega} = a\widetilde{\nu}$ like in the previous case can explain the computational data and the dashed line represents the best linear fit produced by the least squared method. The corresponding coefficient is $a \approx 1.5475$ and the likelihood of this linear fit is from the same order of magnitude like for the full collision operator, namely $\chi^2 \approx 7.6 \cdot 10^{-4}$. A comparison of this result with

the previous one shows that the Van Kampen eigenvalue still approaches the least damped Landau solution but in this case the convergence is more than two times faster, i.e., the second term in (4.38), which we have excluded here, slows down the convergence of the Van Kampen eigenvalue but introduces no qualitative changes in the spectrum. However, one should also note that, in terms of absolute values, the full matrix M_ν gives always a smaller $\Delta\widetilde{\omega}$ for the same velocity resolution and collision frequency (at least for the values that we investigated).

Hermite polynomial representation

After we have seen the effect of collisions modelled via the Lenard-Bernstein collision operator in our numerical scheme we would like to make a small change of the numerical approach. The previous analysis was inspired by [15]. However, in this work the authors do not discretize the velocity space. Instead, the perturbation is expanded in a separate functional basis and the coefficients of the expansion play the role of the isolated points in velocity space used in our numerical scheme. For the analysis that follows, we change the velocity normalization and introduce the new variable u such that $u := \widetilde{v}/\sqrt{2}$. However, in order to facilitate comparison with our previous results in the complex $\widetilde{\omega}$-plane we keep the normalization of the frequency and wave number. With the new variable, (4.40) transforms into

$$\widetilde{\omega}\widehat{\widetilde{f}}_1 = \sqrt{2}\widetilde{k}u\widehat{\widetilde{f}}_1 + \sqrt{\frac{2}{\pi}}\frac{u}{\widetilde{k}}e^{-u^2}\int_{-\infty}^{+\infty}\widehat{\widetilde{f}}_1(\widetilde{k},u',\widetilde{\omega})du + i\widetilde{\nu}\left(\widehat{\widetilde{f}}_1 + u\frac{\partial\widehat{\widetilde{f}}_1}{\partial u} + \frac{1}{2}\frac{\partial^2\widehat{\widetilde{f}}_1}{\partial u^2}\right), \tag{4.51}$$

where we have used the explicit form of the equilibrium distribution function rewritten in the new coordinate. For the perturbation $\widehat{\widetilde{f}}_1$ we write the expansion

$$\widehat{\widetilde{f}}_1(\widetilde{k},u,\widetilde{\omega}) = \sum_{n=0}^{\infty} a_n(\widetilde{k},\widetilde{\omega})b_n(u). \tag{4.52}$$

For this expansion to be applicable, the perturbation should belong to a separable functional space over $\mathbb{R}$ in which the set of functions $\{b_n(u)\}$ forms a complete basis. We follow [15] and choose as basis vectors

$$b_n(u) = \widetilde{H}_n(u)e^{-u^2}, \tag{4.53}$$

where $\widetilde{H}_n(u)$ denotes the normalized nth Hermite polynomial defined as

$$\widetilde{H}_n(u) := \frac{(-1)^n}{\sqrt{2^n n!\sqrt{\pi}}}e^{u^2}\frac{d^n e^{-u^2}}{du^n}. \tag{4.54}$$

One should note that the vectors of the basis $\{b_n(u)\}$ are neither orthogonal to each other nor do they have the same norm. In this notation we have that

$$\int_{-\infty}^{+\infty} \widetilde{H}_n(u)\widetilde{H}_m(u)e^{-u^2}du = \delta_{mn} \; ; \; \frac{d\widetilde{H}_n(u)}{du} = \sqrt{2n}\widetilde{H}_{n-1}(u) \; , \tag{4.55}$$

$$\sqrt{2}u\widetilde{H}_n(u) = \sqrt{n+1}\widetilde{H}_{n+1}(u) + \sqrt{n}\widetilde{H}_{n-1}(u). \tag{4.56}$$

The strategy when working with such an expansion is to use the properties (4.55) in such a way that the sum in every term is the same (e.g., from $n = 0$ to ∞), and $\widetilde{H}_n(u)e^{-u^2}$ appears in every term so it can be factored out. The equation that is left in the brackets gives the connection between different coefficients a_n. This procedure for the first and the collision term is straightforward, therefore we show only the calculation regarding the second expression on the right-hand side of (4.51). The integral gives

$$\int_{-\infty}^{+\infty} \widetilde{\widehat{f}}_1(\widetilde{k},u,\widetilde{\omega})du = \sum_{n=0}^{\infty} \frac{(-1)^n}{\sqrt{2^n n!\sqrt{\pi}}} a_n(\widetilde{k},\widetilde{\omega}) \int_{-\infty}^{+\infty} \frac{d^n e^{-u^2}}{du^n}du =$$

$$= \frac{a_0(\widetilde{k},\widetilde{\omega})}{\sqrt[4]{\pi}} \underbrace{\int_{-\infty}^{+\infty} e^{-u^2}du}_{=\sqrt{\pi}} + \sum_{n=1}^{+\infty} \frac{(-1)^n}{\sqrt{2^n n!\sqrt{\pi}}} a_n(\widetilde{k},\widetilde{\omega}) \underbrace{\left.\frac{d^{n-1}e^{-u^2}}{du^{n-1}}\right|_{-\infty}^{+\infty}}_{\propto e^{-u^2}\big|_{-\infty}^{+\infty}=0} = \sqrt[4]{\pi}a_0(\widetilde{k},\widetilde{\omega}). \tag{4.57}$$

It is worth to make one side remark at this point. We could have chosen the basis vectors b_n as $\widetilde{H}_n e^{-u^2/2}$. In that case the basis $\{b_n\}$ would have been orthonormal but then the integral of $\widetilde{\widehat{f}}_1$ over velocity would not have consisted of only one term proportional to a_0 but it would have included contributions from all coefficients a_n with even index n and this would have made the further analysis more cumbersome. In this case the second term in (4.51) is

$$\sqrt{\frac{2}{\pi}}\frac{u}{\widetilde{\widetilde{k}}}e^{-u^2} \int_{-\infty}^{+\infty} \widetilde{\widehat{f}}_1(\widetilde{k},u',\widetilde{\omega})du' = \frac{1}{\widetilde{\widetilde{k}}} \sum_{n=0}^{\infty} a_{n-1}(\widetilde{k},\widetilde{\omega})\delta_{1n}\widetilde{H}_n(u)e^{-u^2} \tag{4.58}$$

and the recursion relation between the coefficients reads

$$\left(\widetilde{k}\sqrt{n} + \frac{1}{\widetilde{\widetilde{k}}}\delta_{1n}\right) a_{n-1} + \widetilde{k}\sqrt{n+1}a_{n+1} - in\widetilde{\nu}a_n = \widetilde{\omega}a_n. \tag{4.59}$$

One way to evaluate (4.59) and find the set of eigenfrequencies is to write it as a matrix eigenvalue equation in the form

$$\left[\widetilde{k}\begin{pmatrix} 0 & 1 & 0 & 0 & \cdots & 0 & \cdots \\ 1+\frac{1}{\widetilde{k}^2} & 0 & \sqrt{2} & 0 & \cdots & 0 & \cdots \\ 0 & \sqrt{2} & 0 & \sqrt{3} & \cdots & 0 & \cdots \\ 0 & 0 & \sqrt{3} & 0 & \cdots & 0 & \cdots \\ \vdots & \vdots & \vdots & \vdots & & \vdots & \end{pmatrix} - i\widetilde{\nu}\begin{pmatrix} 0 & 0 & 0 & 0 & \cdots \\ 0 & 1 & 0 & 0 & \cdots \\ 0 & 0 & 2 & 0 & \cdots \\ 0 & 0 & 0 & 3 & \cdots \\ \vdots & \vdots & \vdots & \vdots & \ddots \end{pmatrix}\right] \cdot \begin{pmatrix} a_0 \\ a_1 \\ a_2 \\ a_3 \\ \vdots \end{pmatrix} = \widetilde{\omega}\begin{pmatrix} a_0 \\ a_1 \\ a_2 \\ a_3 \\ \vdots \end{pmatrix}. \tag{4.60}$$

For a practical computation, of course, one has to cut the infinite matrices in (4.60) at some point. However, the matrix elements in the equation above get bigger with increasing the number of the corresponding row or column. As also noted in [15], this feature of the matrix leads to problems with convergence of the solutions derived by this approach. Nevertheless, we will evaluate (4.59) in this way and use the same ideas as for our previous discretization scheme in order to determine wich part of the spectrum is converged and can therefore be trusted.

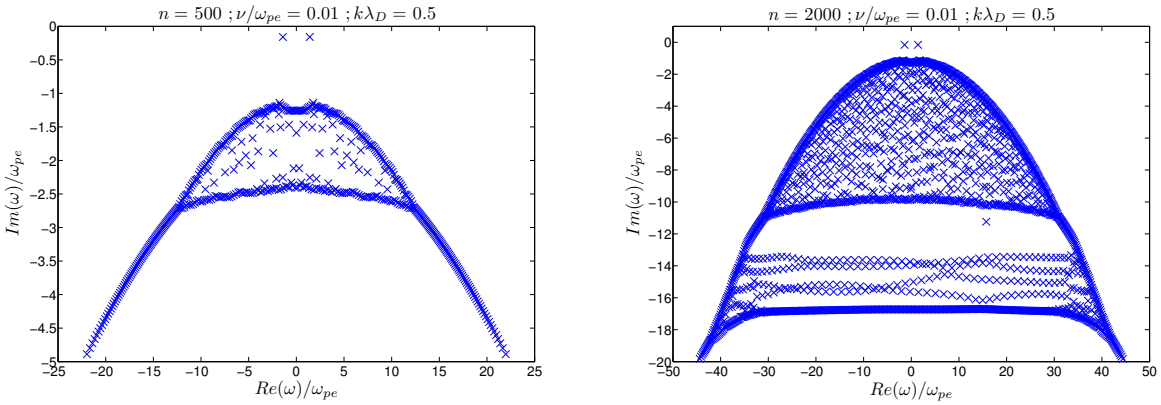

(a) $N = 500$ (b) $N = 2000$

Figure 4.18: Van Kampen spectrum in the Hermite polynomial representation for fixed collision frequency ($\widetilde{\nu} = 0.01$) and different number of polynomials.

In Figure 4.18 we have show the Van Kampen spectrum for fixed collision frequency ($\widetilde{\nu} = 0.01$) and different resolution in the space of Hermite polynomials. (High resolution means here that polynomials up to high n have been considered.) One sees that in this case there is also an area of stochasticity in the middle of the spectrum where the Van Kampen eigenvalues do not adhere to the analytic symmetry of the equation. However, even for high n (at least up to $n = 2000$) this area does not shrink into a line situated on the imaginary axis. With the discretization in velocity space a line of Van Kampen eigenvalues formed that was near the real line. In the Hermite polynomial representation these eigenvalues are missing which might be due to the fact that they were not physical but rather a remnant of the velocity grid.

On the two plots in Figure 4.18, one can also notice the two eigenvalues that are separated from the rest of the spectrum and their position is close to where the two least damped Landau solutions are situated. In order to verify this, we conduct the same analysis as in the case of the velocity discretization. The result is that two of the Van Kampen eigenvalues tend linearly to the least damped Landau solution, as was expected based on our previous analysis. However, in this representation one can see how also other Van Kampen eigenvalues tend to the Landaus solutions which are stronger damped. This situation is represented on the four plots in Figure 4.19. It is clear how part of the Van Kampen eigenvalues (blue crosses) steadily approach the Landau solutions (red circles) when collision frequency is decreased. In Figure 4.19 the collision frequency has been kept relative high because when lowering $\widetilde{\nu}$ the area of stochasticity approaches the real $\widetilde{\omega}$-axis and steadily encloses the stronger damped Landau solutions. Nevertheless, qualitatively it is clear that all Landau roots are approached by Van Kampen eigenvalues when the collision frequency tends to zero.

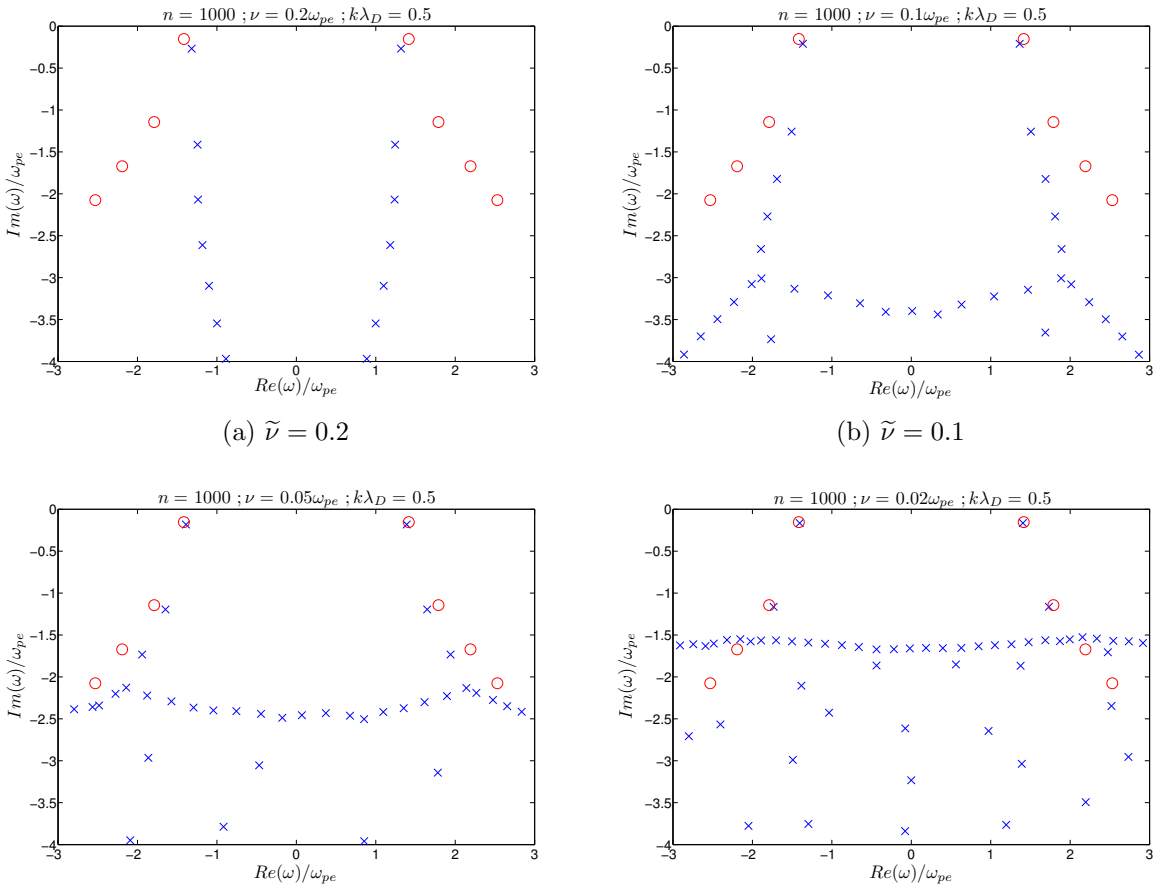

(a) $\widetilde{\nu} = 0.2$ (b) $\widetilde{\nu} = 0.1$

(c) $\widetilde{\nu} = 0.05$ (d) $\widetilde{\nu} = 0.02$

Figure 4.19: Limit of part of the Van Kampen spectrum in the Hermite polynomial representation for fixed resolution ($n = 1000$).

Chapter 5

Extension to ion temperature gradient (ITG) modes

In this chapter we shall discuss some consequences of temperature and density gradients in the framework of drift-kinetics. After introducing the physics of the slab ITG model and deriving a few analytical results, a numerical evaluation of the equations follows. We consider again first the collisionfree case and then introduce collisions into the system via the Lenard-Bernstein collision operator.

5.1 The slab ITG model

Our starting point in this chapter will be the drift-kinetic equation used extensively in plasma physics. For the derivation of this equation we follow [3]. First, let us assume that we have a strongly magnetized plasma and a constant (in time as well as in space) magnetic field $\vec{B} = B\vec{e}_z$ in the z-direction. In this case, the particles (ions and electrons) gyrate rapidly around the field lines and are effectively bound to them while being able to move freely along the field lines. As long as one is only interested in low-frequency dynamics, one can average out the phase dependence of the rapid gyromotion and thus reduce the velocity space of the particles by one dimension. If $f_{i,gc}(\vec{r}, \vec{v}, t)$ denotes the distribution function of ion gyrocentres, one can write that $f_{i,gc}(\vec{r}, \vec{v}, t) \rightarrow f_{i,gc}(\vec{r}, v_{||}, v_{\perp}, t)$. From now on we will suppress for the ease of notation the subscript gc. This reduction of the six-dimensional phase space is called 'gyro-kinetic approximation'. However, here we also neglect finite Larmor radius (FLR) effects which is not done in gyro-kinetics. Therefore, one should call the approximative model used here drift-kinetics. In mathematical terms, we have introduced cylindrical coordinates in velocity space and have integrated out the angle dependence such that now the volume element in velocity space is given by $2\pi v_{\perp} dv_{\perp} dv_{||}$. If the number of particles remains constant, then in analogy with the usual kinetic theory one can write that

$$0 = \frac{\partial f_i}{\partial t} + \nabla^{(5)} \cdot (\vec{u} f_i) = \frac{\partial f_i}{\partial t} + \nabla \cdot (\dot{\vec{r}} f_i) + \frac{1}{v_\perp} \frac{\partial}{\partial v_\perp} (v_\perp \dot{v}_\perp f_i) + \frac{\partial}{\partial v_{||}} (\dot{v}_{||} f_i), \tag{5.1}$$

where $\nabla^{(5)}$ denotes a divergence in the five dimensional phase space with cylindrical velocity coordinates and the five-dimensional vector $\vec{u}$ is defined as $\vec{u} := (\vec{r}, v_\perp, v_{||})$. The velocity $v_\perp$ perpendicular to the magnetic field is usually much smaller than the parallel velocity $v_{||}$. Since our primary goal is to gain a qualitative understanding of this model, we consider only first order effects, which in this case is the $\vec{E} \times \vec{B}$ drift. With this approximation the velocity reads

$$\dot{\vec{r}} = \vec{v}_D + v_{||} \vec{e}_z, \tag{5.2}$$

where $\vec{v}_D = \vec{E} \times \vec{B}/B^2$. Using this expression for the drift velocity and the fact that the magnetic field is constant, one can easily show that $\nabla \cdot \vec{v}_D = 0$. The gyromotion of the ions is related to the magnetic moment which is given by $\mu = m_i v_\perp^2/(2B)$, where m_i is the ion mass. In a magnetic field that is constant in space and in time, this magnetic moment is also constant and, therefore, $\dot{v}_\perp = 0$. According to the second Newton's law, the time derivative of $v_{||}$ equals the force acting on the ion that is parallel to the magnetic field divided by its mass. The force of the magnetic field has no component that is tangent to it, so in the z-direction the only contribution comes from the z-component of the electric field, i.e., $\dot{v}_{||} = eE_{||}/m_i$. Using these results in (5.1), one arrives at

$$\frac{\partial f_i}{\partial t} + \left(\vec{v}_{||} + \vec{v}_D\right) \cdot \nabla f_i + \frac{e}{m_i} E_{||} \frac{\partial f_i}{\partial v_{||}} = 0. \tag{5.3}$$

Since the drift velocity is much smaller than the parallel velocity, one can neglect the $v_\perp$-dependence of f_i. Setting $\frac{\partial B}{\partial t} = 0$ means that we can express the electric field as $\vec{E} = -\nabla\varphi$, where φ is the electrostatic potential. Subsequently, we are going to introduce gradients of the equilibrium temperature and density which we take for simplicity in the x direction. In order to circumvent unnecessary mathematical complications arising from the Fourier transformation in y and z of the approximate drift kinetic equation, we consider an electrostatic potential which is a function only of y, z and t: $\varphi = \varphi(y, z, t)$. This assumption implies also the same dependency of the electric field and that $E_x = 0$. Strictly speaking, we can consider also an electric field with a non-vanishing component in x-direction. However, this is not going to influence the model qualitatively and, therefore, we take E_x to be zero. In physical terms this is equivalent to setting k_x to zero.

At this point, we interrupt the exact quantitative description of the slab ITG model and give a more physical explanation of the ITG instability with the help of the simple picture shown in Figure 5.1 which represents the geometry of our model. Although this explanation comes from fluid theory, it will still be useful to gain some physical insight. We are not going to present the fluid equations here but merely adopt the results derived in [20]. Assume that the temperature gradient points in the positive x-direction and that a wavelike ion density perturbation is formed in the plasma with a maximum at $x = y = 0$.

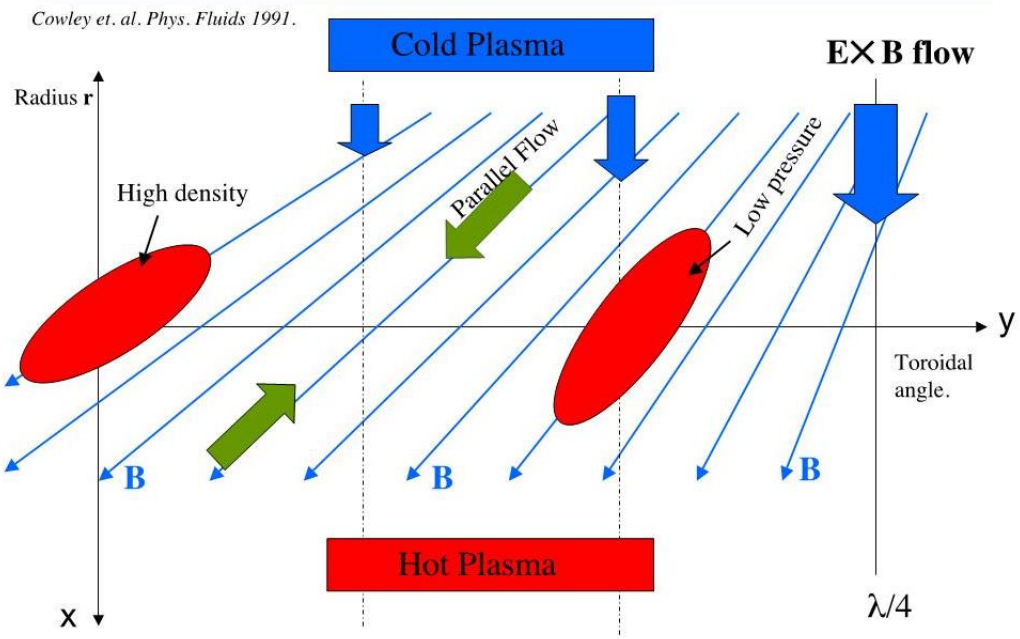

Figure 5.1: Simplified picture of the ITG instability (source: Cowley et. al., Phys. Fluids 1991).

This instantaneously induces an electric field towards the the origin of the coordinate system. Together with the magnetic field, this electric field gives rise to a $\vec{E} \times \vec{B}$ drift that in this situation is parallel to the temperature gradient, as shown in the figure, i.e., this drift brings plasma from the cold to the hot areas. The effect of this advection of colder plasma is that it cools the perturbation and thus decreases its pressure which, however, causes a flow of ions into the perturbation, since the pressure there is lower. This feedback mechanism leads to a growth of this perturbation in the ion density, i.e., an instability. If one does the corresponding calculation, then one sees that there is a slight phase shift between the quantities involved. The $\vec{E} \times \vec{B}$ drift does not peak at $y = 0$ where the maximum of the ion density perturbations. Since the drift 'feeds' the perturbation, this phase shift leads to a movement of the instability in the plasma.

Now we continue with the description of the kinetic slab ITG model. In order to approximate (5.3), we will use the same linearisation procedure as in the previous chapter. So we write

$$f_i(\vec{r}, v_{||}, t) = f_{0i}(x, v_{||}) + f_{1i}(\vec{r}, v_{||}, t), \tag{5.4}$$

where the subscripts 0 and 1 denote the equilibrium and the perturbation of the distribution function of gyrocentres. The only difference here is that we will allow for f_{0i} to depend on one of the spatial coordinates, namely the same coordinate on which also the temperature and density depend. It should be noted that the electric field arises due to the perturbation.

Since the drift velocity is proportional to the electric field, we will consider it to be also a first order quantity. Substituting the last expression for f_i into (5.3) and neglecting second order terms we arrive at

$$\frac{\partial f_{1i}}{\partial t} + v_{||}\frac{\partial f_{1i}}{\partial z} - \frac{\partial \varphi}{\partial y}\frac{1}{B}\frac{\partial f_{0i}}{\partial x} - \frac{e}{m_i}\frac{\partial \varphi}{\partial z}\frac{\partial f_{0i}}{\partial x} = 0. \tag{5.5}$$

For the derivation of the last equation one should take into account that

$$\vec{E} \times \vec{B} = -\nabla\varphi(y,z,t) \times \vec{B} = -\frac{\partial \varphi}{\partial y} B\vec{e}_x \text{ and } E_{||} := -\frac{\partial \varphi}{\partial z}. \tag{5.6}$$

In order to get a self consistent equation determining f_{1i}, we need a relation between the electrostatic potential φ and f_{1i}. Similar to the MHD case, we can assume some equation of state which gives us self-consistency. Since the ion mass is much greater than the electron mass, the average electron velocity is much higher than the average ion velocity when both electron and ion temperatures are nearly the same. In physical terms this means that the electrons react on the potential differences, caused by f_{1i}, on time scales much faster than the time scales on which f_{1i} and therefore the electrostatic potential changes, i.e., we say that the electrons are adiabatic. Mathematically, this means that at every moment of time, the electrons will have a linearised Boltzmann distribution corresponding to the electrostatic potential $\varphi(y,z,t)$ they experience:

$$n_{1e}(\vec{r},t) = n_{0e}(x)\frac{e\varphi(y,z,t)}{k_B T_e(x)}, \tag{5.7}$$

where n_{1e} and n_{0e} are the perturbed and equilibrium electron densities respectively and T_e is the electron temperature which can also vary in x. Using the quasi-neutrality of the plasma (here the ions have the charge e), namely that

$$n_{0i}(x) = n_{oe}(x) \text{ and } n_{1e}(\vec{r},t) = n_{1i}(\vec{r},t) := \int_{-\infty}^{+\infty} f_{1i}(\vec{r}, v_{||}, t)dv_{||}, \tag{5.8}$$

we derive the desired connection between f_{1i} and the electrostatic potential which reads

$$\varphi(y,z,t) = \frac{k_B T_e(x)}{e n_{0i}(x)} \int_{-\infty}^{+\infty} f_{1i}(\vec{r}, v_{||}, t)dv_{||}. \tag{5.9}$$

In order to work with (5.5) in a more comfortable way (especially in the case of a numerical analysis), it is convenient to normalize the quantities in the equation. Since the densities and temperatures are continuous functions of space, we will normalize them over their maximal values:

$$T_{i,e}^{(m)} := \sup\left\{T_{i,e}(x)\right\} \ ; \ n^{(m)} := \sup\left\{n_{0i}(x)\right\} = \sup\left\{n_{0e}(x)\right\}. \tag{5.10}$$

Given these definitions, we can now define a typical ion thermal velocity given by

$$v_{th,i} := \sqrt{\frac{k_B T_i^{(m)}}{m_i}}. \tag{5.11}$$

One should also note that there are different spatial scales in this problem. For strongly magnetized plasmas the mean free path of the particles along the magnetic field is large, so all plasma quantities vary slowly in the z-direction. The equilibrium distribution function f_{0i} also experiences considerable changes over a scale length comparable to the length of the system (which we call a). Therefore spatial derivatives of f_{0i} and derivatives with respect to z will be normalized with respect to a.[1] Perpendicular to the magnetic field the movement of particles is bound by their gyromotion, so it is physically meaningful to normalize derivatives of the perturbed quantities with respect to x or y over the Larmor radius of a particle whose velocity perpendicular to the magnetic field equals $v_{th,i}$, i.e.,

$$r_L := \frac{\sqrt{k_B T_i^{(m)} m_i}}{eB}. \tag{5.12}$$

The time scales of interest are set by the ion gyro-frequency ω_g of the particles which in terms of magnetic field and particle properties is given by

$$\omega_g = \frac{eB}{m_i} = \frac{v_{th,i}}{r_L}. \tag{5.13}$$

One should notice that ω_g does not depend on the particle energy (at least for non-relativistic energies) and is therefore the same for all ions. We can now define the normalized quantities (denoted by a tilde over the corresponding letter) we will work with via:

$$\widetilde{f}_{1,0i} := \frac{v_{th,i}}{n^{(m)}} f_{1,0i} \; ; \; \widetilde{t} := t\omega_g \; ; \; \widetilde{v}_{||} := \frac{v_{||}}{v_{th,i}} \; ; \; \widetilde{\varphi} := \frac{e}{k_B T_i^{(m)}} \varphi. \tag{5.14}$$

Using these definitions, one can transform (5.5) and arrives at

$$\frac{1}{\rho_*} \frac{\partial \widetilde{f}_{1i}}{\partial \widetilde{t}} + \widetilde{v}_{||} \frac{\partial \widetilde{f}_{1i}}{\partial \widetilde{z}} - \frac{\partial \widetilde{\varphi}}{\partial \widetilde{y}} \frac{\partial \widetilde{f}_{0i}}{\partial \widetilde{x}} - \frac{\partial \widetilde{\varphi}}{\partial \widetilde{z}} \frac{\partial \widetilde{f}_{0i}}{\partial \widetilde{x}} = 0, \tag{5.15}$$

where ρ_* is the ratio between the Larmor radius, r_L, and a, the system length in perpendicular direction. In order to simplify (5.15) we Fourier transform it with respect to $\widetilde{z}$, $\widetilde{y}$ and $\widetilde{t}$ according to the convention

$$g(\widetilde{z}, \widetilde{y}, \widetilde{t}) = \frac{1}{(2\pi)^{3/2}} \int_{-\infty}^{+\infty} \int_{-\infty}^{+\infty} \int_{-\infty}^{+\infty} \widehat{g}(\widetilde{k}_{||}, \widetilde{k}_y, \widetilde{\omega}) e^{-i\widetilde{k}_{||}\widetilde{z}} e^{-i\widetilde{k}_y \widetilde{y}} e^{i\widetilde{\omega}\widetilde{t}} d\widetilde{k}_y d\widetilde{k}_{||} d\widetilde{\omega}. \tag{5.16}$$

[1] Strictly speaking the mean free path of a particle in a typical tokamak is a few kilometres which exceeds the system length by three orders of magnitude. However, from a mathematical point of view there is nothing wrong in normalizing the derivatives w.r.t. z over a and later on such a normalization will turn out to be useful.

Furthermore, we will assume that the equilibrium distribution f_{0i} is a local Maxwell distribution in which the equilibrium density and temperature vary with x, i.e.,

$$f_{0i}(x, v_{||}) = \frac{n_{0i}(x)}{\sqrt{2\pi k_B T_i(x)/m_i}} \exp\left(-\frac{m_i v_{||}^2}{2k_B T_i(x)}\right). \tag{5.17}$$

Normalizing this expression with respect to the aforementioned quantities gives

$$\widetilde{f}_{0i}(\widetilde{x}, \widetilde{v}_{||}) = \frac{\widetilde{n}_{0i}(\widetilde{x})}{\sqrt{2\pi \widetilde{T}_i(\widetilde{x})}} \exp\left(-\frac{1}{2}\frac{\widetilde{v}_{||}^2}{\widetilde{T}_i(\widetilde{x})}\right), \tag{5.18}$$

where we have normalized the temperature via $\widetilde{T}_{i,e}(\widetilde{x}) := T_{i,e}(\widetilde{x})/T_i^{(m)}$. From this follows immediately that $\partial \widetilde{f}_{0i}/\partial \widetilde{v}_{||} = (\widetilde{v}_{||}/\widetilde{T}_i)\widetilde{f}_{0i}$. Substituting this, after Fourier transforming (5.15), leads to

$$\left(\frac{\widetilde{\omega}}{\rho_*} - \widetilde{k}_{||}\widetilde{v}_{||}\right)\widehat{\widetilde{f}}_{1,i} + \left(\widetilde{k}_y \frac{\partial \widetilde{f}_{0i}}{\partial \widetilde{x}} - \frac{\widetilde{k}_{||}\widetilde{v}_{||}}{\widetilde{T}_i(x)}\widetilde{f}_{0i}\right)\widehat{\widetilde{\varphi}} = 0. \tag{5.19}$$

The relation between $\widehat{\widetilde{\varphi}}$ and $\widehat{\widetilde{f}}_{1,i}$ is derived by normalizing and Fourier-transforming (5.9):

$$\widehat{\widetilde{\varphi}} = \frac{\tau^{(m)}\widetilde{T}_e(\widetilde{x})}{\widetilde{n}_{0i}(\widetilde{x})} \int_{-\infty}^{+\infty} \widehat{\widetilde{f}_{1i}}(..., \widetilde{v}_{||}, ...) d\widetilde{v}_{||}, \tag{5.20}$$

where $\tau^{(m)}$ is given by the ratio $T_e^{(m)}/T_i^{(m)}$. The only parameters in $\widetilde{f}_{0i}$ which depend on $\widetilde{x}$ are density and temperature, so using (5.18) we can easily express the derivative $\partial \widetilde{f}_{0i}/\partial \widetilde{x}$ through the gradients of temperature and density. A straightforward calculation gives

$$\widetilde{k}_y \frac{\partial \widetilde{f}_{0i}}{\partial \widetilde{x}} - \frac{\widetilde{k}_{||}\widetilde{v}_{||}}{\widetilde{T}_i(\widetilde{x})}\widetilde{f}_{0i} = \left(-\frac{1}{2}\frac{\widetilde{k}_y}{\widetilde{T}_i(\widetilde{x})}\frac{d\widetilde{T}_i(\widetilde{x})}{d\widetilde{x}} + \frac{1}{2}\frac{\widetilde{k}_y \widetilde{v}_{||}^2}{\widetilde{T}_i^2(\widetilde{x})}\frac{d\widetilde{T}_i(\widetilde{x})}{d\widetilde{x}} + \frac{\widetilde{k}_y}{\widetilde{n}_{0,i}(\widetilde{x})}\frac{d\widetilde{n}_{0i}(\widetilde{x})}{d\widetilde{x}} - \right.$$
$$\left. - \frac{\widetilde{k}_{||}\widetilde{v}_{||}}{\widetilde{T}_i(\widetilde{x})}\right)\widetilde{f}_{0i}(\widetilde{x}, \widetilde{v}_{||}) =: \alpha(\widetilde{x}, \widetilde{v}_{||})\widetilde{f}_{0i}(\widetilde{x}, \widetilde{v}_{||}). \tag{5.21}$$

Combining this expression with (5.20) and substitution in (5.19) yields

$$\frac{\widetilde{\omega}}{\rho_*}\widehat{\widetilde{f}}_{1i} = \widetilde{k}_{||}\widetilde{v}_{||}\widehat{\widetilde{f}}_{1i} \underbrace{- \frac{\tau^{(m)}\widetilde{T}_e(\widetilde{x})}{\widetilde{n}_{0i}(\widetilde{x})}\alpha(\widetilde{x}, \widetilde{v}_{||})\widetilde{f}_{0i}(\widetilde{x}, \widetilde{v}_{||})}_{=\psi(\widetilde{x}, \widetilde{v}_{||})} \int_{-\infty}^{+\infty} \widehat{\widetilde{f}}_{1i}(..., \widetilde{v}'_{||}, ...) d\widetilde{v}'_{||}. \tag{5.22}$$

One can view this equation as an eigenvalue equation of a linear operator acting on $\widehat{\widetilde{f}}_{1i}$, where the eigenvalues this time are denoted by $\widetilde{\omega}/\rho_*$. If one compares (5.22) with (3.1), it

becomes immediately apparent that this is qualitatively the same operator that we studied in chapter 3. The only difference with respect to the case of Langmuir waves is that now the explicit form of the function $\psi(v)$ is more complicated. However, this is not going to be a problem here, since in chapter 3 we investigated the properties and the spectrum of this operator without specifying the exact form of $\psi(v)$. We only assumed that it belongs to the space H which is also the case in (5.22). We derived that this operator has a spectrum that consists of a continuous part situated on the entire real line and a discrete part that obeys the condition (3.16), where the integral is to be understood in the sense of the Cauchy principle value. We also agreed on the prescription that, if the integral is done along the Landau contour, then this condition gives the corresponding Landau solutions. Here this leads to

$$1 - \frac{\tau^{(m)}\widetilde{T}_e(\widetilde{x})}{\widetilde{n}_{0i}(\widetilde{x})\widetilde{k}_{||}} \int\limits_L \frac{\alpha(\widetilde{x},\widetilde{v}_{||})\widetilde{f}_{0i}(\widetilde{x},\widetilde{v}_{||})}{\widetilde{v}_{||} - \widetilde{\omega}_L/(\widetilde{k}_{||}\rho_*)} d\widetilde{v}_{||} = 0. \tag{5.23}$$

Before further transforming (5.23), it is useful to note some relations between the integrals one encounters in this equation and the plasma dispersion function Z. Using the definition of Z given in [1] one can derive[2] the following expressions:

$$\begin{gathered} \int\limits_L \frac{e^{-bx^2}}{x-a}dx = \sqrt{\pi}Z(a\sqrt{b}) \ ; \ \int\limits_L \frac{xe^{-bx^2}}{x-a}dx = \sqrt{\frac{\pi}{b}} + a\sqrt{\pi}Z(a\sqrt{b}) \ ; \\ \int\limits_L \frac{x^2e^{-bx^2}}{x-a}dx = a\sqrt{\frac{\pi}{b}} + a^2\sqrt{\pi}Z(a\sqrt{b}), \end{gathered} \tag{5.24}$$

where $a \in \mathbb{C}$ and $b \in \mathbb{R}_+$ are fixed parameters. In the expression for $\alpha(\widetilde{x},\widetilde{v}_{||})$ one encounters gradients of the ion temperature and equilibrium density. For ease of notation we define

$$\frac{d\ln\widetilde{T}_i(\widetilde{x})}{d\widetilde{x}} := -\frac{1}{\widetilde{L}_T(\widetilde{x})} \text{ and } \frac{d\ln\widetilde{n}_{0i}(\widetilde{x})}{d\widetilde{x}} := -\frac{1}{\widetilde{L}_n(\widetilde{x})}, \tag{5.25}$$

where L_T and L_n have the physical dimension of length and are normalized over the typical system length a. The usefulness of the definitions above will become clear later on. With these definitions and the explicit form of $\alpha(\widetilde{x},\widetilde{v}_{||})$ given in (5.21) we can now express (5.23) in way that involves the plasma dispersion function and is more convenient for numerical analysis, namely

[2]The exact derivation is shown in the Appendix.

$$1+\tau^{(m)}\frac{\widetilde{T}_e(\widetilde{x})}{\widetilde{T}_i(\widetilde{x})}+\tau^{(m)}\frac{\widetilde{T}_e(\widetilde{x})}{2\widetilde{T}_i(\widetilde{x})}\frac{\widetilde{k}_y}{\widetilde{k}_{||}}\frac{1}{\widetilde{L}_T(\widetilde{x})}\left(\frac{\widetilde{\omega}}{\rho_*\widetilde{k}_{||}}\right)+\tau^{(m)}Z\left(\frac{\widetilde{\omega}}{\sqrt{2\widetilde{T}_i(\widetilde{x})}\rho_*\widetilde{k}_{||}}\right)\cdot\left[\frac{\widetilde{T}_e(\widetilde{x})}{\sqrt{2}\widetilde{T}_i^{3/2}(\widetilde{x})}\left(\frac{\widetilde{\omega}}{\rho_*\widetilde{k}_{||}}\right)+\right.$$
$$\left.+\frac{\widetilde{T}_e(\widetilde{x})}{\sqrt{2\widetilde{T}_i(\widetilde{x})}}\frac{\widetilde{k}_y}{\widetilde{k}_{||}}\left(\frac{1}{\widetilde{L}_n(\widetilde{x})}-\frac{1}{2}\frac{1}{\widetilde{L}_T(\widetilde{x})}\right)+\frac{\widetilde{T}_e(\widetilde{x})}{\sqrt{2}\widetilde{T}_i^{3/2}(\widetilde{x})}\frac{\widetilde{k}_y}{\widetilde{k}_{||}}\frac{1}{\widetilde{L}_T(\widetilde{x})}\left(\frac{\widetilde{\omega}}{\sqrt{2}\rho_*\widetilde{k}_{||}}\right)^2\right]=0. \quad (5.26)$$

The special case of a plasma in a global thermal equilibrium with homogeneous equilibrium ion density is derived in this approximated model by taking the limit $\widetilde{L}_T \to +\infty$ and $\widetilde{L}_n \to +\infty$. This leads to

$$1+\tau^{(m)}+\tau^{(m)}\left(\frac{\widetilde{\omega}}{\sqrt{2}\rho_*\widetilde{k}_{||}}\right)Z\left(\frac{\widetilde{\omega}}{\sqrt{2}\rho_*\widetilde{k}_{||}}\right)=0, \quad (5.27)$$

which one recognises as the dispersion relation of ion acoustic waves in a strongly magnetized plasma.

In our further analysis we are going to work with a commonly used approximation for the temperature and density gradients. In this model, one considers small volumes in the plasma such that it can be assumed that both temperature and density vary only weakly over the distances under consideration, so we set $\widetilde{T}_i(\widetilde{x})=\widetilde{T}_e(\widetilde{x})=\widetilde{n}_i(\widetilde{x})=1$. However, we do not want to neglect the gradients entirely and, therefore, approximate them by taking $\widetilde{L}_T$ and $\widetilde{L}_n$ to be constant but finite. The physical meaning of the quantities L_T and L_n is that they represent the length scales over which temperature and density vary considerably. Since these length scales are usually considerably bigger than the Larmor radius and of the same order of magnitude as the perpendicular system length a, they are normalized with respect to a. With this approximation the dispersion relation reads

$$1+\tau^{(m)}+\tau^{(m)}\frac{\widetilde{k}_y}{\widetilde{k}_{||}}\frac{1}{2\widetilde{L}_T}\left(\frac{\widetilde{\omega}_L}{\rho_*\widetilde{k}_{||}}\right)+\tau^{(m)}Z\left(\frac{\widetilde{\omega}_L}{\sqrt{2}\rho_*\widetilde{k}_{||}}\right)\cdot\left[\frac{\widetilde{k}_y}{\widetilde{k}_{||}\sqrt{2}}\left(\frac{1}{\widetilde{L}_n}-\frac{1}{2}\frac{1}{\widetilde{L}_T}\right)+\right.$$
$$\left.+\frac{\widetilde{\omega}_L}{\rho_*\widetilde{k}_{||}\sqrt{2}}+\frac{\widetilde{k}_y}{\widetilde{k}_{||}\sqrt{2}}\frac{1}{\widetilde{L}_T}\left(\frac{\widetilde{\omega}_L}{\sqrt{2}\rho_*\widetilde{k}_{||}}\right)^2\right]=0, \quad (5.28)$$

where we have denoted the solutions of this equation by $\widetilde{\omega}_L$ in order to keep in mind that they arise when one integrates along the Landau contour in order to avoid ambiguity in the integral in (5.23). We can avoid the ambiguity also by taking the Cauchy principal value of the integral and, as we saw in chapter 3, this treatment would give us the discrete part of the Van Kampen spectrum. Therefore, these Van Kampen eigenfrequencies, denoted here by $\widetilde{\omega}_V$, fulfil the equation

$$1-\frac{\tau^{(m)}\widetilde{T}_e(\widetilde{x})}{\widetilde{n}_{0i}(\widetilde{x})\widetilde{k}_{||}}p.v.\int_{-\infty}^{+\infty}\frac{\alpha(\widetilde{x},\widetilde{v}_{||})\widetilde{f}_{0i}(\widetilde{x},\widetilde{v}_{||})}{\widetilde{v}_{||}-\widetilde{\omega}_V/(\widetilde{k}_{||}\rho_*)}d\widetilde{v}_{||}=0, \tag{5.29}$$

which is analogous to (5.23). The situation here is similar to the one we already investigated in subsection 4.1.2. By comparing (5.23) and (5.29) and recalling the definition of the Landau contour we immediately conclude that, if one of them has a solution with a positive imaginary part, then it is also a solution to the second equation, since for poles in the upper half of the complex $\widetilde{\omega}$-plane the Landau contour reduces to a simple integration along the real line as also the Cauchy principal value. In analogy to 4.1.2, we would like to say something about the symmetry of the discrete part of the Van Kampen spectrum. By using the definition of $\alpha(\widetilde{x},\widetilde{v}_{||})$ and the explicit form of $\widetilde{f}_{0,i}(\widetilde{x},\widetilde{v})$ one can split the integral in (5.29), which for ease of notation we denote here as the function $g(a)$, into a sum of three terms, namely

$$\begin{aligned}g(a)=&\frac{\widetilde{n}_{0,i}(\widetilde{x})\widetilde{k}_y}{\sqrt{2\pi\widetilde{T}_i(\widetilde{x})}}\left(-\frac{1}{\widetilde{L}_n(\widetilde{x})}+\frac{1}{2\widetilde{L}_T(\widetilde{x})}\right)p.v.\int_{-\infty}^{+\infty}\frac{e^{-bt^2}}{t-a}dt-\\&-\frac{\widetilde{n}_{0,i}(\widetilde{x})\widetilde{k}_y}{2\widetilde{T}_i(\widetilde{x})\widetilde{L}_T(\widetilde{x})\sqrt{2\pi\widetilde{T}_i(\widetilde{x})}}p.v.\int_{-\infty}^{+\infty}\frac{t^2e^{-bt^2}}{t-a}dt-\frac{\widetilde{n}_{0,i}(\widetilde{x})\widetilde{k}_{||}}{\widetilde{T}_i(\widetilde{x})\sqrt{2\pi\widetilde{T}_i(\widetilde{x})}}p.v.\int_{-\infty}^{+\infty}\frac{te^{-bt^2}}{t-a}dt,\end{aligned} \tag{5.30}$$

where we have introduced the substitutions $t:=\widetilde{v}_{||}$, $a:=\widetilde{\omega}_V/(\rho_*\widetilde{k}_{||})$ and $b:=1/(2\widetilde{T}_i(\widetilde{x}))$. For a non-vanishing imaginary part of a we can split these three integrals into real and imaginary in the same way as we proceeded in subsection 4.1.2. This gives

$$\begin{aligned}Re(g(a))=&\frac{\widetilde{n}_{0,i}(\widetilde{x})}{\sqrt{2\pi\widetilde{T}_i(\widetilde{x})}}\left(\frac{-\widetilde{k}_y}{2\widetilde{T}_i(\widetilde{x})\widetilde{L}_T(\widetilde{x})}\int_{-\infty}^{+\infty}\frac{t^2(t-a_r)e^{-bt^2}}{|t-a|^2}dt-\frac{\widetilde{k}_{||}}{\widetilde{T}_i(\widetilde{x})}\int_{-\infty}^{+\infty}\frac{t(t-a_r)e^{-bt^2}}{|t-a|^2}dt+\right.\\&\left.+\widetilde{k}_y\left(\frac{-1}{\widetilde{L}_n(\widetilde{x})}+\frac{1}{2\widetilde{L}_T(\widetilde{x})}\right)\int_{-\infty}^{+\infty}\frac{(t-a_r)e^{-bt^2}}{|t-a|^2}dt\right)\end{aligned} \tag{5.31}$$

and

$$\begin{aligned}Im(g(a))=&a_i\frac{\widetilde{n}_{0,i}(\widetilde{x})}{\sqrt{2\pi\widetilde{T}_i(\widetilde{x})}}\left(\frac{-\widetilde{k}_y}{2\widetilde{T}_i(\widetilde{x})\widetilde{L}_T(\widetilde{x})}\int_{-\infty}^{+\infty}\frac{t^2e^{-bt^2}}{|t-a|^2}dt-\frac{\widetilde{k}_{||}}{\widetilde{T}_i(\widetilde{x})}\int_{-\infty}^{+\infty}\frac{te^{-bt^2}}{|t-a|^2}dt+\right.\\&\left.+\widetilde{k}_y\left(\frac{-1}{\widetilde{L}_n(\widetilde{x})}+\frac{1}{2\widetilde{L}_T(\widetilde{x})}\right)\int_{-\infty}^{+\infty}\frac{e^{-bt^2}}{|t-a|^2}dt\right)\end{aligned} \tag{5.32}$$

From this decomposition follows that $Re(g(a^*)) = Re(g(a))$ and $Im(g(a^*)) = -Im(g(a))$, which is equivalent to $g^*(a) = g(a^*)$. In terms of the function g, (5.29) reads

$$1 - \frac{\tau^{(m)}\widetilde{T}_e(\widetilde{x})}{\widetilde{n}_{0i}(\widetilde{x})\widetilde{k}_{||}} g\left(\frac{\widetilde{\omega}_V}{\rho_*\widetilde{k}_{||}}\right) = 0. \tag{5.33}$$

When we take the complex conjugate of both side of this equation and use the property of g, that we just derived, we see that

$$1 - \frac{\tau^{(m)}\widetilde{T}_e(\widetilde{x})}{\widetilde{n}_{0i}(\widetilde{x})\widetilde{k}_{||}} g\left(\frac{\widetilde{\omega}_V^*}{\rho_*\widetilde{k}_{||}}\right) = 0, \tag{5.34}$$

i.e., if $\widetilde{\omega}_V$ is a solution of (5.29), then so is also its complex conjugate. Since, the other part of the Van Kampen spectrum lies on the real line, then the same symmetry applies to every eigenvalue. We summarize our conclusions as follows:

- The Van Kampen spectrum possesses a mirror symmetry with respect to the real $\widetilde{\omega}$-axis.
- The Van Kampen eigenvalues with positive imaginary part (i.e., unstable) are also Landau solutions.

One should note that the above properties of the Van Kampen spectrum and the set of Landau solutions does not depend on the gradient approximations we introduced and, therefore, hold for arbitrary functions $T_i(x)$, $T_e(x)$ and $n_{0,i}(x)$.

The equations in this subsection are even more complicated than those that we had before, so in order to gain more insights into this model, we have to solve them numerically. For this we use the same numerical scheme as before, namely we discretize the $\widetilde{v}_{||}$-axis and consider only a finite interval on it that is symmetric with respect to zero. At this point, we go to the approximation that was already introduced, namely

$$\widetilde{T}_i(\widetilde{x}) \equiv 1 \; ; \; \widetilde{T}_e(\widetilde{x}) \equiv 1 \; ; \; \widetilde{n}_{0,i}(\widetilde{x}) \equiv 1 \; ; \; \widetilde{L}_T(\widetilde{x}) = const \; ; \; \widetilde{L}_n(\widetilde{x}) = const. \tag{5.35}$$

In this framework our model has six parameters: $\widetilde{k}_y$, $\widetilde{k}_{||}$, ρ_*, $\tau^{(m)}$, $\widetilde{L}_T$ and $\widetilde{L}_n$ which we are allowed to choose freely.

5.2 Numerical description of collisionless ITG modes

The way we implement the discretization in velocity space follows the same scheme as in the case of Langmuir waves: we approximate the continuous operator on the right-hand side of (5.22) with a matrix the rank of which equals the number of velocity points. The only difference here is the explicit form of the vector $\vec{G}$, namely we now have

$$G_j = \frac{\tau^{(m)}\widetilde{k}_y}{\sqrt{2\pi}}\left(\frac{1}{2\widetilde{L}_T} - \frac{1}{\widetilde{L}_n} - \frac{\widetilde{k}_{||}}{\widetilde{k}_y}\widetilde{v}_{||,j} - \frac{\widetilde{v}_{||,j}^2}{2\widetilde{L}_T}\right) e^{-\widetilde{v}_{||,j}^2/2}. \tag{5.36}$$

The Van Kampen approach reduces again to finding the eigenvalues of the matrix that corresponds to the continuous operator, and in the slab ITG model this matrix is also defined via equation (4.9). For finding the positions of the Landau solutions we proceed in the same way as in section 2.2 and draw a contour plot of the absolute value of the function on the right hand side of (5.28). The combined results of both approaches are shown in Figure 5.2 where the Van Kampen eigenvalues are denoted by blue crosses. One notices that there is only one unstable Van Kampen eigenvalue and one unstable Landau solution and their positions in the complex $\widetilde{\omega}$-plane are the same. This is also what we expected from our mathematical analysis. The Van Kampen spectrum has the mirror symmetry with respect to the real axis that we derived. In the case of Langmuir waves, the set of Landau solutions was symmetric with respect to the imaginary axis. Here, this symmetry is broken because of the gradients that set a preferable direction in space.

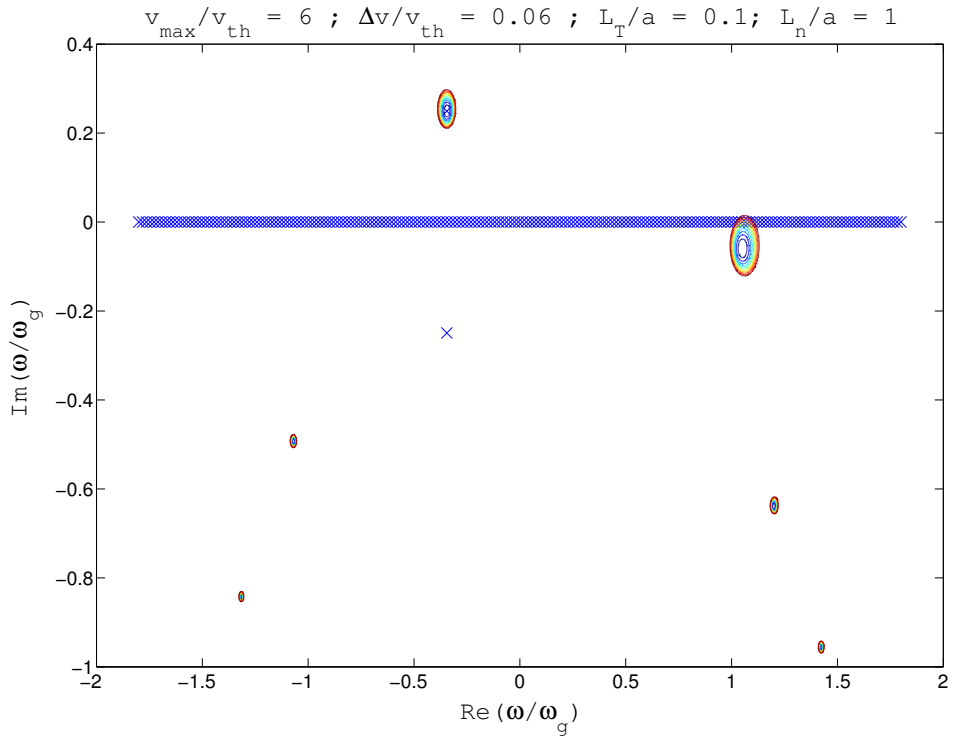

Figure 5.2: Landau solutions and Van Kampen spectrum in the case of slab ITG for $\widetilde{k}_{||} = \widetilde{k}_y = 0.3$ and $\rho_* = 1$.

It is noteworthy that only the temperature gradient produces the instability. When introduced, a density gradient stabilizes the system, i.e., for a fixed $\widetilde{L}_T$ decreasing $\widetilde{L}_n$ (that corresponds to an increase of the density gradient) lowers the growth rate of the

instability and if $\widetilde{L}_n$ falls below a certain threshold, the pair of one unstable and one damped solution disappears and all Van Kampen eigenvalues lie on the real line. As explained in [3], one can formulate this condition in mathematical terms. If the quantity $\Lambda := (L_n/L_T)(k_y/k_{par})^2(v_D/v_{th,i})^2$ is large compared to one, then the threshold for an instability is that $\eta_i := L_n/L_T > 2$. Since $v_D/v_{th,i}$ is of the order of r_L/a, then in our units of normalization the parameter Λ is

$$\Lambda = \eta_i \left(\frac{k_y}{k_{||}}\right)^2 \left(\frac{v_D}{v_{th,i}}\right)^2 \sim \eta_i \left(\frac{k_y}{k_{||}}\right)^2 \left(\frac{r_L}{a}\right)^2 = \eta_i \left(\frac{\widetilde{k}_y}{\widetilde{k}_{||}}\right)^2$$

which does not depend on ρ_*. If one sets the parameters of our program appropriately, e.g., $\widetilde{k}_y = 0.3$ and $\widetilde{k}_{||} = 0.03$, then it reproduces this threshold. When dealing with the ITG instability in the framework of gyrokinetics, one usually performs what is called a scan in the perpendicular wave number, namely for fixed gradients and parallel wave number, k_y is varied. This gives us the growth rate of the instability as a function of k_y. In such scans one sees that the growth rate initially increases, peaks at some value of the perpendicular wave number and then decreases monotonically while it reaches zero for $\widetilde{k}_y$ in the vicinity of one. Since the perpendicular wave number is normalized over the gyroradius, the effect of r_L being finite, that becomes prominent for $\widetilde{k}_y > 1$, stabilized the wave. In our model we did not include finite gyroradius effects and, thus, such a scan with respect to the perpendicular wave number shows a different picture, namely the growth rate of the instability increases monotonically with $\widetilde{k}_y$.

In analogy to subsection 4.1.1, we investigate the density of eigenmodes (strictly speaking, the density of the projection of the eigenmodes onto the real $\widetilde{\omega}$-axis). One example that corresponds to the set of parameters of the previous plot is shown in Figure 5.3. The large spike is due to the fact that the real part of the frequency for the unstable and the damped eigenvalue is the same, i.e., at this point $\Delta\widetilde{\omega}$ is zero. When the gradients are chosen such that there is no instability, then there is still a peak at that point that gets higher and sharper when the $\widetilde{L}_n$ increases and approaches the threshold for producing an instability.[3] This suggests that in the stable case, two of the Van Kampen eigenvalues around this point approach each other until they have the same position. If one increases $\widetilde{L}_n$ further (or decreases $\widetilde{L}_T$), then these eigenvalues separate again but this time in a direction perpendicular to the real axis, i.e., they get a non-zero imaginary part and the pair of an unstable and a damped eigenmode is formed.
The smaller peak in the spectral density, situated to the right of the big one, lies above the least damped Landau solution shown on Figure 5.2. This indicates that also in the ITG model, the Van Kampen eigenvalues 'sense' the Landau solutions. The red dashed line corresponds to the constant density of eigenvalues (at $1/\widetilde{k}_{||} = 1/3$) that comes from the multiplication operator $\widetilde{k}_{||}\widetilde{v}_{||}$ in the first part of (5.22), i.e., the variations of the spectral

[3]When the condition $\widetilde{k}_y \gg \widetilde{k}_{||}$ is not met, there is still a threshold. However, it depends not only on the ratio of the gradients but also on their explicit values.

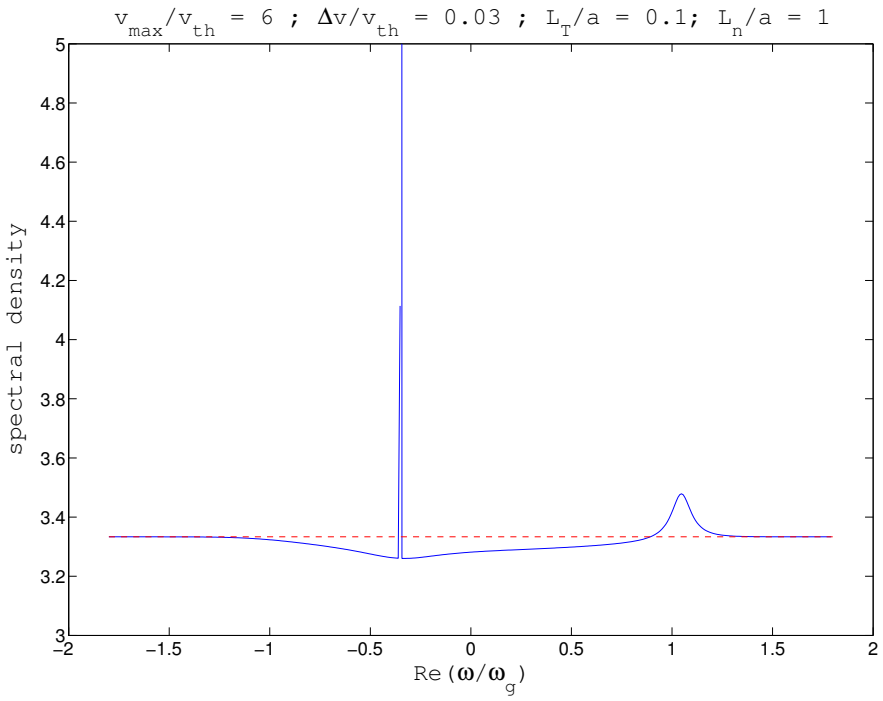

Figure 5.3: Density of the projection of the Van Kampen eigenvalues on the real line in the case of slab ITG model for $\widetilde{k}_{||} = \widetilde{k}_y = 0.3$ and $\rho_* = 1$.

density are due to the second term in (5.22) that involves the electrostatic potential.
One can also compute the coefficients when a given perturbation that evolves in time is decomposed in the basis of Van Kampen modes. In this case the calculation in (4.16) still holds. However, if there is an instability, then its coefficient is going to grow in time exponentially and dominate over the others.

It is useful to make a connection between the results derived here and those of other more sophisticated models. We will compare the Van Kampen spectrum from our model with those achieved with the gyrokinetic simulation code GENE. This abbreviation stands for 'gyrokinetic electromagnetic numerical experiment' and a description of the code can be found in [21] as well as at http://gene.rzg.mpg.de where also the entire code can be downloaded. The applicability of GENE is much wider than the simple example presented here. It can treat plasmas in a variety of conditions that involve realistic geometries of the magnetic field, perturbations of the magnetic field, finite Larmor radius effects, etc. In the framework of gyrokinetics, the ion distribution function is defined in a five dimensional phase space, since the velocity space is reduced by one dimension and only the parallel velocity and the energy of the gyromotion (proportional to the magnetic moment μ of the gyrating particle) are left. The distribution of both variables is similar to a Maxwellian, i.e., for $|v_{||}|, \mu \to \infty$ it falls rapidly to zero. In slab geometry, the magnetic moment can be factored and integrated out of the equations implemented in GENE. Then the program

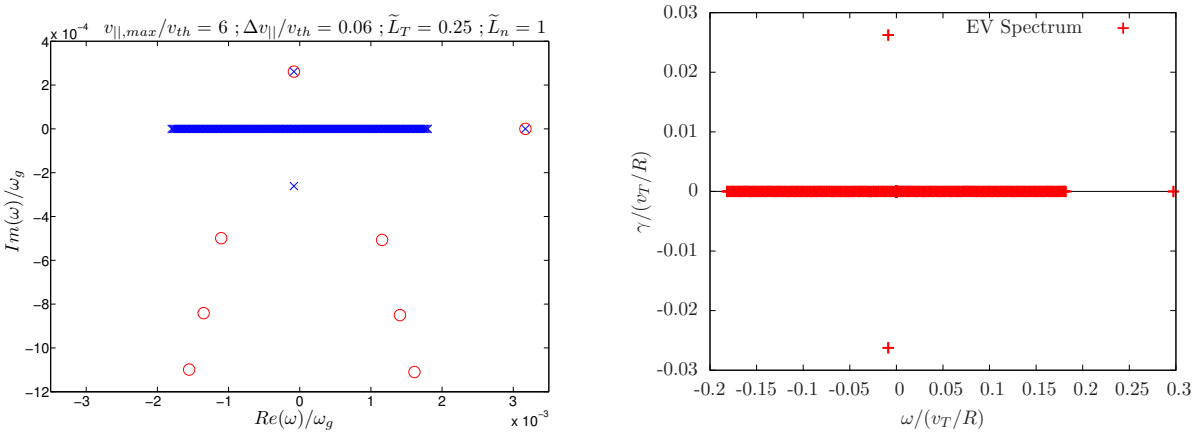

(a) Slab ITG model described in this work.

(b) GENE equivalent of the slab ITG.

Figure 5.4: Comparison of Van Kampen spectra between the slab ITG model described in this work and the equivalent problem solved with GENE; $\widetilde{k}_{||} = 0.03$, $\widetilde{k}_y = 0.3$ and $\rho_* = 0.01$.

solves almost the same set of equations. The only difference is that in GENE there is no Fourier transformation with respect to $k_{||}$ [27]. This issue was solved by David Hatch with a Fourier filter with respect to $k_{||}$ for the modes. After this step, one can compare the results of both approaches directly. Such a comparison is shown in Figure 5.4. The left plot has been produced by the program *drift_eigenvalue.m* and the right one has been made by David Hatch with GENE such that it corresponds to the same parameters. In Figure 5.4, the Van Kampen eigenvalues are denoted by blue crosses and also the eight Landau solutions that are closest to the real line are shown (red circles). The Van Kampen eigenvalues produced by GENE are represented by red pluses. The immediate comparison between the two plots shows a good agreement which is not only qualitative but also quantitative. For example one could compare the position of the instability. Our program produces an instability at $\widetilde{\omega} \approx (-0.82 + 2.6i) \cdot 10^{-4}$ and GENE at $\widetilde{\omega} \approx (-0.87 + 2.6i) \cdot 10^{-4}$. The discrepancy between the two results is small and it appears in the real part, so it is probably due to the fact that one takes only a finite number of points in velocity space.
It is also noteworthy that one of the real Van Kampen eigenvalues is separated from the rest. (Its position is the same on both plots.) This is due to the fact that this eigenvalue belongs to the discrete part of the Van Kampen spectrum that is defined as the set of solutions of (5.29). The length of the box in which the other eigenvalues are situated is directly related to the length of the interval in velocity space that is used, namely $\widetilde{\omega}_{max} = \rho_* \widetilde{k}_{max} \widetilde{v}_{||,max}$. One can also easily compute the discrete Van Kampen eigenvalues directly by plotting the right-hand side of (5.29) and find the values of the argument for which this real valued function gives zero. For the set of parameters used for producing Figure 5.4 there are in total four discrete Van Kampen eigenvalues, namely $\widetilde{\omega}_{V,1} = -0.493 \cdot 10^{-3}$, $\widetilde{\omega}_{V,2} = -0.020 \cdot 10^{-3}$, $\widetilde{\omega}_{V,3} = 0.519 \cdot 10^{-3}$ and $\widetilde{\omega}_{V,4} = 3.171 \cdot 10^{-3}$. The last of these four solutions equals exactly

the separated real eigenvalue that our program produced. This was not expected, since in our discretization scheme we approximated velocity integrations like in (5.29) with a finite sum that extends from $-v_{||,max}$ to $v_{||,max}$. However, despite this fact, our matrix apparently 'knows' something about the position of the discrete Van Kampen solutions, at least when they are outside the frequency 'box' on the real line. In Figure 5.4(a) one sees that the one of the Landau solutions seems to have the same position as the discrete Van Kampen eigenvalue. In fact, it is very close to it but not at the same spot. The Van Kampen value is real, while the Landau solution has a small imaginary part of approximatively $2.3 \cdot 10^{-8}$. Using an approximation of the plasma dispersion function for arguments with a small imaginary part, whose absolute value is much smaller than that of the real part of the argument, one can show that such solutions of (5.23) are almost solutions of (5.29).

It is also interesting to look at the mode structure of the numerical Van Kampen eigenmodes. First, we write down the analytical eigenfunctions. By the result (3.17) in chapter 3 they read

$$\widehat{\widetilde{f}}_{\widetilde{\omega}}(\widetilde{v}_{||}) = \frac{\tau^{(m)}\widetilde{T}_e(\widetilde{x})}{\widetilde{n_{0i}}(\widetilde{x})\widetilde{k}_{||}} \frac{\alpha(\widetilde{x},\widetilde{v}_{||})f_{0i}(\widetilde{x},\widetilde{v}_{||})}{\widetilde{v}_{||} - \widetilde{\omega}/(\rho_*\widetilde{k}_{||})} + \\ + \widetilde{k}_{||}\delta(\widetilde{k}_{||}\widetilde{v}_{||} - \widetilde{\omega}) \left(1 - \frac{\tau^{(m)}\widetilde{T}_e(\widetilde{x})}{\widetilde{n}_{0i}(\widetilde{x})\widetilde{k}_{||}} p.v. \int_{-\infty}^{+\infty} \frac{\alpha(\widetilde{x},\widetilde{v}'_{||})\widetilde{f}_{0i}(\widetilde{x},\widetilde{v}'_{||})}{\widetilde{v}'_{||} - \widetilde{\omega}/(\widetilde{k}_{||}\rho_*)} d\widetilde{v}'_{||}\right). \quad (5.37)$$

For eigenmodes that correspond to the discrete part of the Van Kampen spectrum, the coefficient in brackets after the delta function is zero, thus only the first part is left. If the eigenfrequency is complex, this first part has also no poles, since $\widetilde{v}_{||}$ and $\widetilde{k}_{||}$ are real.

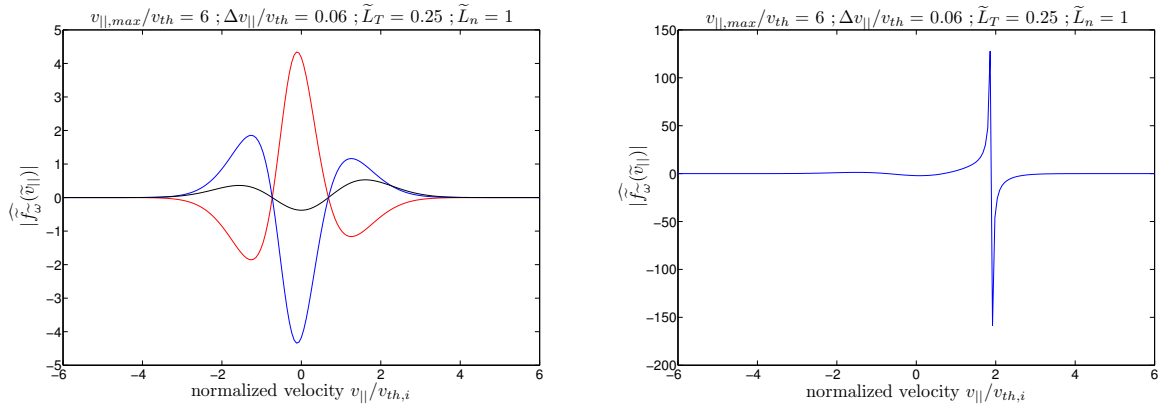

(a) Eigenmodes corresponding to the unstable, damped and the isolated real eigenvalue.

(b) Eigenmode corresponding to an eigenvalue from the continuum.

Figure 5.5: Mode structure of different numerical eigenvectors.

In Figure 5.5 we show some of the eigenvectors that our program produces. On the left are the imaginary parts of the eigenvectors corresponding to the unstable (red line) and damped (blue line) eigenvalues, and also the numerical eigenvector that corresponds to the real eigenvalue that is isolated from the others. One sees that the blue and the red lines differ by a minus sign and that they are not sharply peaked. This was also expected from (5.37). The black line is not peaked either, although the analytical eigenfunction has a singularity. However, the parallel velocity that corresponds to $\widetilde{\omega} = 3.171 \cdot 10^{-3}$ does not lie in the interval $[-6, 6] \cdot v_{th,i}$. Therefore, the numerical eigenvector cannot develop a sharp peak. The situation with the mode shown in Figure 5.5 is different. The numerical eigenmode represented there corresponds to the eigenvalue that is closest to $(1/\sqrt{3}) \cdot 10^{-3}$ and, as expected, it develops a sharp peak at $\widetilde{v}_{||} = 1/(0.3\sqrt{3}) \approx 1.92$.

5.3 Collisional ITG modes

As we observed in subsection 4.2.2, the Van Kampen spectrum for a collisionless plasma in the linear electrostatic regime changes dramatically when collisions are introduced in the system (at least when collisions are modelled via an operator of the type of the Lenard-Bernstein collision operator that involves a second derivative with respect to velocity, i.e., diffusion in velocity space). Therefore, it is interesting to study the effect of collisions in this case. From a physical point of view, one might expect that the ITG modes are fundamentally different from the electrostatic Langmuir waves, since now the plasma is strongly magnetized and there are gradients of temperature and density. On the other hand, we saw in section 5.1 that from a mathematical point of view, the sets of equations that describe the two models are very similar. It is particularly easy to conceive this by comparing equations (5.22) and (3.1). Therefore, we expect that the Lenard-Bernstein collision operator has qualitatively the same effect on the slab ITG modes as on the Langmuir waves. If one adds the Lenard-Bernstein collision operator, formulated in terms of parallel velocity, on the right-hand side of (5.15) and performs again all the transformations described in the first subsection of this chapter, one eventually arrives at

$$\frac{\widetilde{\omega}}{\rho_*}\widehat{\widetilde{f}}_{1i} = \widetilde{k}_{||}\widetilde{v}_{||}\widehat{\widetilde{f}}_{1i} - \frac{\tau^{(m)}\widetilde{T}_e(\widetilde{x})}{\widetilde{n}_{0i}(\widetilde{x})}\alpha(\widetilde{x},\widetilde{v}_{||})\widetilde{f}_{0i}(\widetilde{x},\widetilde{v}_{||})\int_{-\infty}^{+\infty}\widehat{\widetilde{f}}_{1i}(...,\widetilde{v}'_{||},...)d\widetilde{v}'_{||} + \\ + i\frac{\widetilde{\nu}}{\rho_*}\left(\widehat{\widetilde{f}}_{1i} + \widetilde{v}_{||}\frac{\partial\widehat{\widetilde{f}}_{1i}}{\partial\widetilde{v}_{||}} + \frac{\partial^2\widehat{\widetilde{f}}_{1i}}{\partial\widetilde{v}_{||}^2}\right). \quad (5.38)$$

The discretization procedure outlined in subsections 4.1.1 and 4.2.2 turns the right-hand side of (5.38) into a matrix with complex elements, and the Van Kampen spectrum is the set of eigenvalues of this matrix. The implementation of this eigenvalue problem was done with MATLAB via the program *drift_eigenvalue_Lenard.m* which has been used to produce the spectrum shown in Figure 5.6.

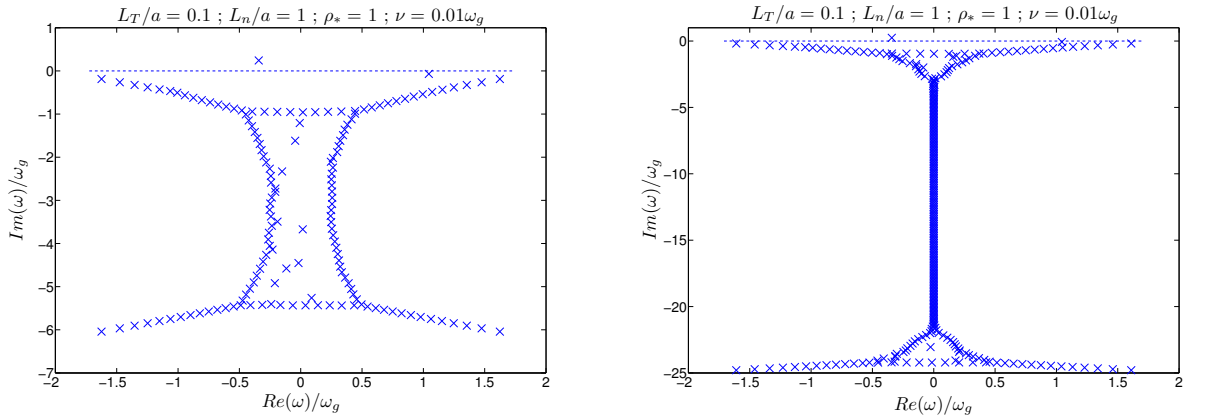

(a) Number of points in velocity space: $N = 150$. (b) number of points in velocity space: $N = 300$.

Figure 5.6: Comparison of Van Kampen spectra in the slab ITG model for fixed collision frequency ($\widetilde{\nu} = 0.001$) and different velocity resolution; $\widetilde{k}_{||} = \widetilde{k}_y = 0.3$.

In the slab ITG model, we observe the same qualitative behaviour as in the case of Langmuir waves. The spectrum consists roughly of the same three parts, and there is again an area of stochasticity that shrinks to the negative imaginary axis when the resolution in velocity space is increased. Therefore, in the limit $\widetilde{\nu} \to 0$, we will follow the same principles. First, we reassure ourselves that this area of stochasticity does not enclose the Landau solutions for which we want to find the corresponding Van Kampen eigenvalues. One prominent feature of the spectra in Figure 5.6 is that one of the damped Van Kampen eigenvalues separates from the rest and its position is close to the position of the least damped Landau solution in Figure 5.2. This foreshadows the correctness of our conjecture that in the slab ITG model the limit $\widetilde{\nu} \to 0$ yields similar results as in the case of Langmuir waves. As in subsection 4.2.2, the mirror symmetry of the collisionless Van Kampen spectrum with respect to the real axis is destroyed by introducing the collision operator considered here, which comes from the factor of i in (5.38). It can be easily checked that the position of the unstable mode has been barely changed by the collision operator. The mode moves indeed a little closer to the real line but the change of the growth rate appears to be one order of magnitude smaller than the collision frequency. However, its damped mirror image in the collisionless case seems to have changed its position abruptly, and there is no eigenmode in the vicinity of the damped mode for $\widetilde{\nu} = 0$. Varying the resolution in velocity space while keeping the collision frequency constant at some low value shows that the position of the unstable Landau solution is quite robust against changes of in the resolution and does not react like the other Van Kampen eigenvalues. For the Lenard-Bernstein collision operator, one can also derive explicitly the analytic dispersion relation and it is an analytic function of $\widetilde{\nu}$ at $\widetilde{\nu} = 0$. Therefore, for small collision frequency, the unstable Landau solution with collision operator lies in the vicinity of the collisionless unstable Landau solution. This fact, together with the observation that the unstable Van Kampen eigenvalue stays nearly the same for small $\widetilde{\nu}$, leads us to the conjecture that also in the case of collisions the

unstable Landau solution coincides with the unstable Van Kampen solution, as it does in the collisionless case.

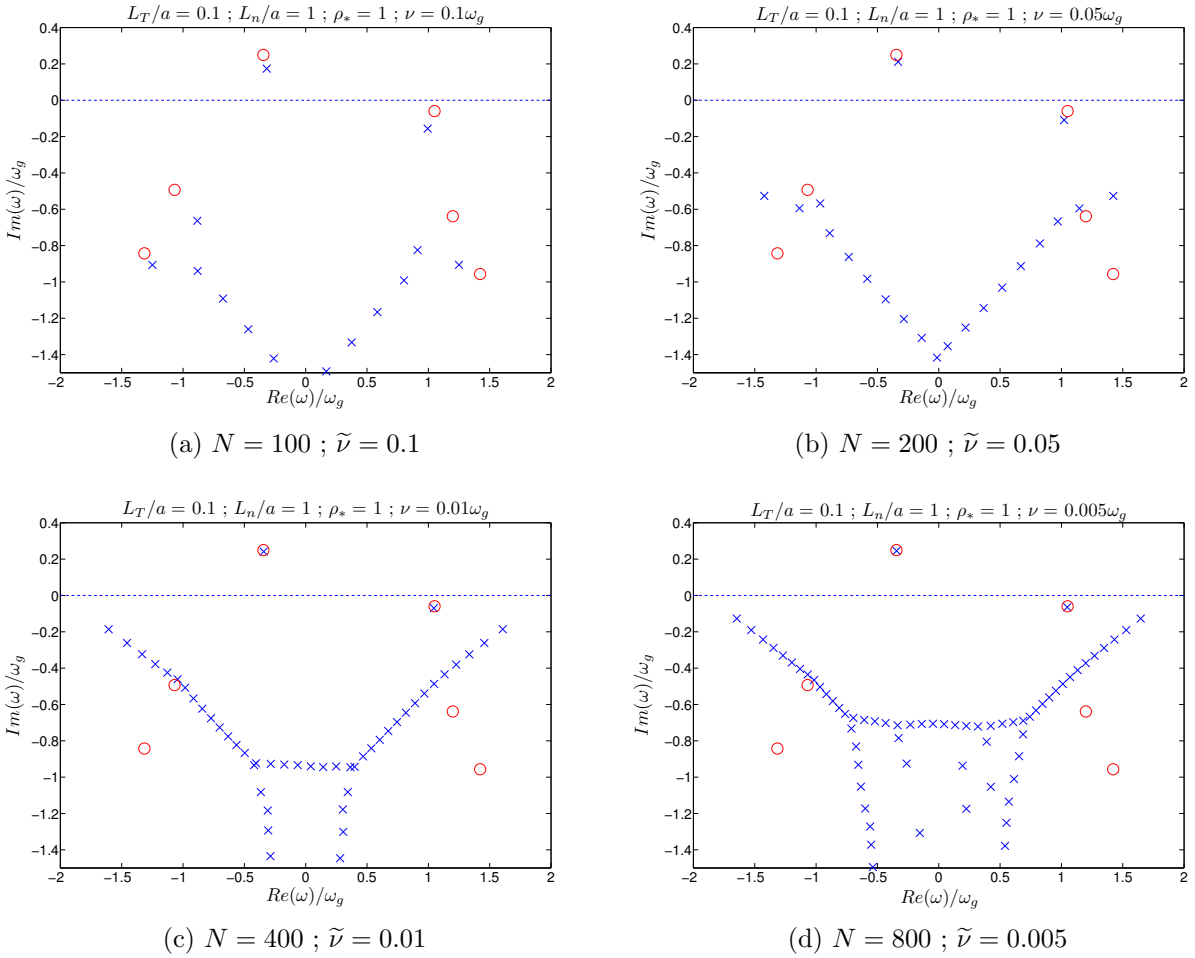

(a) $N = 100$; $\widetilde{\nu} = 0.1$

(b) $N = 200$; $\widetilde{\nu} = 0.05$

(c) $N = 400$; $\widetilde{\nu} = 0.01$

(d) $N = 800$; $\widetilde{\nu} = 0.005$

Figure 5.7: Visualization of the limit $\widetilde{\nu} \to 0$ of the Van Kampen spectrum in the case of the slab ITG model.

Finally, we investigate more precisely what happens with the Van Kampen spectrum when the collision frequency is decreased such that at least the upper part of the spectrum is converged. This process is presented in Figure 5.7 where we have reduced the range of the axes in order that the upper part of the spectrum, which is the one we are interested in, is clearly visible. Blue crosses denote again the Van Kampen eigenvalues and red circles the collisionless Landau solutions. One sees that the least damped Van Kampen eigenvalue approaches the least damped Landau solution. This qualitative observation can also be confirmed numerically. Like in subsection 4.2.2, we compute the difference $\Delta\widetilde{\omega}$ between the least damped Landau solution and the corresponding Van Kampen eigenvalue for small collision frequencies. From the data that our program produces one sees that the dependence is again linear, and for $\widetilde{\nu} \to 0$ also $\Delta\widetilde{\omega} \to 0$.

Having validated numerically this conjecture, the next step is to investigate the mode structures of typical Van Kampen eigenmodes. This is done in the same way as in subsection 4.2.2, namely by numerically computing the second derivative of the corresponding mode with respect to velocity, and taking the maximum of its absolute value which we call again d_{max}. We focus our attention on three modes: the unstable mode, the one that approaches the least damped Landau solution and the mode in the upper left corner of the Van Kampen spectrum. For the unstable mode, we observed that d_{max} indeed grows when the collision frequency is decreased but the changes were very small. For a decrease of $\widetilde{\nu}$ by a factor of 10, d_{max} increased by a factor of nearly 2. From this follows that the product $\widetilde{\nu} \cdot d_{max}$ will tend to zero in the limit $\widetilde{\nu} \to 0$, i.e., the unstable Van Kampen mode has a trivial limit which is what we expected, since the unstable Landau solution is a continuous function of $\widetilde{\nu}$. Next, we perform the same numerical computation for the Van Kampen mode that approaches the least damped Landau solution. Here d_{max} scales approximately linearly with the inverse collision frequency which means that the product $\widetilde{\nu} \cdot d_{max}$ does not tend to zero in the limit $\widetilde{\nu} \to 0$, confirming our observations of the Van Kampen spectrum. For the Van Kampen mode in the upper left corner of the spectrum noticeable changes of d_{max} were observed when collision frequency decreased. Therefore, the functional dependence of the second derivative was parametrized as $d_{max} = y_1 \cdot (1/\widetilde{\nu})^{y_2} + y_3$, since this parametrization was successful in the case of Langmuir waves. The best such fit to our data yielded for the parameter y_2 a value of approximatively 0.83. This means that the product $\widetilde{\nu} \cdot d_{max}$ scales like $\widetilde{\nu}^{0.17}$, i.e., this mode also has a trivial limit when the collision frequency goes to zero.
As one sees in this chapter, many features of the Langmuir waves carry over to the slab ITG model. From a physical point of view, this can be considered as an unexpected result, since in the second case, one deals with strongly magnetized plasmas where also gradients in density and temperature are present.

Chapter 6

Summary and conclusions

In chapter 1, we motivated this work by highlighting the importance of kinetic effects like Landau damping for the physical understanding turbulent plasmas. In chapter 3, we formulated the problem of Langmuir waves in a mathematically rigorous way. To our knowledge, such an in-depth treatment cannot be found anywhere in the literature. Although this did not change the fundamental physics of Landau damping, of course, it helped to gain useful insights into the structure and origin of the Van Kampen spectrum. At the end of that chapter, we also arrived at the conclusion that some standard references about Landau damping such as [13] do not give the correct picture of the conditions under which the Van Kampen spectrum arises. The consequences of this finding should be investigated further.

In chapter 4, we treated the problem of Langmuir waves numerically. One of the most interesting aspects in the collisionless case was to explore which of the Van Kampen eigenmodes are most important for the large-time evolution of the system and the occurrence of an exponentially damped electric field. It was expected that these are the modes that lie above the least damped Landau solutions in the complex frequency plane where an accumulation of eigenvalues was observed, since they also have the largest coefficients when a typical initial condition is decomposed into the basis of Van Kampen modes. However, it turned out that these modes alone are not sufficient for reproducing Landau damping and that one should also consider the modes that lie in the middle part of the spectrum, although their coefficients are rather small.
Another important part of this work was to show numerically that the Van Kampen spectrum changes abruptly when collisions are introduced into the system via the Lenard-Bernstein collision operator as stated in [18], [15], and [16]. Since this conjecture has been proved analytically, our goal was rather to investigate if a numerical discretization in velocity space, that is widely used in computer simulations in plasma physics, reproduces this effect. From our analysis, this appears to be the case. We also went one step further and investigated which part of the Lenard-Bernstein collision operator is responsible for this behaviour. It became clear that the reason was the term in the operator which involves a second derivative of the perturbation with respect to velocity. One usually refers to this as diffusion in velocity space, and it is also present into the full Focker-Planck collision

operator. Therefore, if one considers simplified models for collision operators, one should also include this feature in order to reproduce physically correct results.
In chapter 5, we studied a slab ITG model. It turned out that it is mathematically very similar to the model of electrostatic Langmuir waves, and we observed that many of its essential features carry over to the slab ITG case. This applies also to the effect of collisions.

The work presented here can be extended to physically more realistic situations. Further investigations of Landau damping can improve our understanding for the influence of kinetic effects on the behaviour of turbulent fusion plasmas. One of its important features that has to be clarified is the saturation of turbulent flows and the energy transfer between unstable and damped modes with similar wave numbers, since this appears to be the greatest difference between plasma turbulence and conventional fluid turbulence. The linear theory used in this work can help us gain important physical insights which can lead to improved models of nonlinear effects, allowing for more efficient computer simulations of fusion plasmas.

Appendix A

Relations involving the plasma dispersion function Z

The exact definition of the plasma dispersion function Z given in [1] is

$$Z(\xi) = \frac{1}{\sqrt{\pi}} \int_{-\infty}^{+\infty} \frac{e^{-x^2}}{x-\xi} dx, \tag{A.1}$$

where $\xi \in \mathbb{C}$ and the above expression applies for $Im\xi > 0$. For $Im\xi \leq 0$, one should take the analytical continuation of (A.1) which, as we saw, is given by doing the integration from $-\infty$ to $+\infty$ along the Landau contour. Here, for convenience, we are going to keep the boundaries of the integrals as in (A.1) but one should keep in mind what the exact integration prescription is. The first relation in (5.24) is clear, so we focus on the second and third one:

$$\begin{aligned} \int_{-\infty}^{+\infty} \frac{xe^{-bx^2}}{x-a} dx = \int_{-\infty}^{+\infty} \frac{(x-a+a)e^{-bx^2}}{x-a} dx = \underbrace{\int_{-\infty}^{+\infty} e^{-bx^2} dx}_{=\sqrt{\frac{\pi}{b}}} + a \underbrace{\int_{-\infty}^{+\infty} \frac{e^{-bx^2}}{x-a} dx}_{=\sqrt{\pi} Z(a\sqrt{b})} = \\ = \sqrt{\frac{\pi}{b}} + a\sqrt{\pi} Z(a\sqrt{b}); \end{aligned} \tag{A.2}$$

$$\int_{-\infty}^{+\infty} \frac{x^2 e^{-bx^2}}{x-a} dx = \int_{-\infty}^{+\infty} \frac{(x^2-a^2+a^2)e^{-bx^2}}{x-a} dx = \underbrace{\int_{-\infty}^{+\infty} xe^{-bx^2} dx}_{=0} + a \underbrace{\int_{-\infty}^{+\infty} e^{-bx^2} dx}_{=\sqrt{\frac{\pi}{b}}} + \tag{A.3}$$

$$+a^2 \underbrace{\int_{-\infty}^{+\infty} \frac{e^{-bx^2}}{x-a} dx}_{=\sqrt{\pi} Z(a\sqrt{b})} = a\sqrt{\frac{\pi}{b}} + a^2 \sqrt{\pi} Z(a\sqrt{b}).$$

In previous chapters of this work, we occasionally used a decomposition of Z into its real and imaginary part for arguments with a positive imaginary part. In that case, one can represent the plasma dispersion function via (A.1), and this integral is well defined since there are no poles lying on the integration path. If $\xi := x + iy$, where $x,y \in \mathbb{R}$, one can write

$$Z(\xi) = Z(x,y) = \frac{1}{\sqrt{\pi}} \int_{-\infty}^{+\infty} \frac{e^{-t^2}(t-(x-iy))}{|t-x-iy|^2} dt = \underbrace{\frac{1}{\sqrt{\pi}} \int_{-\infty}^{+\infty} \frac{(t-x)e^{-t^2}}{(t-x)^2+y^2} dt}_{=ReZ(x,y) \text{ for } y>0} +$$
$$+ \underbrace{i\, y \frac{1}{\sqrt{\pi}} \int_{-\infty}^{+\infty} \frac{e^{-t^2}}{(t-x)^2+y^2} dt}_{=ImZ(x,y) \text{ for } y>0}. \quad \text{(A.4)}$$

In section 2.2, we also used that the partial derivative of $ImZ(x,y)$ with respect to x can be commuted with the integration with respect to t. In order to prove this, we first note that the derivative of the integrand is

$$\frac{\partial}{\partial x}\left(\frac{e^{-t^2}}{(t-x)^2+y^2}\right) = \frac{2(t-x)e^{-t^2}}{((t-x)^2+y^2)^2}$$

which exist for all x and t, since $y \in \mathbb{R}_+$. Now, we only have to verify that the integral of this expression over t is finite, which can be done as follows:

$$\int_{-\infty}^{+\infty} \frac{2(t-x)e^{-t^2}}{((t-x)^2+y^2)^2} dt = 2\int_{-\infty}^{+\infty} \frac{te^{-t^2}}{((t-x)^2+y^2)^2} dt - 2x \underbrace{\int_{-\infty}^{+\infty} \frac{e^{-t^2}}{((t-x)^2+y^2)^2} dt}_{\leq \frac{1}{y^4}\int_{-\infty}^{+\infty} e^{-t^2} dt = \frac{\sqrt{\pi}}{y^4} < +\infty} \quad \text{(A.5)}$$

and the first integral can be estimated with

$$\left| \int_{-\infty}^{+\infty} \frac{te^{-t^2}}{((t-x)^2+y^2)^2} dt \right| \leq \int_{-\infty}^{+\infty} \frac{|t|e^{-t^2}}{((t-x)^2+y^2)^2} dt \leq \frac{1}{y^4} \int_{-\infty}^{+\infty} |t|e^{-t^2} dt =$$

$$= \frac{2}{y^4} \int_{0}^{+\infty} te^{-t^2} dt = \frac{1}{y^4} < +\infty, \quad \text{(A.6)}$$

i.e., the left-hand side of (A.5) is a sum of two finite terms and is therefore also finite.

Appendix B

Employed MATLAB codes

In this part of the Appendix, we present the codes that we used to produce the results described in this thesis.

```
function[nooutput,f] = landau(n,kapa)

v = [0:.001:0.02];
[Re_w,Im_w] = meshgrid(-n:.001:n, -n:.001:0);
f1 = 1 + kapa^2 + 1i*(1/kapa)*sqrt(pi/2).*(Re_w +
    1i*Im_w).*faddeeva((Re_w+1i*Im_w)/(sqrt(2)*kapa));
f = sqrt(real(f1).^2 + imag(f1).^2);

plot([n -n], [0 0], '--');
hold on
contour(Re_w, Im_w, f, v);
xlabel('$Re(\omega)/\omega_{pe}$', 'Interpreter', 'latex', 'FontSize', 30,
    'FontName','Courier');
ylabel('$Im(\omega)/\omega_{pe}$', 'Interpreter', 'latex', 'FontSize', 30,
    'FontName','Courier');
title(['contour plot of the Landau solutions for k = ', num2str(kapa),
    '\lambda_{D}']);
```

```
% calculates eigenvalues, eigenvectors and spectral density of the matrix M

function[nooutput,E] = eigenvalue(v_max,N,kapa)

v = linspace(-v_max,v_max,N+1);  % row of the vector v
delta_v = v(2) - v(1);
G = -v.*exp(-(v.^2)/2)/sqrt(2*pi);
a = 1:N+1;
```

```
b = ones(1,N+1);

M1 = -kapa*v_max*((N+2)/N)*eye(N+1);
M2 = kapa*delta_v*diag(a);
M3 = -(delta_v*G.'*b)/kapa;

M = M1 + M2 + M3;

[V,E] = eig(M);
E = diag(E);
[new_E,inds] = sort(E);
V = V(:,inds);

V = V*diag(1./sum(V))/delta_v;

plot(real(E), imag(E), 'x', 'MarkerSize', 15);
hold on
plot(real(new_E(1:end-1)), delta_v./diff(real(new_E)));

xlabel('$Re(\omega)/\omega_{pe}$', 'Interpreter', 'latex',
    'FontSize', 34, 'FontName','Courier');
ylabel('$Im(\omega)/\omega_{pe}$', 'Interpreter', 'latex',
    'FontSize', 34, 'FontName','Courier');
ylabel('spectral density', 'FontSize', 34, 'FontName', 'Courier')
title(['$v_{max} = $ ' , num2str(v_max), '$v_{th}$ ', ' $ ; \Delta v = $ ',
num2str(delta_v), '$v_{th}$ ', ' $ ; k\lambda_{D} = $ ', num2str(kapa)],
'Interpreter', 'latex', 'FontSize', 34, 'FontName', 'Courier');
set(gca, 'FontSize', 24)
```

```
% calculates the perturbation of the distribution function as an
% initial value problem

function[kapa,D,V,W,F] = initial_value(v_max,N,t_max,N_time)

kapa = 0.5;
t = linspace(0,t_max,N_time);
v = linspace(-v_max,v_max,N+1);
delta_v = v(2) - v(1);

a = 1:N+1;
G = -v.*exp(-(v.^2)/2)/sqrt(2*pi);
```

```
b = ones(1,N+1);

M1 = -kapa*v_max*((N+2)/N)*eye(N+1);
M2 = kapa*delta_v*diag(a);
M3 = -(delta_v*G.'*b)/kapa;

M = M1 + M2 + M3;

[V,D] = eig(M);
D = diag(D);
[D,inds] = sort(D);
V = V(:,inds);

V = V*diag(1./sum(V))/delta_v;

[W,E_l] = eig(M.');
E_l = diag(E_l);
[~,inds] = sort(E_l);
W = W(:,inds);

W = W*diag(1./sum(W))/delta_v;

clear M;

F_0 = exp(-(v).^2/2);

COEF = zeros(1,N+1);
for j = 1:N+1
    COEF(j) = (W(:,j)'*F_0')/(W(:,j)'*V(:,j));
end


B = exp(multiprod(-1i*diag(D),permute(t,[1 3 2])))-repmat(ones(N+1,'single')
    -eye(N+1,'single'),[1 1 N_time]);
C = multiprod(multiprod(V,B),inv(V));
clear B;
F = squeeze(multiprod(C,F_0'));
clear C;
```

```
% Van Kampen spectrum in the case of a 'bump-on-tail' background distribution
% in velocity space
```

```
function[nooutput,f] = bump(v_max,N,C_a,v_b,tau)

v = linspace(-v_max,v_max,N+1);
delta_v = v(2) - v(1);
kapa = 0.5;
G = - (C_a/sqrt(2*pi))*v.*exp(-v.^2/2) -
((1-C_a)*tau^(3/2)/sqrt(2*pi))*(v-v_b).*exp(-tau*((v-v_b).^2)/2);
a = 1:N+1;
b = ones(1,N+1);

M1 = -kapa*v_max*((N+2)/N)*eye(N+1);
M2 = kapa*delta_v*diag(a);
M3 = -(delta_v*G.'*b)/kapa;

M = M1 + M2 + M3;

[~,E] = eig(M);
E = diag(E);
[new_E,inds] = sort(real(E));
V = V(:, inds);

V = V*diag(1./sum(V))/delta_v;


plot(real(E), imag(E), 'x', 'MarkerSize', 15);
hold on
landau_bump(kapa,C_a,v_b,tau);
xlabel('$Re(\omega)/\omega_{pe}$', 'Interpreter', 'latex', 'FontSize',
    34, 'FontName', 'Courier');
ylabel('$Im(\omega)/\omega_{pe}$', 'Interpreter', 'latex', 'FontSize',
34, 'FontName', 'Courier');
title(['$v_{max} = $ ', num2str(v_max), '$v_{th}$ ', ' $; \Delta v = $ ',
    num2str(delta_v), '$v_{th}$', ' $; C_{a} = $ ', num2str(C_a), ' $;
    v_{b} = $ ', num2str(v_b), '$v_{th}$', ' $; \tau = $ ', num2str(tau)],
    'Interpreter', 'latex', 'FontSize', 34, 'FontName', 'Courier');
set(gca, 'FontSize', 24)
```

```
% Landau approach for the 'bump-on-tail' instability

function[nooutput,f] = landau_bump(kapa,C_a,v_b,tau)
```

```
v = [0:.004:0.02];
[Re_w,Im_w] = meshgrid(-4:10^(-4):4, -1:10^(-4):0.5);
f1 = kapa^2 + tau + C_a*(1-tau) + 1i*sqrt(pi)*C_a*((Re_w +
1i*Im_w)/(sqrt(2)*kapa)).*faddeeva((Re_w+1i*Im_w)/(sqrt(2)*kapa)) +...
    + 1i*sqrt(pi)*(1-C_a)*tau*sqrt(tau/2)*(((Re_w +
1i*Im_w)/kapa)-v_b).*faddeeva(sqrt(tau/2)*(((Re_w + 1i*Im_w)/kapa)-v_b));
f = sqrt(real(f1).^2 + imag(f1).^2);

contour(Re_w, Im_w, f, v);
xlabel('$Re(\omega)/\omega_{pe}$', 'Interpreter', 'latex', 'FontSize', 34,
    'FontName', 'Courier');
xlabel('$Im(\omega)/\omega_{pe}$', 'Interpreter', 'latex', 'FontSize', 34,
    'FontName', 'Courier');
title(['$v_{max} = $ ', num2str(v_max), '$v_{th}$ ', ' $; \Delta v = $ ',
    num2str(delta_v), '$v_{th}$', ' $; C_{a} = $ ', num2str(C_a),
    ' $; v_{b} = $ ', num2str(v_b), '$v_{th}$', ' $; \tau = $ ', num2str(tau)],
    'Interpreter', 'latex', 'FontSize', 34, 'FontName', 'Courier');
set(gca, 'FontSize', 24)
```

```
% calculates eigenvalues and spectral density of the matrix M for the slab
% ITG model

function[nooutput,E] = drift_eigenvalue(v_max,N,L_T,L_n)

v = linspace(-v_max,v_max,N+1);
delta_v = v(2) - v(1);
a = 1:N+1;
b = ones(1,N+1);
tau = 1;
k_y = 0.3;
k_par = 0.03;
ro = 0.01;

G = tau*exp(-(v.^2)/2).*( k_y/(2*L_T) - (k_y/(2*L_T))*v.^2 - k_y/L_n -
    k_par*v )/sqrt(2*pi);

M1 = k_par*v_max*((N+2)/N)*eye(N+1);
M2 = -k_par*delta_v*diag(a);
M3 = (delta_v*G.'*b);
```

```
M = -(M1 + M2 + M3);

[V,E] = eig(M);
E = ro*diag(E);
[new_E,inds] = sort(real(E));
V = V(:,inds);

V = V*diag(1./sum(V))/delta_v;

clear M;

plot(real(E), imag(E), 'x', 'MarkerSize', 24);
hold on
plot(new_E(1:end-1), delta_v./diff(new_E));
hold on
drift_landau(ro,L_T,L_n);
xlabel('$Re(\omega)/\omega_{g}$', 'Interpreter', 'latex', 'FontSize', 40,
    'FontName', 'Courier');
ylabel('$Im(\omega)/\omega_{g}$', 'Interpreter', 'latex', 'FontSize', 40,
    'FontName', 'Courier');
title(['$v_{||,max}/v_{th} = $ ', num2str(v_max), ' $ ; \Delta v_{||}/v_{th} = $ ',
    num2str(delta_v), ' $ ; \widetilde{L}_{T} = $ ',num2str(L_T), ' $ ;
    \widetilde{L}_{n} = $',num2str(L_n)], 'Interpreter', 'latex', 'FontSize',
    40, 'FontName', 'Courier');
set(gca, 'FontSize', 30)
```

```
% This program computes the Landau solutions arising from the linerized
% drift-kinetic equation for the distribution function gyrocenters where
% only a ExB drift has benn considered

function [nooutput,f] = drift_landau(ro,L_T,L_n)

tau = 1;
k_y = 0.3;
k_par = 0.3;
v = [0:0.1:1]*10^(-4);
[Re_w,Im_w] = meshgrid(1.418:10^(-5):1.428, -0.962:10^(-5):-0.952);

f1 = 1 + tau + 0.5*tau*(k_y/k_par)*(1/L_T)*(Re_w + 1i*Im_w)/(k_par*ro) +
1i*tau*sqrt(pi).*faddeeva((Re_w + 1i*Im_w)/(sqrt(2)*k_par*ro)).*( (Re_w +
1i*Im_w)/(sqrt(2)*k_par*ro) - (k_y/k_par)*( 1/(2*L_T) - 1/L_n )/sqrt(2) +
```

```
sqrt(1/2)*(k_y/k_par)*((Re_w + 1i*Im_w)/(sqrt(2)*k_par*ro)).^2/L_T );
f = real(f1).^2 + imag(f1).^2;

contour(Re_w, Im_w, f, v);
xlabel('$Re(\omega)/\omega_{g}$', 'Interpreter', 'latex', 'FontSize', 30);
ylabel('$Im(\omega)/\omega_{g}$', 'Interpreter', 'latex', 'FontSize', 30);
title(['v_{max}/v_{th} = ', num2str(v_max), ' ; \Deltav/v_{th} = ',
    num2str(delta_v) ' ; k_{||}*a = ', num2str(k_par), ' ; k_{y}*r_{L} = ',
    num2str(k_y), ' ; L_{T}/a = ',num2str(L_T), '; L_{n}/a = ',num2str(L_n),
    ' ; \rho_{*} = ', num2str(ro)], 'FontSize', 24, 'FontName', 'Courier');
set(gca, 'FontSize', 18)
```

```
% calculates eigenvalues and spectral density of the matrix M for Langmuir
% waves where collisions are involved via the Lenard-Bernstein collision
% operator

function[nooutput,E] = Lenard_Bernstein(v_max,N,nu)

v = linspace(-v_max,v_max,N+1);
delta_v = v(2) - v(1);
G = -v.*exp(-(v.^2)/2)/sqrt(2*pi);
kapa = 0.5;
a = 1:N+1;
b = ones(1,N+1);

M = -kapa*v_max*((N+2)/N)*eye(N+1) + kapa*delta_v*diag(a) - (delta_v*G.'*b)/kapa
    + 1i*nu*(eye(N+1) + (-((N+2)/4)*eye(N+1) + (1/2)*diag(a))*(diag(b(1:N),1) -
    diag(b(1:N),-1))+(diag(b(1:N),1)-2*eye(N+1)+diag(b(1:N),-1))*(1/(delta_v^2)));

[V,E] = eig(M);
E = diag(E);
[~,inds] = sort(abs(E - 1.41566179 + 1i*0.15335939));
V = V(:,inds);

V = V*diag(1./sum(V))/delta_v;


plot(real(E), imag(E), 'x', 'MarkerSize', 24);
xlabel('$Re(\omega/\omega_{pe})$', 'Interpreter', 'latex', 'FontSize', 40,
    'FontName', 'Courier');
```

```
ylabel('$Im(\omega/\omega_{pe})$', 'Interpreter', 'latex', 'FontSize', 40,
    'FontName', 'Courier');
title(['$v_{max} = $ ', num2str(v_max), '$v_{th}  ;  \nu = $ ', num2str(nu),
    '$\omega_{pe}$' ,' $ ; N = $ ', num2str(N)], 'Interpreter', 'latex',
    'FontSize', 40, 'FontName', 'Courier');
set(gca, 'FontSize', 40)
```

```
% calculates eigenvalues and spectral density of the matrix M for the slab
% ITG model where collisions are involved via the Lenard-Bernstein collision
% operator

function[nooutput,E] = drift_eigenvalue_Lenard(v_max,N,L_T,L_n,nu)

v = linspace(-v_max,v_max,N+1);
delta_v = v(2) - v(1);
a = 1:N+1;
b = ones(1,N+1);
tau = 1;
k_y = 0.3;
k_par = 0.3;
ro = 1;

G = tau*exp(-(v.^2)/2).*( k_y/(2*L_T) - (k_y/(2*L_T))*v.^2 - k_y/L_n -
    k_par*v )/sqrt(2*pi);

M1 = k_par*v_max*((N+2)/N)*eye(N+1);
M2 = -k_par*delta_v*diag(a);
M3 = (delta_v*G.'*b);

M = -(M1 + M2 + M3) + 1i*(1/ro)*nu*( eye(N+1) + (-(N/4)*eye(N+1) -
    (1/2)*eye(N+1) + (1/2)*diag(a))*(diag(b(1:N),1) - diag(b(1:N),-1)) +
    (diag(b(1:N),1) - 2*eye(N+1) + diag(b(1:N),-1))*(1/(delta_v^2)) );

[V,E] = eig(M);
E = ro*diag(E);
[~,inds] = sort(imag(E), 'descend');
V = V(:,inds);

V = V*diag(1./sum(V))/delta_v;
```

```
plot(real(E), imag(E), 'x', 'Markersize', 24);
hold on
drift_landau(ro,L_T,L_n);
xlabel('$Re(\omega)/\omega_{g}$', 'Interpreter', 'latex', 'FontSize', 40,
    'FontName', 'Courier');
ylabel('$Im(\omega)/\omega_{g}$', 'Interpreter', 'latex', 'FontSize', 40,
    'FontName', 'Courier');
title(['$L_{T}/a = $ ',num2str(L_T), ' ; $L_{n}/a = $ ',num2str(L_n),
    ' ; $\rho_{\ast}= $ ',num2str(ro), ' ; $\nu = $ ', num2str(nu),
    '$\omega_{g}$'], 'Interpreter', 'latex', 'FontSize', 40, 'FontName',
    'Courier');
set(gca, 'FontSize', 30)
```

```
% reduced Lenard-Bernstein collision operator (only the first and the
% third part are present)

function[nooutput,E] = Lenard_Bernstein_2(v_max,N,nu)

v = linspace(-v_max,v_max,N+1);
delta_v = v(2) - v(1);
G = -v.*exp(-(v.^2)/2)/sqrt(2*pi);
kapa = 0.5;
a = 1:N+1;
b = ones(1,N+1);

M1 = -kapa*v_max*((N+2)/N)*eye(N+1);
M2 = kapa*delta_v*diag(a);
M3 = -(delta_v*G.'*b)/kapa;

M = M1 + M2 + M3 + 1i*nu*( eye(N+1) + (diag(b(1:N),1) - 2*eye(N+1) +
diag(b(1:N),-1))*(1/(delta_v^2)) );

[V,E] = eig(M);
E = diag(E);
[E_new,inds] = sort(E);
V = V(:,inds);


plot(real(E), imag(E), 'x', 'MarkerSize', 24);
hold on
```

```
xlabel('$Re(\omega/\omega_{pe})$', 'Interpreter', 'latex', 'FontSize',
    40, 'FontName', 'Courier');
ylabel('$Im(\omega/\omega_{pe})$', 'Interpreter', 'latex', 'FontSize',
    40, 'FontName', 'Courier');
title(['$v_{max} = $ ', num2str(v_max), '$v_{th} $ ', ' $  ;  N = $ ',
    num2str(N)], 'Interpreter', 'latex', 'FontSize', 40, 'FontName',
    'Courier');
set(gca, 'FontSize', 40)
```

```
% implements the Newton-Rapson method for finding zeros of a given function

function [nooutput,w] = my_newton(start,max,tol,kapa)

for j = 1:max
    w = start;
    w = w - sqrt(2)*kapa*(1 + kapa^2 + (w/(sqrt(2)*kapa))*1i*sqrt(pi)*
        *faddeeva(w/(sqrt(2)*kapa)))/(1i*sqrt(pi)*faddeeva(w/(sqrt(2)*kapa))*
        *(1 - 2*(w/(sqrt(2)*kapa))^2) - 2*w/(sqrt(2)*kapa));

    if (abs((w - start)/w) < tol)
      fprintf(1,'Newton converged\n\n answer is: omega = %11.8f %+11.8fi\n\n',
           real(w), imag(w));
      break
    end

    start = w;
end
```

```
% implements the decomposition in a basis involving Hermite polynomials
% according to Ng and Bhattacharjee


function[nooutput,M] = test_Ng(n,nu)

a = 1:n;
b = 1:n+1;
kapa = 0.5;

M1 = diag(sqrt(a),-1) + diag(sqrt(a),1);
```

```
M1(2,1) = M1(2,1) + 1/kapa^2;
M = kapa*M1 - 1i*nu*diag(b-1);

[~,E] = eig(M);
E = diag(E);

plot(real(E), imag(E), 'x', 'MarkerSize', 24);

xlabel('$Re(\omega)/\omega_{pe}$', 'Interpreter', 'latex', 'FontSize', 40,
    'FontName', 'Courier');
ylabel('$Im(\omega)/\omega_{pe}$', 'Interpreter', 'latex', 'FontSize', 40,
    'FontName', 'Courier');
title(['$n = $ ' , num2str(n), '  $ ; \nu = $ ', num2str(nu), '$\omega_{pe}$',
    ' $ ; k\lambda_{D} = $ ' , num2str(kapa)], 'Interpreter', 'latex',
    'FontSize', 40, 'FontName', 'Courier');
set(gca, 'FontSize', 30)
```

The program *faddeeva.m* implements the plasma dispersion function and has been downloaded from www.mathworks.com.

Bibliography

[1] The Plasma Dispersion Function, Burton D. Fried and Samuel D. Conte (Academic Press, London 1961)

[2] Theoretische Plasmaphysik, K. H. Spatschek (Teubner, Stuttgart 1990)

[3] Plasmaphysik, Robert J. Goldstone and Paul H. Rutherford (Vieweg, 1998)

[4] Introduction to Plasma Theory, Dwight R. Nicholson (John Wiley, 1983)

[5] Plasma Confinement, R. D. Hazeltine and J. D. Meiss (Dover Publications, 2003)

[6] Methods of Modern Mathematical Physics, IV: Analysis of Operators, M. Reed and B. Simon (Academic Press, 1978)

[7] Lineare Operatoren in Hilberträumen, Teil I Grundlagen, J. Weidmann (Teubner, 2000)

[8] Theoretical Methods in Plasma Physics, N. G. Van Kampen and B. U. Felderhof (North-Holland, Amsterdam 1967)

[9] Fundamentals of Plasma Physics and Controlled Fusion, Kenro Miyamoto (Iwanami Book Service Center, 1997)

[10] Modern Plasma Physics, Volume 1, P. H. Diamond, S.-I. Itoh and K. Itoh (Cambridge University Press, 2010)

[11] L. Landau, J. Phys. USSR 10, 25 (1946)

[12] N. G. Van Kampen, Physica 21, 949 (1955)

[13] K. M. Case, Ann. Phys. (N. Y.) 7, 349 (1959)

[14] K. M. Case, Phys. Fluids 8, 96 (1965)

[15] C. S. Ng, A. Bhattacharjee, and F. Skiff, Phys. Rev. Lett. 83, 1974, (1999)

[16] C. S. Ng, A. Bhattacharjee, and F. Skiff, Phys. Rev. Lett. 92, 065002 (2004)

[17] P. L. Bhatnagar, E. P. Gross, and M. Krook, Phys. Rev. 94, 511 (1954)

[18] A. Lenard and I. B. Bernstein, Phys. Rev. 112, 1456 (1958)

[19] T.-H. Watanabe and H. Sugama, Phys. Plasmas 11, 1476 (2004)

[20] S. C. Cowley, R. M. Kulsrud and R. Sudan, Phys. Fluids B 3, 2767 (1991)

[21] F. Jenko, W. Dorland, M. Kotschenreuther, B. N. Rogers, Phys. Plasmas 7, 1904 (2000)

[22] G. W. Hammett, W. Dorland and F. W. Perkins, Phys. Rev. Lett. 106, 115003 (2011)

[23] C. H. Su and C. Oberman, Phys. Rev. Lett. 20, 427 (1968)

[24] D. R. Hatch, P. W. Terry, F. Jenko, F. Merz, M. J. Pueschel, W. M. Nevins and E. Wang, Phys. Plasmas 18, 055706 (2011)

[25] D. R. Hatch, P. W. Terry, F. Jenko, F. Merz and W. M. Nevins, Phys. Rev. Lett. 106, 115003 (2011)

[26] R. W. Short and A. Simon, Phys. Plasmas 9, 3245 (2002)

[27] private correspondence with D. Hatch

[28] private correspondence with F. Jenko